ABSTRACT

Title of dissertation: NONLINEAR OPTICS QUANTUM COMPUTATION AND QUANTUM SIMULATION WITH CIRCUIT-QED
Prabin Adhikari, Doctor of Philosophy, 2014

Dissertation directed by: Dr. Jacob M. Taylor
Joint Quantum Institute
University of Maryland

Superconducting quantum circuits are a promising approach for realizations of large scale quantum information processing and quantum simulations. The Josephson junction, which forms the basis of superconducting circuits, is the only known nonlinear non-dissipative circuit element, and its inherent nonlinearities have found many different applications. In this thesis I discuss specific implementations of these circuits. I show that strong two-photon nonlinearities can be induced by coupling photons in the microwave domain to Josephson nonlinearities. I then propose a method to simulate a parent Hamiltonian that can potentially be used to observe fractional quantum Hall states of light. I will also explore how superconducting circuits can be used to modify system-bath couplings to emulate a chemical potential for photons. Finally, I consider the limitations of devising a scheme to couple superconducting circuits to trapped ions, and consider the challenges for such hybrid approaches.

NONLINEAR OPTICS QUANTUM COMPUTATION AND QUANTUM SIMULATION WITH CIRCUIT-QED

by

Prabin Adhikari

Dissertation submitted to the Faculty of the Graduate School of the
University of Maryland, College Park in partial fulfillment
of the requirements for the degree of
Doctor of Philosophy
2014

Advisory Committee:
Dr. Mohammad Hafezi, Chair
Dr. Jacob M. Taylor, Co-Chair/Advisor
Dr. Frederick C. Wellstood, Co-Chair
Dr. Eite Tiesinga
Dr. Dionisios Margetis

Acknowledgments

The past seven years at the University of Maryland have been intellectually stimulating, challenging, and very rewarding. During my time here, I have learned a lot of physics and acquired many skills necessary for scientific research. More importantly, I feel that I have acquired the skills for reasoning and critical thinking, which are important in many areas of life besides the academic world. I have also gotten to know many interesting and hardworking people from whom I have benefited greatly. I am very grateful to everyone I have been in touch with for their unwavering support in making this possible.

First of all I would like to thank my advisor Dr. Jacob Taylor for his mentorship. He has consistently encouraged me to work hard and supported me throughout my time as a graduate student. He has provided me everything I needed– from logistical resources, scientific advice and moral support, to grant support for participation in very illuminating conferences and schools. I am very grateful for the wonderful group outings, kickball games, and informal meetings both inside and outside the University that enabled our research group as a whole to communicate and disseminate ideas. Furthermore, I want to acknowledge the support of the Physics Frontier Center, funded by the National Science Foundation, without which my research would not have been possible.

I also want to thank Dr. Mohammad Hafezi whose support has been pivotal in my research, and my understanding of physics. It has been an honor to collaborate both with Dr. Taylor and Dr. Hafezi. I have also had the opportunity to do

independent study with Dr. Eite Tiesinga from the JQI, and Dr. Frank Gaitan from LPS. During my work with them, I learned a lot of new physics besides my immediate research area. I would like to offer many thanks to them for their valuable time and feedback.

I am also indebted to a great mentor and a friend of mine, Dr. William Wallace, who supported me throughout my undergraduate years at St. John's University. Without him I would not have made it to the University of Maryland. I also want to thank Dr. Robert Finkel for the guidance he provided me when I was an undergraduate. I will always cherish the wonderful memories from the four valuable years at St. John's University.

I have developed deep friendships during my time at Maryland. First, I want to acknowledge my office mate Ranchu Mathew for his camaraderie. I will always cherish the interesting scientific and philosophical discussions that I have had with him. I also want to thank my past and present group colleagues Dvir Kafri, Xunnong Xu, Haitan Zhu, Steve Ragole, and Vanita Srinivasa for their friendship and their advice on scientific matters. Additionally, I want to thank my experimentalist friends Varun Vaidya, Rajibul Islam, Elizabeth Goldschmidt, and Baladitya Suri for enlightening me with experimental knowledge. Outside the University, I want to acknowledge my friends Jesus Anguiano, James Creznic, and Pradeep Subedi for their friendship over the past decade.

Finally, I want to thank all my family members in Nepal for their love. Despite the great distance separating us, my family has been a source of unwavering encouragement throughout my life, especially while in America. Specifically, I am very

grateful to my parents Kamal and Kalpana and my two younger brothers Prabal and Prajesh for their love and support.

My journey over the past seven years would not have been possible without my wife Clare. I thank her for supporting me all these years with patience and understanding, and working hard for our future.

Table of Contents

List of Tables

List of Figures

Chapter 1

Introduction to Quantum Computation and Quantum Simulation

1.1 Church-Turing Thesis and Classical Computers

The key assumption from the modern theory of classical computation can be summarized by the Church-Turing thesis: *Any algorithmic process can be efficiently simulated using a Turing Machine* [1]. A Turing Machine is a device that consists of a tape, a read-write head, and a set of instructions from an alphabet. The tape is divided into cells and each cell carries one symbol from the alphabet. The read-write head moves along the tape according to a given set of instructions and changes symbols on the tape as it moves. The output of the Turing Machine are the contents of the tape when the instructions have been completed.

Alan Turing proposed the Church-Turing thesis in a seminal 1936 paper [2]. This thesis cannot be proven, but is supported by empirical evidence. This thesis essentially claims that what we think of as algorithms can be *completely captured*

by a Turing Machine. Intuitively, an algorithm is simply a set of steps to be carried out for any given input in order to get a desired output. At the same time Turing's thesis advisor Alonzo Church introduced a universal model of computation called the *lambda calculus*. He and Turing then showed that the Turing machine and the lambda calculus were equivalent in their capabilities [3].

Not long after Turing's paper, the first computers constructed from electronic components were developed. John von Neumann developed a simple theoretical model for putting together in a practical fashion all the components required for a computer to be fully capable as a Turing Machine [4]. Although the early computers were slow and bulky by today's standards, after the development of the trasistor by John Bardeen, Walter Brattain, and Will Shockley in 1947 [5,6], computer hardware began a long process of becoming faster and more powerful. Computer power has grown at an amazing pace ever since, so much so that this growth was codifed by Gordon Moore in 1965 in what is now known as *Moore's law*. This "law" states that computer power will double for constant cost every 18 months. Today, a small hand-held cell phone has much more computing power than all but the fastest computers of a few decades ago.

It is clear, however, that we cannot make computing devices arbitrarily small without altering the physical basis of computation. Traditional or so-called classical computers are based on Boolean or classical logic. As computer hardware is made even smaller, quantum effects can become significant. The classical physics that we use in the macroscopic world starts to break down. For example, in quantum physics, a system may not have a definite classical state. For example, one may

not be able to say whether an electron has a spin up, corresponding to a classical 0 (say), or spin down corresponding to a classical 1 (say). That is, an electron spin, which is a simple quantum system, can be in a superposition of both up and down at the same time, and if one measures the spin, the results 0 or 1 are obtained with equal probability.

Not only that, there is a limit to how many transistors can be fabricated within a given planar area. The Intel Core $I7$ processors of today have more than 2.2×10^9 transistors. This type of computation requires energy, and hence, with many components operating at high computing speeds, one has to start considering the dissipation of energy [7]. This can be characterized by Landauer's principle which states that for every bit of information erased, an entropy $S = k_B \ln 2$ is generated, where k_B is Boltzmann's constant [8]. The power density of modern day computers is around 130 W cm^{-2}. For comparison, the power density at the surface of the sun is around 6000 W cm^{-2} [9]. But the temperature at the surface of the sun is around 5778 K. A computer on the other hand, needs to be maintained at room temperature. This suggests that this type of computers cannot be made arbitrarily fast.

One potential solution to these problems may be offered by quantum computation, which as the name suggests, uses quantum logic. Quantum computation is reversible in principle, and seems to offer exponential speedup over classical computers. However, as Richard Feynman pointed out in 1982 [10], typical quantum systems cannot be simulated by classical computers using efficient algorithms. Roughly speaking, an efficient algorithm is one which runs in time polynomial in the "size" of

the input. In contrast, an inefficient algorithm typically requires exponential time. One well-known example from mathematics is the problem of factoring a number into its prime factors. The fastest known classical algorithms require a time for obtaining the factor, that is exponential in the number of bits in the binary representation of the input. In contrast, there are some quantum algorithms that are much faster than their classical counterparts [11] including Grover's search algorithm and Shor's factoring algorithm. Grover's search algorithm [12] can search for an entry in an unsorted database consisting of N elements in $O(\sqrt{N})$ time, while Shor's factoring algorithm [13] can factorize a number N in time poly$(\log N)$. However, despite these successes, it is not clear for what general class of problems quantum algorithms can perform better than their classical counterparts. It should also be kept in mind that many problems can be solved today by classical computers, as efficiently as they could be solved by a quantum computer, if it existed.

1.2 Universal Quantum Computation

In classical computation there are various Boolean operations like AND, NOT, OR, $NAND$ *etc.* However, a two-bit gate such as AND or OR and a single-bit gate such as NOT are sufficient to perform all classical logic operations [14]. We call a set of such gates *universal*. An analogous result holds for universal quantum computation. In order to do universal quantum computation, it is sufficient to be able to perform all single-qubit gates and the controlled-not two-qubit gate [15, 16]. All unitary operations on arbitrarily many qubits can then be constructed from a

polynomial number of these gates.

One approach to universal Quantum Information Processing (QIP) which I will discuss more in the first part of the thesis, involves the use of single photons. An advantage of using single photons to do QIP is that many critical techniques are well developed in quantum optics. Also, photons interact weakly with the surroundings resulting in slow decoherence, which is essential for quantum computing. Optical photons, for instance, can be experimented with at room temperature, unlike, say ion traps, which require low temperatures for best operation [17]. However, one of the major obstacles to using single photons for QIP is that two photons will not interact with each other unless they are in a nonlinear medium. This makes it difficult to implement two-qubit gates using photons. Reliably producing single photons on demand and detecting them also remains a major challenge [18].

A single-qubit gate is a unitary operator U that acts on a single-qubit state $|\Psi\rangle = \alpha |0\rangle_q + \beta |1\rangle_q \in \mathcal{H}$, where α and β are arbitrary complex numbers on the unit circle and $|0\rangle_q$ and $|1\rangle_q$ are logical basis states of the Hilbert space $\mathcal{H}$. In principle, in a photon system any single-qubit gate can be created using linear optical elements such as beam-splitters and phase-shifters. More precisely, any unitary operator U acting on a single qubit can be decomposed into rotations about the Z and Y axes on the Bloch Sphere [1] modulo a phase factor. That is:

$$U = e^{i\alpha} R_z(\beta) R_y(\gamma) R_z(\delta). \tag{1.1}$$

Here the rotation operators are $R_z(\beta) = e^{-i\frac{\beta}{2}\sigma_z}$ and $R_y(\gamma) = e^{-i\frac{\gamma}{2}\sigma_y}$ with σ_y and σ_z being the Pauli matrices. A rotation by angle θ about the X axis can be written

as $R_x(\theta) = R_z(\frac{\pi}{2})R_y(-\theta)R_z(-\frac{\pi}{2})$. Thus one can perform arbritrary rotations about the X, Y, or Z axes, and one can perform any arbitary single-qubit operation.

To understand how to build two-qubit optical gates, I next consider the dual rail basis with $|0\rangle_q \equiv |01\rangle$ and $|1\rangle_q = |10\rangle$, where a single photon can be in one of two modes [1]. Let us analyze the effect of a ϕ phase shift. Consider a qubit state $|\Psi\rangle = \alpha|0\rangle_q + \beta|1\rangle_q$ that transforms to

$$\begin{aligned} & \alpha|01\rangle + \beta e^{i\phi}|10\rangle \\ = \;& e^{i\frac{\phi}{2}}(e^{-i\frac{\phi}{2}}\alpha|01\rangle + e^{i\frac{\phi}{2}}\beta|10\rangle) \\ = \;& e^{i\frac{\phi}{2}}e^{-i\frac{\phi\sigma_z}{2}}(\alpha|0\rangle_q + \beta|1\rangle_q) \\ = \;& e^{i\frac{\phi}{2}}R_Z(\phi)(\alpha|0\rangle_q + \beta|1\rangle_q) \\ = \;& e^{i\frac{\phi}{2}}R_Z(\phi)|\Psi\rangle \end{aligned} \tag{1.2}$$

One can see that upto a global phase, this phase shift is equivalent to a rotation about the Z axis.

In a similar manner one can show that rotations of -2θ about the Y axis can be achieved by using a beam splitter tilted at angle θ. In general, an ideal lossless beam splitter can be represented by a unitary transformation [1]

$$U(\theta,\phi) = \begin{pmatrix} \cos\theta & -e^{i\phi}\sin\theta \\ e^{-i\phi}\sin\theta & \cos\theta \end{pmatrix}. \tag{1.3}$$

The input and output modes are related by $\hat{a}_l^\dagger \rightarrow \sum_m U_{ml}\hat{a}_m^\dagger$ with $l, m \in \{1, 2\}$ representing the two modes of the beam splitter. Using this relation one can show that a beam splitter with $\phi = 0$ will convert an incident state $|\Psi\rangle$ according to

$$|\Psi\rangle = \alpha|0\rangle_q + \beta|1\rangle_q \rightarrow R_Y(-2\theta)(\alpha|0\rangle_q + \beta|1\rangle_q) = R_Y(-2\theta)\,|\Psi\rangle\,. \tag{1.4}$$

Since an arbitrary single-qubit rotation can be decomposed into rotations about the Y and Z axes, this implies that all single-qubit operations can be achieved by linear optics alone.

A two-qubit gate is a unitary operation which acts on a state $|\Psi\rangle$ of two qubits. An example of a two-qubit gate is a controlled-not (CNOT) gate [1]. A CNOT gate performs the following operation on the basis states $\{|00\rangle, |01\rangle, |10\rangle, |11\rangle\}$ of two qubits:

$$|00\rangle \rightarrow |00\rangle,\ |01\rangle \rightarrow |01\rangle,\ |10\rangle \rightarrow |11\rangle,\ |11\rangle \rightarrow |10\rangle. \tag{1.5}$$

Another example of a two-qubit gate is the controlled-phase (CP) gate [1] which implements a controlled π phase shift.

$$|00\rangle \rightarrow |00\rangle,\ |01\rangle \rightarrow |01\rangle,\ |10\rangle \rightarrow |10\rangle,\ |11\rangle \rightarrow e^{i\pi}|11\rangle. \tag{1.6}$$

As noted earlier, it is not possible to perform these gates using linear optics alone. Nevertheless, one of the first proposals for quantum computation in this modality was the quantum optical Fredkin gate [19]. The gate used single-photon optics and the Kerr effect, which occurs in media with an intensity dependent refractive index [20]. A Fredkin gate is a three-qubit gate which can be used to do controlled-swap operations. The first qubit is the control qubit and the second and third are target qubits respectively.

The Hamiltonian for the Kerr effect is [21]

$$H_I \ = \ -\hbar\chi\hat{a}_1^\dagger\hat{a}_1\hat{a}_2^\dagger\hat{a}_2, \tag{1.7}$$

where χ is a coupling constant that depends on the third-order nonlinear suscepti-

bility of the material. Here, $\hat{a}_1$ and $\hat{a}_2$ are the annihilation operators corresponding to two input modes of light entering a Mach-Zender interferometer. By using a Mach-Zender interferometer with a nonlinear medium in either arm, one can implement the Fredkin gate. However, in practice there are two major problems with this approach. The nonlinearities at the single-photon level in optical systems are too small to create a large phase (π), and crystals with high nonlinearities exhibit appreciable absorption.

Although there has been tremendous progress on both theoretical and experimental fronts, the subject of quantum information processing remains an active area of research. Besides photons, many other physical sytems have been considered for the physical realization of quantum computers including ions in a trap [22], quantum dots [23], nitrogen vacancy (NV) centers in diamond [24], and superconducting devices [25]. Each system has its own advantages and drawbacks. David DiVincenzo suggested that a sucessful physical implementation of a quantum computer must satisfy certain criteria. The ones that are important for superconducting qubits can be summarized as [26]:

1. A scalable physical system with well characterized qubits.

2. The ability to initialize the state of the qubits to a simple fiducial state like $|000\ldots\rangle$.

3. Decoherence times which are much longer than the gate operation times.

4. A *universal* set of quantum gates.

5. A qubit-specific measurement capability.

1.3 Introduction to Quantum Simulation

I have already remarked that quantum systems cannot by efficiently simulated by classical computers. It can even be a difficult problem to study quantum systems with a few tens of particles. Because a system of N spin-half particles has a Hilbert space of dimension 2^N, for $N = 40$, a 4 TB classical memory register is needed to store the elements of the Hamiltonian matrix. For $N = 300$, the dimension of the Hilbert space is more than the number of particles in the entire observable universe! This exponential explosion is unavoidable unless approximation methods are used, or the system contains symmetries that can be exploited. However, good approximations are not always available and are not always reliable.

Feynman proposed a possible way around this problem by using the features of quantum mechanics. I quote Feynman [10]: "Let the computer itself be built of quantum mechanical elements which obey quantum mechanical laws." Quantum systems have the capacity to contain an exponentially large amount of information without using an exponentially large amount of physical resources, thus making it a natural tool to perform quantum simulation. The storage capacity of N qubits, for example, is exponentially larger than that of N classical bits. As was shown by Seth Lloyd more than a decade after Feynman's proposal, a quantum computer can indeed act as a universal quantum simulator [27].

To simulate a given quantum system with a Hamiltonian H_{sys}, one can con-

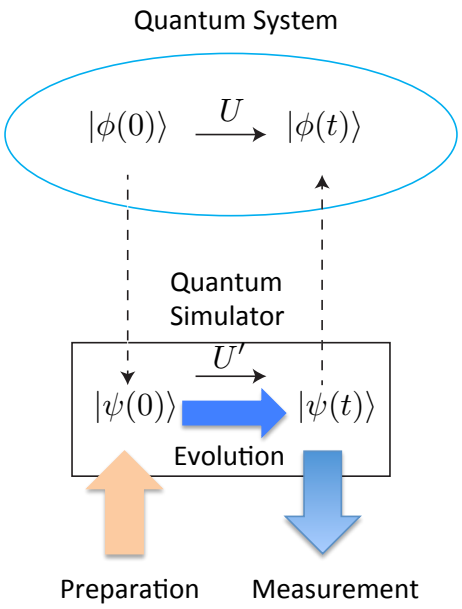

Figure 1.1: Schematic representation of a quantum system and a corresponding quantum simulator.

struct another quantum system which can be accurately initialized and controlled with a Hamiltonian H_{sim} [28]. The initial quantum state $|\phi(0)\rangle$ evolves to $|\phi(t)\rangle$ via the unitary transformation $U = e^{-iH_{sys}t}$. The quantum simulator evolves from the prepared state $|\psi(0)\rangle$ to $|\psi(t)\rangle$ via $U = e^{-iH_{sym}t}$. The simulator is designed such that there is a mapping between the simulator and the simulated system, in particular, the mappings $|\phi(0)\rangle \leftrightarrow |\psi(0)\rangle$, $|\phi(t)\rangle \leftrightarrow |\psi(t)\rangle$, and $U \leftrightarrow U'$, and is assumed to be controllable, as depicted by the colored arrows in Figure 1.1. The controllabilty of the quantum simulator is very important. The information about the quantum system can only be extracted through measurements of the quantum simulator. Although the basic idea underlying a quantum simulator is very simple, implementation of a universal quantum simulator remains highly non-trivial.

Outlook and Overview of Thesis

The importance of making advancements in the field of quantum science to harness its many potentials cannot be overstated. In this thesis, I will explore some problems in quantum computation and quantum simulation, dealing mainly with hybrid quantum systems. Hybrid systems, as the name suggests, are systems which are constructed from a combination of subsystems, sometimes with widely different properties [29]. Hybrid systems take advantage of the desirable features of each subsystem. For example, microwave photons in a cavity or in a transmission line coupled to superconducting qubits comprise a hybrid quantum system [30], and so do trapped-ions coupled to superconducting qubits. Similarly, nanomechanical resonators magnetically coupled to electron spins also form a hybrid system [31].

In the following chapter, I review the basic physics of superconducting circuits and circuit quantization. In the third chapter, I will show how strong two-photon nonlinearities have been attained by coupling photons in the microwave domain to superconducting circuits. These nonlinearites will then be used to create two-photon CP gates in the dual-rail basis. In the fourth chapter I construct a parent Hamiltonian with excitations that exhibit many interesting properties, and in the fifth chapter I propose an architecture to emulate a chemical potential for light. In the sixth chapter, I investigate the potential of coupling trapped-ions to superconducting circuits. Finally, in the seventh chapter I briefly conclude by summarizing my main findings. The eighth chapter includes the appendices.

Chapter 2

Superconducting Circuits and Quantized Hamiltonians

2.1 Introduction

Superconductivity was discovered in 1911 by H. Kamerlingh Onnes [32, 33] only three years after he liquefied helium which gave him the refrigeration technique required for cooling to a few degrees Kelvin. He observed that, when cooled, the electrical resistance of metals such as mercury, lead, and tin vanished completely in a small temperature range at some critical temperature T_c, which is characteristic of the material. Once a current was set up in a superconducting ring for instance, the currents were observed to flow without measurable decrease for an entire year.

However, for decades, a fundamental understanding of this phenomenon was absent, until Ginzburg and Landau introduced a phenomenological theory now known as the Ginzburg-Landau (GL) theory of superconductivity [34] in 1950. This theory concentrated entirely on the superconducting electrons rather than the

quasi-particle excitations in the system. In particular, they proposed a complex pseudowave-function ψ as an order parameter within Landau's general theory of second-order phase transitions, with the local density of superconducting electrons n_s given by $n_s = |\psi(x)|^2$.

A microscopic theory of superconductivity came seven years later in 1957 when Bardeen, Cooper and Schrieffer proposed what is now known as the BCS theory [35]. Their basic idea was that the interaction between electrons resulting from virtual exchange of phonons is attractive when the energy difference between the electron states involved is less than the phonon energy. This leads to the formation of bound states of electrons called Cooper pairs when the thermal energy $k_B T$ is less than an energy scale 2Δ, which is typically on the order of 10^{-3} eV for conventional low-T_c superconductors. The Cooper pairs are responsible for conductivity without dissipation.

2.2 Isolated Josephson Junction

In 1962, Josephson made the remarkable prediction [36] that a zero-voltage supercurrent can flow between two superconducting electrodes (S) separated by a thin insulating (I) barrier. This type of structure is now called a Josephson junction. If the insulating layer is thin enough, Cooper pairs have a small but nonvanishing probability ($p \sim 10^{-5}$ – 10^{-3}) of penetrating from one electrode to another via quantum tunneling through the energy barrier created by the insulator [37]. The Cooper pairs in the superconducting electrodes have no net spin, and a

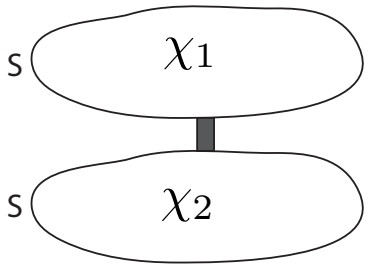

Figure 2.1: An SIS junction with phases χ_1 and χ_2 on the two electrodes.

pair, therefore, obeys Bose-Einstein statistics.

For typical insulators in use currently, when the thickness d of the insulating layer is roughly ($d \sim 10^{-9}$m), the net current I flowing through the contact —the *Josephson junction* —contains a significant supercurrent I_S [37]. The supercurrent is a direct function of the phase difference

$$\phi = \chi_1 - \chi_2, \tag{2.1}$$

where χ_1 and χ_2 are the phases of the condenstate wavefunctions inside the two superconducting electrodes. This function is 2π-periodic, and in the simplest case, is sinusoidal [37]. That is

$$I \equiv I_S = I_c \sin\phi. \tag{2.2}$$

Here, the critical current I_c is a constant that is determined by the shape and structure of the Josephson junction. It is the maximum current that can flow in the superconducting state. When a voltage V is applied across the junction, the phase ϕ evolves according to the ac Josephson relation [37]

$$\frac{d\phi}{dt} = \frac{2eV}{\hbar}. \tag{2.3}$$

One can define an effective inductance of a junction L_J from the relation

$$V = L_J \frac{dI}{dt}. \tag{2.4}$$

From (2.2) the rate of change of current is

$$\frac{dI}{dt} = (I_c \cos\phi)\dot{\phi} = I_c \cos\phi \frac{2eV}{\hbar}. \tag{2.5}$$

Combining (2.4) and (2.5) one gets

$$L_J = \frac{\hbar}{2eI_c \cos\phi} = \frac{\Phi_0}{2\pi I_c \cos\phi}, \tag{2.6}$$

where $\Phi_0 = h/(2e)$ is the superconducting flux quantum. One can see that L_J becomes arbitrarily large as $\phi \to \pi/2$. The corresponding energy U_J stored in the junction by virtue of its nonlinear inductance can be found as follows:

$$\begin{aligned} U_J &= \int_{t_0}^{t} I(t)V(t)dt \\ &= \int_{t_0}^{t} I_c \sin\phi(t)V(t)dt \\ &= \int_{\phi_0}^{\phi} I_c \sin\phi \frac{\hbar}{2e} d\phi \\ &= \frac{\hbar I_c}{2e}(\cos\phi_0 - \cos\phi) \\ &= -\frac{\Phi_0 I_c}{2\pi}(\cos\phi - \cos\phi_0). \end{aligned} \tag{2.7}$$

From this result, I can define the Josephson energy E_J by

$$E_J = \frac{\Phi_0 I_c}{2\pi}. \tag{2.8}$$

Ignoring the constant term in (2.7), one gets $U_J = -E_J \cos\phi$.

A real Josephson junction will have a capacitance C_J between its electrodes and an associated charging energy defined as $E_C = (2e)^2/(2C_J)$. This is the energy required for a Cooper-pair to tunnel through the junction.

2.3 Quantum Description of an Isolated Junction

When the quantum fluctuation of the junction is large compared to thermal fluctuations, which occurs when $k_B T \leq \hbar\omega$, with ω the characteristic frequency of the junction, and T the temperature, a quantum description is required. One characteristic frequency of the junction is the plasma frequency ω_p given by

$$\omega_p = \sqrt{\frac{2eI_c}{\hbar C_J}} = \frac{\sqrt{2E_C E_J}}{\hbar}. \tag{2.9}$$

The basic principles of quantum mechanics state that variables like ϕ, V, and I that describe the junction classically, cannot simultaneously be known quantum mechanically. Therefore, in the quantum regime, one needs to introduce non-commuting conjugate pairs. One pair is given by $\hat{N} = \hat{Q}/(2e)$ and $\hat{\phi}$, with the commutation relation $[\hat{\phi}, \hat{N}] = i$. Here, $\hat{N}$ describes the number of Cooper pairs tunneling through the junction and $\hat{\phi}$ is the phase of the junction. The commutation relation implies that $\Delta\hat{\phi}\Delta\hat{N} \geq 1/2$. The Hamiltonian of the junction can then be written as

$$H = \frac{\hat{Q}^2}{2C_J} - E_J \cos\hat{\phi} = E_C\hat{N}^2 - E_J\cos\hat{\phi}. \tag{2.10}$$

Note that sometimes the charging energy is defined as $E_C = e^2/(2C_J)$ so that the kinetic term becomes $4E_C\hat{N}^2$. In the coordinate or phase representation $\hat{\phi} = \phi$ and $\hat{N} = -i\partial/\partial\phi$. This leads to

$$H = -E_C\frac{\partial^2}{\partial\phi^2} - E_J\cos\phi. \tag{2.11}$$

In the limit $\hbar\omega_p \ll E_J$, the energy levels of the system are localized at the bottom of the cosine well. The minima of the potential occur at $\phi_n = 2n\pi$ where

$n \in \mathbb{Z}$. One can explore quantum fluctuations $\tilde{\phi} = \phi - \phi_n$ around this minima so that

$$U = -E_J \left(1 - \frac{\tilde{\phi}^2}{2}\right). \tag{2.12}$$

The Hamiltonian is reduced to that of a harmonic oscillator with frequency ω_p. Thus, the lowest energy levels of the junction become approximately linear and are given by

$$E_n = \left(n + \frac{1}{2}\right) \hbar\omega_p. \tag{2.13}$$

2.4 Josephson Junctions Connected to External Circuits

So far I have only discussed an isolated junction. However, one can realize many different architectures by connecting Josephson junctions to external circuits. These externally shunted junctions can have very different properties, but they all have one property in common. That is, these systems can exhibit large nonlinearities depending on the choice of parameters. The nonlinearities in the junctions enable one to approximate some circuits as a qubit or two-level system, while others can be treated as a harmonic oscillator with a moderate or large anharmonicity. The various regimes in which a shunted junction operate are outlined in Table 2.1. The ratio E_J/E_L is approximately equal to the number of minima in the potential landscape, while the ratio E_J/E_C is roughly equal to the number of energy levels per well around each minima. This is outlined in a "Mendeleev" table of superconducting circuits in Figure 2.2 [25].

Regime	Energy Relationships
Phase	$E_C \ll E_L < E_J$
Fluxonium	$E_L < E_C < E_J$
Flux	$E_C < E_L < E_J$
Hybrid	$E_C < E_L \sim E_J$
Transmon	$E_C \ll E_J$
Charge	$E_J \ll E_C$

Table 2.1: The various regimes in which a shunted Josephson junction can operate.

2.4 Charge Qubit

The first such architecture, a Cooper pair box, is an example of a charge qubit (Figure 2.3). A Josephson junction with Josephson energy E_J and a capacitance C_J is connected to a gate voltage V_g through a gate capacitance C_g. The Cooper pair box (CPB) is made of an electrode of the Josephson junction and an electrode of the gate capacitor and the superconducting lead connecting them.

The Lagrangian L of the system is

$$L = \frac{1}{2}C_J V_J^2 + \frac{1}{2}C_g(V_g - V_J)^2 + E_J \cos\phi. \tag{2.14}$$

Recall the relation

$$V_J = -\frac{\hbar}{2e}\dot{\phi}. \tag{2.15}$$

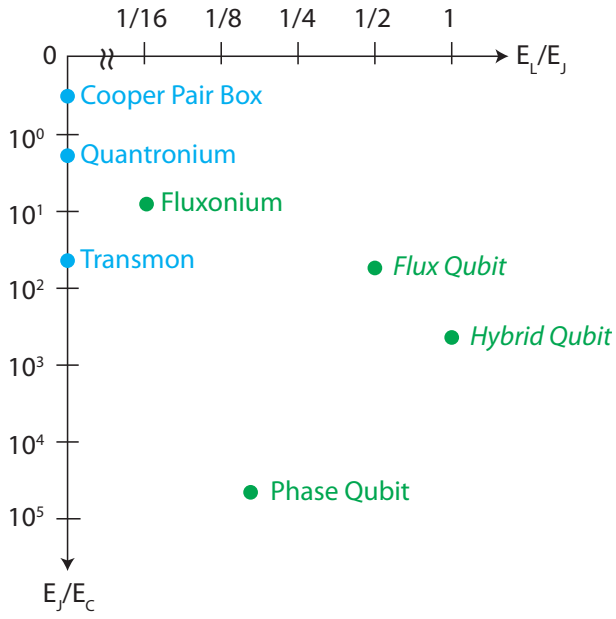

Figure 2.2: A "Mendeleev table" of superconducting circuits. I will consider flux and hybrid circuits (italicized).

The kinetic energy is

$$\begin{aligned} T &= \frac{1}{2}\left(\frac{\hbar}{2e}\right)^2 C_J\dot{\phi}^2 + \frac{1}{2}C_g\left(V_g + \frac{\hbar}{2e}\dot{\phi}\right)^2 \\ &= \frac{1}{2}(C_J + C_g)\left(\frac{\hbar}{2e}\right)^2\dot{\phi}^2 + \frac{\hbar}{2e}C_g V_g\dot{\phi}, \end{aligned} \tag{2.16}$$

where the constant term $C_g V_g^2/2$ has been dropped. The conjugate momentum is

$$\pi = \frac{\partial L}{\partial\dot{\phi}} = \left(\frac{\hbar}{2e}\right)^2 (C_J + C_g)\dot{\phi} + \frac{\hbar}{2e}C_g V_g. \tag{2.17}$$

The Hamiltonian is

$$\begin{aligned} H &= \pi\dot{\phi} - L \\ &= \frac{1}{2}\frac{(2e)^2}{C_J + C_g}(N - N_g)^2 - E_J\cos\phi, \end{aligned} \tag{2.18}$$

where $N_g = C_g V_g/(2e)$, and $Q = -2eN$ is the number of Cooper pairs on the island.

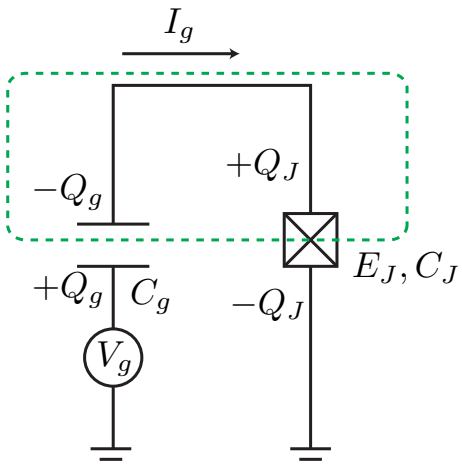

Figure 2.3: Schematic of a Cooper pair box. The parts inside the dashed box comprises the Cooper pair island whose excess charge corresponds to the qubit degree of freedom. I_g is the current flowing through the circuit.

Let $E_C = (2e)^2/(C_g + C_J)$. Then the quantum Hamiltonian is

$$H = \frac{1}{2}E_C(\hat{N} - N_g)^2 - E_J \cos\hat{\phi}. \tag{2.19}$$

The charge qubit operates in the regime where $E_C \gg E_J$. This means physically that the tunneling between states with different N is suppressed and N is therefore a good quantum number. This assumption breaks down when $N \sim N_g$ where the tunneling energy dominates over the Coulomb energy.

From the commutation relation $[\hat{\phi}, \hat{N}] = i$, one gets $\phi = i\partial/\partial N$, and $e^{\pm i\hat{\phi}} |N\rangle = |N \mp 1\rangle$. Therefore, the Hamiltonian in the $\{|N\rangle\}$ basis can be written as

$$H = \sum_{N\in\mathbb{Z}} \frac{E_C}{2}(N - N_g)^2 |N\rangle \langle N| - \frac{E_J}{2}(|N\rangle \langle N+1| + |N+1\rangle \langle N|). \tag{2.20}$$

N_g is a controllable parameter. If N_g is set in the vicinity of $(N + 1/2)$ with $N \in \mathbb{N}$, then states $|N\rangle$ and $|N+1\rangle$ have almost degenerate energies. All other states have

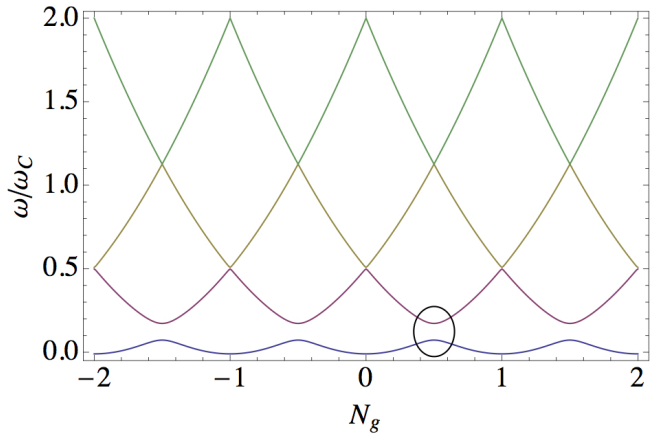

Figure 2.4: Energy levels of a Cooper pair box for $\omega_C/\omega_J = 10$. The ellipse denotes the region where the ground and the first excited state are nearly degenerate, at $N_g = 1/2$. These states form a qubit.

higher energies and can be ignored. Then

$$\begin{aligned} H &= \frac{E_C}{2}\left[N_g^2 \left|N\right\rangle \left\langle N\right| + (1-N_g)^2 \left|N+1\right\rangle \left\langle N+1\right|\right] \\ &\quad -\frac{E_J}{2}\left[\left|N\right\rangle \left\langle N+1\right| + \left|N+1\right\rangle \left\langle N\right|\right] \\ &= -\frac{1}{2}B_z\sigma_z - \frac{1}{2}B_x\sigma_x, \end{aligned} \tag{2.21}$$

where $B_z = E_C/2(1-2N_g)$, $B_x = E_J$, and I have ignored the constant terms. σ_x and σ_z are the familiar Pauli matrices. Note that because of the discrete nature of N, ϕ is compact and the wavefunction $\psi(\phi)$ is the same as $\psi(\phi + 2n\pi)$ for $n \in \mathbb{Z}$.

2.4 Flux Qubit

The simplest flux qubit is an rf-SQUID. It consists of a Josephson junction connected by a superconducting loop with inductance L as depicted in Figure 2.5.

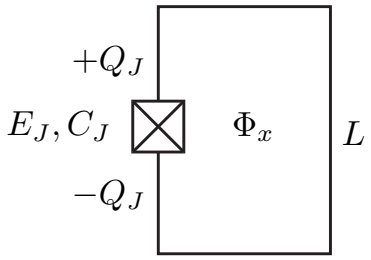

Figure 2.5: A flux qubit with flux Φ_x threading the inductive loop.

The Hamiltonian of a flux qubit in the ϕ representation is

$$H = -E_C \frac{\partial^2}{\partial \phi^2} - E_J \cos\phi + \frac{1}{2} E_L (\phi + \phi_x)^2, \tag{2.22}$$

with $E_C = (2e)^2/(2C_J)$.

In contrast to the Cooper pair box, ϕ is now non-compact and is defined on all of $\mathbb{R}$. This is because $N = q/(2e)$ is no longer discrete as the presence of the inductive loop allows continuous charge to move from one side of the junction to the other. In the limit where $E_J > E_C > E_L$, the device is called a fluxonium. Similarly, if $E_J < E_L$ and there is only one minimum in the potential, it is called a hybrid superconducting circuit. Figure 2.6 shows the energy levels of inductively shunted junction for various energy regimes. If $E_L \gg E_J$, the potential can be well approximated around the minima by a harmonic well. Then the circuit can be regarded as a harmonic oscillator with a nonlinear perturbation.

In experiments the noise characteristics of superconducting circuits have to be taken into account. Qubits are characterized by two times denoted T_1 and T_2. The *relaxation time* T_1 is the time required for the qubit to relax from the first excited state to the ground state. This process involves energy loss. The dephasing

time T_2 is the time over which the phase difference between two eigenstates become randomized. Both relaxation and dephasing can be theoretically described using a model where the system is weakly coupled to the quantum noise produced by the environment [38,39]. This approach predicts that energy relaxation from the excited to the ground state occurs due to the spectral density of the noise at the frequency difference of the two states. The dephasing rate, by contrast, has two contributions so that

$$\frac{1}{T_2} = \frac{1}{2T_1} + \frac{1}{T_\phi}. \tag{2.23}$$

The first contribution arises from relaxation processes whereas the second contribution, also called *pure dephasing* arises from other energy-conserving processes. One can distinguish the dephasing time T_2, which is an intrinsic timescale for decoherence of a single qubit, from another timescale T_2^*, which is the result of measurements on an ensemble of such qubits [40]. It is the case that $T_2^* < T_2$.

At the present time, Cooper pair boxes discussed above suffers from excessive charge noise. By decreasing the ratio of E_C to E_J one can form a so called transmon which is much less sensitive to charge noise [41]. Similarly, flux noise has an adverse effect on flux qubits [42, 43]. However, over the past decade, clever engineering as well as the understanding of sources of noise [44,45] has led to improvement in qubit lifetimes by almost six orders of magnitude [25, 46].

2.5 Circuit-QED

Circuit Quantum Electrodynamics (circuit-QED) [47] borrows techniques from the field of atomic cavity Quantum Electrodynamics (QED), which investigates the interaction of matter with light at the quantum scale [48]. When confined to a cavity, the radiative properties of an atom differ fundamentally from the atom's radiative properties in free space [49]. Spontaneous emission is inhibited if the cavity has characteristic dimensions which are small compared to the radiation wavelength, and enhanced if the cavity is resonant. Surprisingly, superconducting circuits which are macroscopic entities containing billions of atoms can behave very much like a single atom, albeit with more tunable properties. They can be used to reach the so called strong coupling regime where the coupling between the excitations in the circuit and light in the cavity exceed the corresponding decay rates, leading to a coherent periodic exchange of a single photon on resonance [30].

In the preceding sections, I wrote down the quantum or circuit-QED Hamiltonian for various shunted Josephson junctions. In this section, I provide a prescription for deriving such Hamiltonians. The reader can refer to [50] for an introductory treatment of circuit quantization. For a more advanced treatment, especially of circuits involving mutual inductances, the reader is advised to consult [51].

To derive a quantum Hamiltonian for a circuit, I first derive the classical Hamiltonian in the lumped element limit. This limit is appropriate when the circuit components are much smaller than the electromagnetic wavelengths in the frequencies of interest. I will assume that each circuit component has two terminals,

although it can have more. Every two terminal component b has a voltage $v_b(t)$ across it and a current $i_b(t)$ through it. In the classical case, these two variables are used to describe a circuit. However, for the purpose of circuit quantization, one can define the flux and charge variables,

$$\Phi_b(t) = \int_{-\infty}^{t} v_b(t')\ dt', \tag{2.24}$$

$$q_b(t) = \int_{-\infty}^{t} i_b(t')\ dt'. \tag{2.25}$$

One can assume that at $t = -\infty$ all voltages and currents are zero, and that any static bias fields such as magnetic fluxes imposed on the inductors are assumed to be switched on adiabatically from $t = -\infty$ to $t = 0$.

One can work with two types of components. The first is of the capacitive type which satisfies a general (possibly nonlinear) relation

$$v_b = f(q_b). \tag{2.26}$$

The second is of the inductive type which satisfies

$$i_b = g(\Phi_b). \tag{2.27}$$

A Josephson junction, for example, would satisfy a nonlinear equation of the inductive type.

Every circuit can be regarded as a graph with the terminals being represented by the nodes of the graph and the elements connected across the terminals by the edges. A *spanning tree* of a graph is a union of edges of the graph that contains all the nodes but does not contain any loops. The branches of the spanning tree are called *tree branches*. All other branches are called *chords*. Each chord is associated

with a unique loop that is formed when it is added to a tree. With these basic ideas, one can follow a series of steps that leads to a classical Hamiltonian of a circuit. The steps are as follows:

1. Represent the circuit as a network or graph of two-terminal capacitors and inductors.

2. It is helpful to simplify the circuit using the standard rules of series and parallel components.

3. Choose the *ground node* of the circuit. The remaining nodes of the graph are called *active nodes*.

4. Choose a spanning tree T of the graph that contains all the capacitors and as few inductors as possible.

5. Introduce a node flux for each active node n as the time integral of the voltage along a path on T from the node to the ground. That is,

$$\phi_n(t) = \sum_b S_{nb}\Phi_b = \sum_b S_{nb} \int_{-\infty}^{t} v_b(t')\ dt'. \tag{2.28}$$

   S_{nb} is 0 if the path on T from the ground to n does not pass through b. Otherwise it is ± 1 depending on the orientation of the path.

6. Write the kinetic T and potential energy V of the components in terms of the node fluxes, and their time derivatives. For a branch b connecting two nodes n and n', the branch voltage v_b is the time derivative of the branch flux Φ_b, *i.e.* $v_b = \dot{\Phi}_b$. The branch flux is $\Phi_b = \phi_n - \phi'_n + \tilde{\Phi}_{l(b)}$, with $\tilde{\Phi}_{l(b)} = 0$ for $b \in T$.

Otherwise, $\tilde{\Phi}_{l(b)}$ is the externally-applied magnetic flux through the loop $l(b)$ that is produced by adding b to T, i.e. the unique loop associated with the chord b.

7. Form the Lagrangian

$$L = T(\phi_1, \dot{\phi}_1, \ldots, \phi_N, \dot{\phi}_N) = T - V. \tag{2.29}$$

8. Define the canonical momenta

$$q_n = \frac{\partial L}{\partial \dot{\phi}_n}. \tag{2.30}$$

9. Perform the Legendre transformation to get the Hamiltonian

$$H(\phi_1, q_1, \ldots, \phi_n, q_n) = \sum_{i=1}^{N} q_i \dot{\phi}_i - L. \tag{2.31}$$

10. To quantize the circuit, promote the canonical variables to operators that satisfy

$$[\hat{\phi}_i, \hat{q}_j] = i\hbar\delta_{ij}. \tag{2.32}$$

For an introductory example, I consider a simple LC circuit driven by a possibly time-dependent external flux $\Phi_x(t)$ as depicted in Figure 2.7. The ground node (black dot) has flux ϕ_g and the only active node (red dot) has flux ϕ. I denote the flux of the branch comprising the inductor by Φ_L, and for the branch comprising the capacitor by Φ_C. The tree (in green) is chosen so that it includes the inductor. One can let $\phi_g = 0$ since the ground flux is arbitrary. According to the sixth rule

$$\Phi_L = \phi, \tag{2.33}$$

$$\Phi_C = \phi + \Phi_x(t). \tag{2.34}$$

The kinetic and potential energies T and V are

$$T = \frac{1}{2}C\dot{\Phi}_C^2 = \frac{1}{2}C(\dot{\phi} + \dot{\Phi}_x(t))^2, \tag{2.35}$$

$$V = \frac{\phi^2}{2L}. \tag{2.36}$$

From this, one can construct the classical Lagrangian

$$\mathcal{L} = T - V = \frac{1}{2}C(\dot{\phi} + \dot{\Phi}_x(t))^2 - \frac{\phi^2}{2L}. \tag{2.37}$$

The canonical momentum is

$$q = \frac{\partial \mathcal{L}}{\partial \dot{\phi}} = C(\dot{\phi} + \dot{\Phi}_x(t)) \implies \dot{\phi} = \frac{q}{C} - \dot{\Phi}_x(t). \tag{2.38}$$

The classical Hamiltonian is then obtained by a Legendre transformation giving

$$\mathcal{H} = q\dot{\phi} - \mathcal{L} = \frac{q^2}{2C} + \frac{\phi^2}{2L} - q\dot{\Phi}_x(t). \tag{2.39}$$

The Hamiltonian can be quantized by promoting $q \to \hat{q}$ and $\phi \to \hat{\phi}$ with $[\hat{\phi}, \hat{q}] = i\hbar$.

2.6 Conclusions and Outlook

Superconducting circuits with Josephson junctions possess an intrinsic nonlinearity which enables the creation of qubits or anharmonic oscillators. In this chapter I showed that they can have widely varying properties. The rapidly improving lifetimes of superconducting circuits has advanced their potential use for large scale quantum information processing. In this chapter, I also showed a general prescription for obtaining quantum Hamiltonians with linear elements. This will pave the way for the derivation of quantum Hamiltonians of nonlinear circuits.

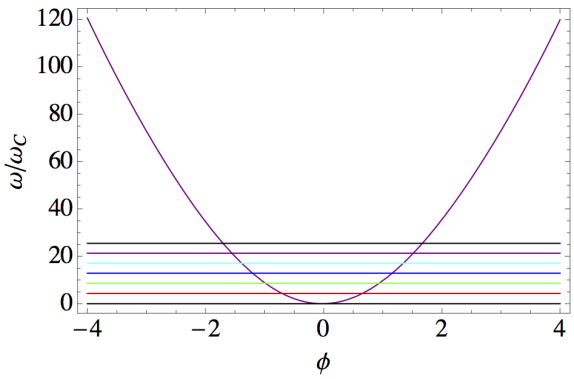

(a)

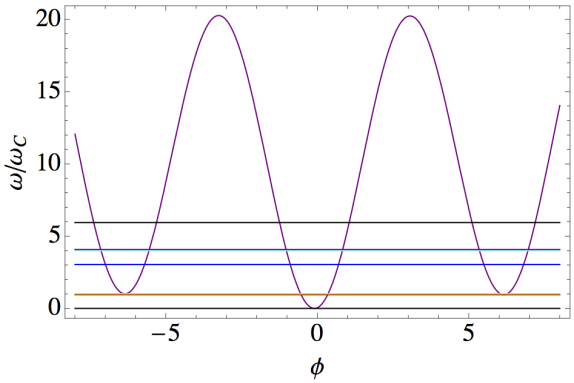

(b)

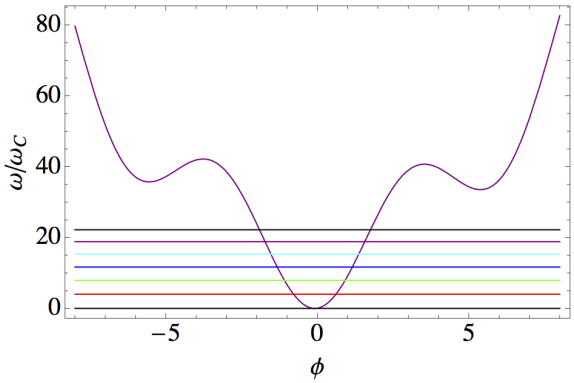

(c)

Figure 2.6: The first few energy levels for $\phi_x = 0.1$ of (a) a hybrid circuit with $\omega_J/\omega_C = 5$, $\omega_L/\omega_C = 10$, (b) fluxonium with $\omega_J/\omega_C = 10$, $\omega_L/\omega_C = 0.05$, and (c) flux qubit with $\omega_J/\omega_C = 15$, $\omega_L/\omega_C = 2$.

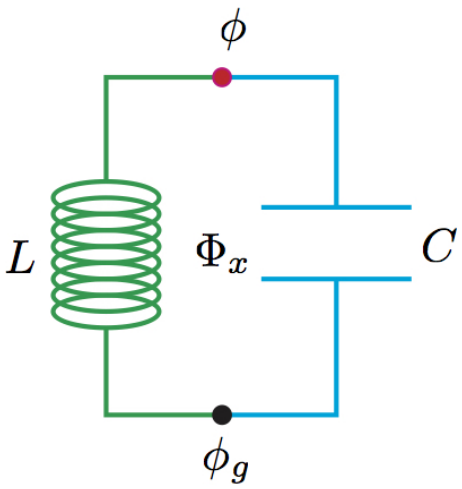

Figure 2.7: An LC circuit

An LC circuit with only one active node (red dot). The spanning tree is in green.

Chapter 3

Nonlinear Optics Quantum Computing with Circuit-QED

3.1 Motivation

In Chapter 1, I introduced universal quantum computation with photons. Specfically, linear optics quantum computing (LOQC) has proven to be one of the conceptually simplest approaches to building novel quantum states and proving the possibility of quantum information processing. This approach relies on the robustness of linear optical elements, but implicitly requires an optical nonlinearity [52–55] as linear optics alone is insufficient to implement universal quantum gates. Unfortunately, progress towards larger scale systems remains challenging due to the limits to optical nonlinearities, as well as the measurement of single photons [18, 56].

In this chapter I explore how recent advances in circuit-QED in which optical and atomic-like systems in the microwave domain are explored for their novel quantum properties [57], provides a new paradigm for quantum computing with

photons [30,58,59], which, in contrast to LOQC, is deterministic. Specifically, using superconducting nonlinearities in the form of Josephson junctions and the related quantum devices such as flux and phase qubits [60,61], key elements of my approach have been realized: the creation of microwave photon Fock states [59, 62–64], controllable beam splitters [59, 65], and single microwave photon detection [66, 67]. In many cases, the photons stored in a transmission line-based resonator or inductor-capacitor resonator have much better coherence times than the attached superconducting qubits [68–70]. This suggests that the main impediment to photon based quantum computing is the realization of appropriate photon nonlinearities to enable two-qubit gates like two-photon phase gates, which are sufficient for universal quantum computation [15, 52].

The key element of a two-photon phase gate is a two-photon nonlinear phase shifter. It imparts a π phase on any state consisting of two photons, while leaving single photon and vacuum states unaffected. A deterministic approach to achieve such photon nonlinearity is based on the Kerr effect [68, 71–73]. In the context of circuit-QED, in Ref. [73], a four level N scheme using a coplanar waveguide resonator and a Cooper pair box is used to arrange for EIT [74] to generate large Kerr nonlinearities. In this chapter I demonstrate a different approach to photon nonlinearity. I explore the possibility of using a dc-SQUID [75] to implement a nonlinear coupling between qubit and resonator, which, through an adiabatic scheme, enables a high fidelity, deterministic two-photon nonlinear phase shift in the microwave domain. Along with the nonlinearity, I envision using dynamically controlled cavity coupling to implement a 50/50 beam splitter operation to construct a two-photon

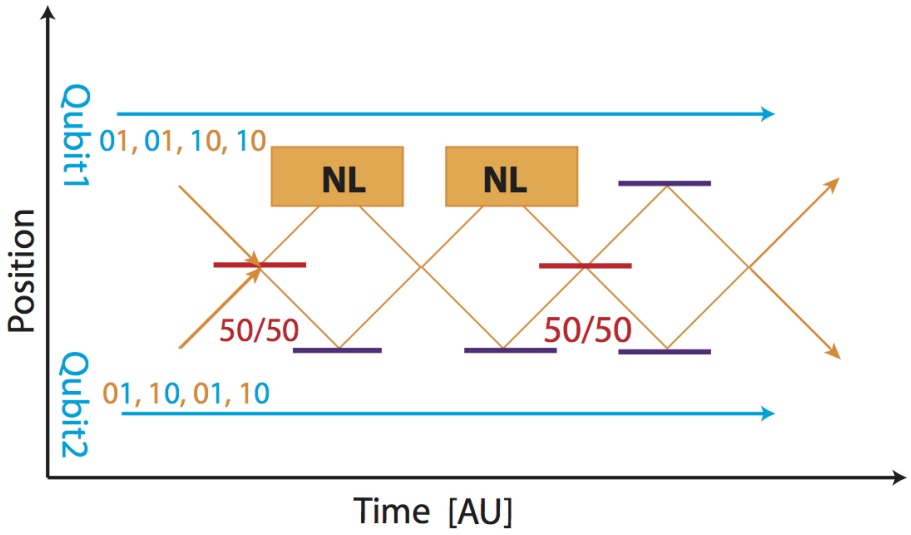

Figure 3.1: Use of two nonlinear phase shifters (NL), combined with 50/50 beam splitters, leads to a deterministic two photon phase gate using dual rail logic. The two photons in the dual rail basis $|0\rangle_L |1\rangle_L = |01\rangle_1 |10\rangle_2$ of the two qubits become bunched into a single mode after passing through the first beam splitter, and then receive a π phase from one of the two phase shifters. Storage cavities are represented by blue lines.

phase gate using so-called dual rail photon qubits [1, 59], in which the logical basis $\{|0\rangle_L = |01\rangle, |1\rangle_L = |10\rangle\}$ corresponds to the existence of a single photon in one of two resonator modes (Figure 3.1). My approach takes best advantage of the relatively long coherence times for microwave photons in resonators, and couples only virtually to superconducting quantum bit devices, minimizing noise and loss due to errors in such devices. When combined with the aforementioned techniques for Fock state generation and detection, along with dynamically controlled beam splitters, this provides the final element for nonlinear optics quantum computing in

the microwave domain.

3.2 Outline of Approach

I now outline the approach. I consider photons stored in a high-impedance microwave resonator [76] coupled inductively with strength $0 < \chi < 1$ to a flux superconducting qubit (SQ) in a dc-SQUID configuration (Figure 3.2). The resonator loops around the dc-SQUID which results in a nonlinear cosine dependent interaction between the resonator and qubit. In this configuration, I get an effective coupling of the form $V \sim E_J \cos(\hat{\phi} + \phi'_x) \cos \hat{\phi}_L$, where an external flux $\phi'_x \equiv 2\pi\chi\Phi'_x/\Phi_0$ is applied to the resonator which consequently threads the smaller loop of the dc-SQUID, Φ_0 being the superconducting flux quantum. The qubit phase variable and the resonator flux are denoted by $\hat{\phi}$ and $\hat{\phi}_L = 2\pi\hat{\Phi}_L/\Phi_0$ respectively. For $\phi'_x \sim \pi/2$, one immediately sees a nonlinear coupling between the qubit and resonator: $V \sim E_J\hat{\phi}\hat{\phi}_L^2$, where two resonator photons can be annihilated to produce one qubit excitation, analogous to parametric up conversion in $\chi^{(2)}$ systems. This causes the two-photon state of the resonator to couple to the first excited state of the SQ with strength g_2 (Figure 3.3(a)). In essence, in this region, the two-photon state with detuning δ from the qubit, becomes slightly qubit-like and acquires some nonlinearity. However, the single-photon state, inspite of its coupling to the first excitation of the SQ with strength g_1, remains mostly photon-like because it is far detuned by Δ from this qubit excitation (Figure 3.3(b)). At the end of the procedure, this leads to an additional phase for the two-photon initial state. The coupling

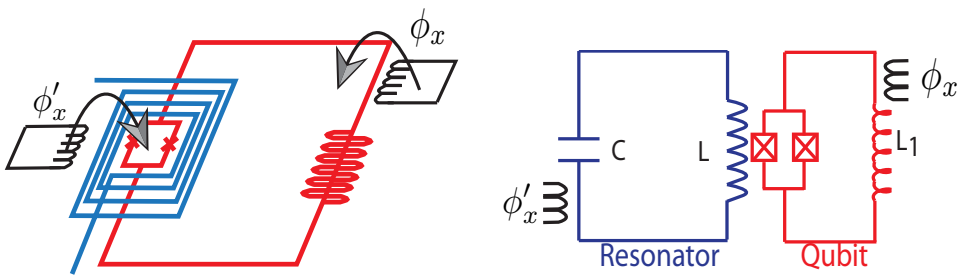

(a) (b)

Figure 3.2: (a) Implementation of a high-impedance coiled resonator (blue) coupled to a dc-SQUID (red) with an inductive outer loop. The flux bias lines are in black. (b) A simple circuit model of the physical implementation.

of the two-photon state to other modes arises via linear coupling at $O(g_1)$ and is assumed to be far detuned.

The noise in the SQ, with a decay rate γ of its first excited state, may slightly limit the nonlinear phase shift operation. Although the overall system will mostly be in the photon-like regime with decay rate κ, there will be an additional probability for it to decay due to its coupling to the lossy qubit. In the limit where $|\delta| \gg |g_2|$ and $|\Delta| \gg |g_1|$ with $|\Delta| > |\delta|$, the two-photon nonlinearity goes like g_2^2/δ, and the two-photon state decays approximately at a rate $\gamma g_1^2/\Delta^2 + \gamma g_2^2/\delta^2$. Thus, the losses due to the qubit go like γ/δ provided one allows g_1 to become close to g_2, which is possible by controlling ϕ'_x. Hence, at large detuning, one will then be limited only by κ. In contrast, a Kerr nonlinearity scales like g_1^4/δ^3 and the noise scales like $\gamma g_1^2/\delta^2$, leading to more loss due to the qubit for large detuning.

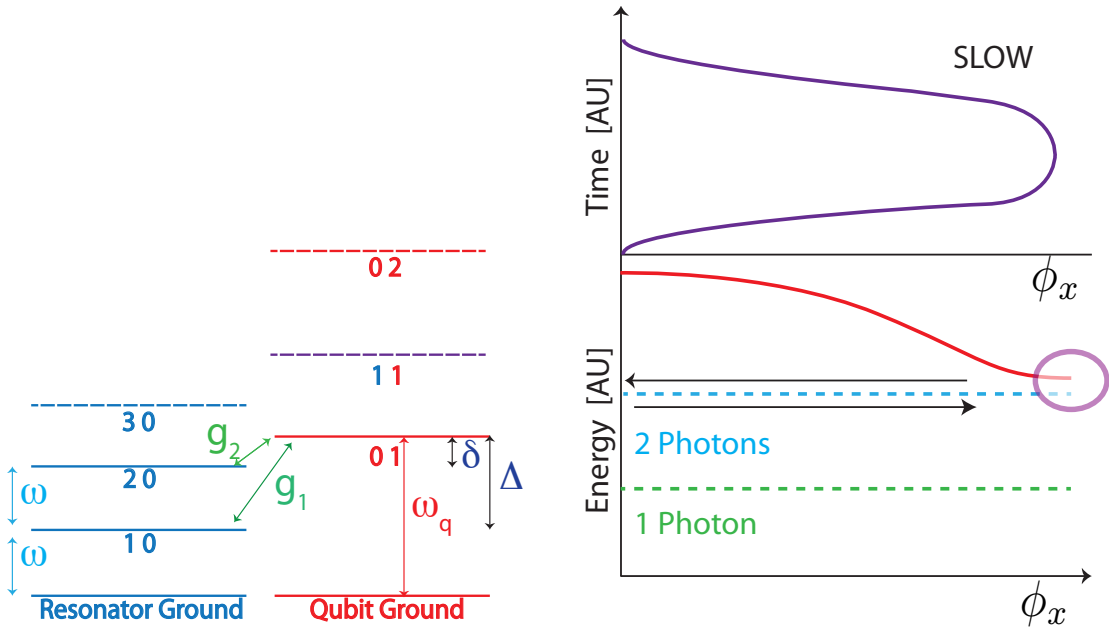

(a) (b)

Figure 3.3: (a) Energy levels of the resonator and qubit system along with the relevant couplings. (b) Top: The suggested flux bias pulse ϕ_x to implement the nonlinear phase shift; a fast but adiabatic sweep and then a very slow variation of the pulse near the avoided crossing. Bottom: The coupling g_2 between the two photon state and the first qubit excited state leads to a sizeable avoided crossing.

3.3 The Circuit Model and Hamiltonian

First I derive the Hamiltonian of the system using a circuit model. The circuit model comprising of an LC circuit coupled inductively with strength $0 < \chi < 1$ to a dc-SQUID configuration is shown in Figure 3.4. The inductance and capacitance of the LC circuit are denoted by L and C respectively. The SQUID consists of two junctions with Josephson energies E_{J1} and E_{J2} respectively, along with capacitances

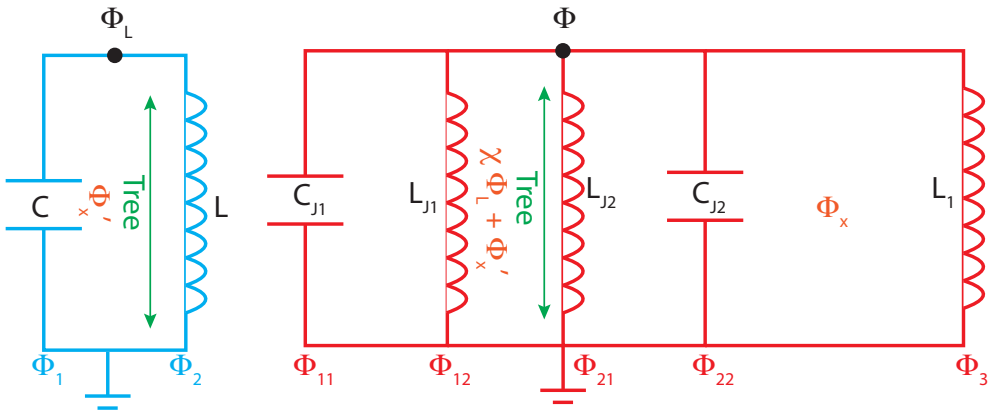

Figure 3.4: The circuit model.

and inductances C_{J1}, L_{J1} and C_{J2}, L_{J2}. The terms Φ_L and Φ represent the node fluxes with the corresponding trees shown in green. The branch fluxes in the LC circuit are denoted in blue by Φ_1 and Φ_2 while the branch fluxes in the qubit are represented in red by the terms Φ_{11}, Φ_{12}, Φ_{21}, Φ_{22}, and Φ_3. The outer loop is threaded by an external flux Φ_x while the loop in the LC circuit has a flux Φ'_x through it. This in turn threads the smaller SQUID loop, along with the resonator flux Φ_L, giving rise to the inductive coupling.

Following the guidelines on circuit quantization, the branch fluxes can be written as

$$\Phi_1 = \Phi_L + \Phi'_x, \tag{3.1}$$

$$\Phi_2 = \Phi_L, \tag{3.2}$$

$$\Phi_{11} = \Phi + \chi\Phi_L + \chi\Phi'_x = \Phi_{12}, \tag{3.3}$$

$$\Phi_{21} = \Phi = \Phi_{22}, \tag{3.4}$$

$$\Phi_3 = \Phi + \Phi_x. \tag{3.5}$$

The kinetic energy term T is [50]

$$\begin{aligned} T &= \frac{1}{2}C\dot{\Phi}_1^2 + \frac{1}{2}C_{J1}\dot{\Phi}_{11}^2 + \frac{1}{2}C_{J2}\dot{\Phi}_{22}^2 \\ &= \frac{1}{2}C(\dot{\Phi}_L + \dot{\Phi}'_x)^2 + \frac{1}{2}C_{J1}(\dot{\Phi} + \chi\dot{\Phi}_L + \chi\dot{\Phi}'_x)^2 + \frac{1}{2}C_{J2}\dot{\Phi}^2 \\ &\approx \frac{1}{2}C\dot{\Phi}_L^2 + \frac{1}{2}C_{J1}(\dot{\Phi} + \chi\dot{\Phi}_L)^2 + \frac{1}{2}C_{J2}\dot{\Phi}^2, \end{aligned} \tag{3.6}$$

where I ignore the time derivative of external fluxes in the adiabatic limit. The potential energy term is

$$V = \frac{\Phi_L^2}{2L} - E_{J1}\cos(\phi + \chi\phi_L + \phi'_x) - E_{J2}\cos\phi + \frac{1}{2}E_L(\phi + \phi_x)^2. \tag{3.7}$$

I have written V in terms of

$$\phi_x = \frac{2\pi\Phi_x}{\Phi_0}, \tag{3.8}$$

$$\phi'_x = \frac{2\pi\chi\Phi'_x}{\Phi_0}, \tag{3.9}$$

$$\phi_L = \frac{2\pi\Phi_L}{\Phi_0}, \tag{3.10}$$

$$E_L = \frac{\Phi_0^2}{4\pi^2 L_1}. \tag{3.11}$$

The Lagrangian of the system is $\mathcal{L} = T - V$. The canonical momenta of the system denoted by q_L and q are

$$q_L = \frac{\partial\mathcal{L}}{\partial\dot{\Phi}_L} \text{ and } q = \frac{\partial\mathcal{L}}{\partial\dot{\Phi}}. \tag{3.12}$$

From the Lagrangian

$$q = (C_{J1} + C_{J2})\dot{\Phi} + \chi C_{J1}\dot{\Phi}_L, \tag{3.13}$$

$$q_L = \chi C_{J1}\dot{\Phi} + (C + \chi^2 C_{J1})\dot{\Phi}_L. \tag{3.14}$$

Solving these equations for $\dot{\Phi}$ and $\dot{\Phi}_L$ I get

$$\dot{\Phi} = \frac{qC - \chi C_{J1}(q_L - \chi q)}{C(C_{J1} + C_{J2}) + \chi^2 C_{J1} C_{J2}}, \tag{3.15}$$

$$\dot{\Phi}_L = \frac{q_L(C_{J1} + C_{J2}) - \chi q C_{J1}}{C(C_{J1} + C_{J2}) + \chi^2 C_{J1} C_{J2}}. \tag{3.16}$$

Using these results I can write the Hamiltonian $\mathcal{H} = q\dot{\Phi} + q_L\dot{\Phi}_L - \mathcal{L}$. The quantum Hamiltonian is then

$$\begin{aligned}\mathcal{H} = & \left[\frac{\hat{\Phi}_L^2}{2L} + \frac{\hat{q}_L^2}{2\tilde{C}}\right] + \left[\frac{\hat{q}^2}{2\tilde{C}_J} - E_{J1}\cos(\hat{\phi} + \chi\hat{\phi}_L + \phi_x') - E_{J2}\cos\hat{\phi} + \frac{1}{2}E_L(\hat{\phi} + \phi_x)^2\right] \\ & - \left(\frac{\chi C_{J1}}{C(C_{J1} + C_{J2}) + \chi^2 C_{J1} C_{J2}}\right)\hat{q}\hat{q}_L,\end{aligned} \tag{3.17}$$

where the effective resonator and junction capacitances are

$$\tilde{C} = \frac{C(C_{J1} + C_{J2}) + \chi^2 C_{J1} C_{J2}}{C_{J1} + C_{J2}} \xrightarrow{\chi=0} C, \tag{3.18}$$

$$\tilde{C}_J = \frac{C(C_{J1} + C_{J2}) + \chi^2 C_{J1} C_{J2}}{C + \chi^2 C_{J1}} \xrightarrow{\chi=0} C_{J1} + C_{J2}. \tag{3.19}$$

Let the dressed resonator frequency be $\omega = 1/\sqrt{L\tilde{C}}$ and $\Phi_L^{(0)} = \sqrt{L\omega\hbar/2}$ be the width of quantum fluctuations in the resonator flux. Introduce the dimensionless parameter $\mu = 2\pi\Phi_L^0/\Phi_0$. In terms of the quantum of conductance $G_0 = 2e^2/h$ and the characteristic impedance of the resonator $Z = \sqrt{L/\tilde{C}}$, I can write $\mu = 2\pi G_0 Z$. Since $\mu \ll 1$, one can expand V in powers of $\chi\hat{\phi}_L \propto \mu$. Performing a series expansion of the term in V proportional to E_{J1} to second order in $\chi\hat{\phi}_L$ I get

$$\begin{aligned} & -\cos(\hat{\phi} + \chi\hat{\phi}_L + \phi_x') \\ = & -\cos(\hat{\phi} + \phi_x') + \chi\sin(\hat{\phi} + \phi_x')\hat{\phi}_L + \frac{\chi^2}{2}\cos(\hat{\phi} + \phi_x')\hat{\phi}_L^2 + O(\hat{\phi}_L^3).\end{aligned} \tag{3.20}$$

This gives the resonator, qubit, and interaction Hamiltonians

$$H_r = \frac{\hat{q}_L^2}{2\tilde{C}} + \frac{\hat{\Phi}_L^2}{2L}, \tag{3.21}$$

$$H_q = \frac{\hat{q}^2}{2\tilde{C}_J} - E_{J1}\cos(\hat{\phi}+\phi_x') - E_{J2}\cos\hat{\phi} + \frac{1}{2}E_L(\hat{\phi}+\phi_x)^2, \tag{3.22}$$

$$V_I = \chi E_{J1}\sin(\hat{\phi}+\phi_x')\hat{\phi}_L + \frac{\chi^2}{2}E_{J1}\cos(\hat{\phi}+\phi_x')\hat{\phi}_L^2 - \frac{\chi C_{J1}}{\tilde{C}(C_{J1}+C_{J2})}\hat{q}\hat{q}_L. \tag{3.23}$$

For simplicity I assume that the junctions are identical with capacitances C_J and Josephson energies E_J. Then I get

$$\tilde{C} = C + \frac{\chi^2}{2}C_J, \tag{3.24}$$

$$\tilde{C}_J = \frac{2CC_J + \chi^2 C_J^2}{C + \chi^2 C_J}, \tag{3.25}$$

along with the simplified terms

$$H_r = \frac{\hat{q}_L^2}{2\tilde{C}} + \frac{\hat{\Phi}_L^2}{2L}, \tag{3.26}$$

$$H_q = \frac{\hat{q}^2}{2\tilde{C}_J} - E_J\cos(\hat{\phi}+\phi_x') - E_J\cos\hat{\phi} + \frac{1}{2}E_L(\hat{\phi}+\phi_x)^2, \tag{3.27}$$

$$V_I = \chi E_J\sin(\hat{\phi}+\phi_x')\hat{\phi}_L + \frac{\chi^2}{2}E_J\cos(\hat{\phi}+\phi_x')\hat{\phi}_L^2 - \frac{\chi}{2\tilde{C}}\hat{q}\hat{q}_L. \tag{3.28}$$

3.4 Linearization and Quantization

In the limit where $E_L \gg E_J > 2E_C$, one can linearize the potential

$$V(\phi,\phi_L) = \left(\frac{\Phi_0}{2\pi}\right)^2\frac{\phi_L^2}{2L} - E_J\cos(\phi+\chi\phi_L+\phi_x') - E_J\cos\phi + \frac{1}{2}E_L(\phi+\phi_x)^2, \tag{3.29}$$

about the classical minima ϕ_c and ϕ_{Lc} of the qubit phase and resonator flux respectively. Thus, in the following, I let curly brackets $\{f(\phi,\phi_L)\}$ denote its evaluation at the classical minima $\phi=\phi_c$ and $\phi_L=\phi_{Lc}$. Hence,

$$V(\phi,\phi_L) \to V(\hat{\phi}+\phi_c, \hat{\phi}_L+\phi_{Lc}), \tag{3.30}$$

where the hats denote quantum fluctuations. I let

$$V_0 = V(\phi_c, \phi_{Lc}), \tag{3.31}$$

$$V_1 = \left\{\frac{\partial V}{\partial \phi}\right\}\hat{\phi} + \left\{\frac{\partial V}{\partial \phi_L}\right\}\hat{\phi}_L. \tag{3.32}$$

Using a Taylor series expansion of V about the classical minima, I get

$$\begin{aligned} & V(\hat{\phi}+\phi_c, \hat{\phi}_L+\phi_{Lc}) \\ = \; & V_0 + V_1 + \frac{1}{2!}\left[\left\{\frac{\partial^2 V}{\partial \phi^2}\right\}\hat{\phi}^2 + 2\left\{\frac{\partial^2 V}{\partial \phi \partial \phi_L}\right\}\hat{\phi}\hat{\phi}_L + \left\{\frac{\partial^2 V}{\partial \phi_L^2}\right\}\hat{\phi}_L^2\right] + O(\hat{\phi}^3). \end{aligned} \tag{3.33}$$

I set the terms

$$\frac{\partial V(\phi, \phi_L)}{\partial \phi} = \frac{\partial V(\phi, \phi_L)}{\partial \phi_L} = 0, \tag{3.34}$$

and solve for the approximate classical values ϕ_c and ϕ_{Lc}. Letting $\tilde{\chi} = 2\pi\chi/\Phi_0$,

$$\phi_c(\phi_x, \phi_x') = -\phi_x + \frac{E_J \sin\phi_x + E_J \sin(\phi_x - \phi_x' - \chi\phi_{Lc})}{E_L + E_J\cos\phi_x + E_J\cos(\phi_x - \phi_x' - \chi\phi_{Lc})}, \tag{3.35}$$

$$\phi_{Lc}(\phi_x, \phi_x') = \left(\frac{2\pi}{\Phi_0}\right)\frac{E_J L\tilde{\chi}\sin(\phi_x - \phi_x')}{1 + E_J L\tilde{\chi}^2\cos(\phi_x - \phi_x')}. \tag{3.36}$$

Explicitly, the linearized potential is

$$\begin{aligned} V_2 = \; & \frac{1}{2}\left[E_L + E_J\cos\phi_c + E_J\cos(\phi_c + \phi_x' + \chi\phi_{Lc})\right]\hat{\phi}^2 \\ & + \frac{1}{2}\left[\left(\frac{\Phi_0}{2\pi}\right)^2\frac{1}{L} + \chi^2 E_J\cos(\phi_c + \phi_x' + \chi\phi_{Lc})\right]\hat{\phi}_L^2 \\ & + \chi E_J\cos(\phi_c + \phi_x' + \chi\phi_{Lc})\hat{\phi}\hat{\phi}_L. \end{aligned} \tag{3.37}$$

The nonlinear correction to the potential has the form

$$V_3 = \frac{1}{3!}\left[\left\{\frac{\partial^3 V}{\partial \phi^3}\right\}\hat{\phi}^3 + 3\left\{\frac{\partial^3 V}{\partial \phi^2 \partial \phi_L}\right\}\hat{\phi}^2\hat{\phi}_L + 3\left\{\frac{\partial^3 V}{\partial \phi \partial \phi_L^2}\right\}\hat{\phi}\hat{\phi}_L^2 + \left\{\frac{\partial^3 V}{\partial \phi_L^3}\right\}\hat{\phi}_L^3\right], \tag{3.38}$$

where the derivatives are given by

$$\frac{\partial^3 V}{\partial \phi^3} = -E_J \sin\phi_c - E_J \sin(\phi_c + \phi'_x + \chi\phi_{Lc}), \tag{3.39}$$

$$\frac{\partial^3 V}{\partial \phi^2 \partial \phi_L} = -\chi E_J \sin(\phi_c + \phi'_x + \chi\phi_{Lc}), \tag{3.40}$$

$$\frac{\partial^3 V}{\partial \phi \partial \phi_L^2} = -\chi^2 E_J \sin(\phi_c + \phi'_x + \chi\phi_{Lc}), \tag{3.41}$$

$$\frac{\partial^3 V}{\partial \phi_L^3} = -\chi^3 E_J \sin(\phi_c + \phi'_x + \chi\phi_{Lc}). \tag{3.42}$$

The coupling I am interested in is

$$\frac{1}{2}\left\{\frac{\partial^3 V}{\partial \phi \partial \phi_L^2}\right\} \hat{\phi}\hat{\phi}_L^2 = -\frac{\chi^2}{2} E_J \sin(\phi_c + \phi'_x + \chi\phi_{Lc}) \hat{\phi}\hat{\phi}_L^2, \tag{3.43}$$

which annihilates two resonator quanta in exchange for a single qubit excitation.

For conciseness of notation I let

$$u(\phi_x, \phi'_x) \equiv \cos(\phi_c + \phi'_x + \chi\phi_{Lc}), \tag{3.44}$$

$$s(\phi_x, \phi'_x) \equiv \sin(\phi_c + \phi'_x + \chi\phi_{Lc}), \tag{3.45}$$

$$r(\phi_x, \phi'_x) \equiv \sin\phi_c, \tag{3.46}$$

$$t(\phi_x, \phi'_x) \equiv \cos\phi_c. \tag{3.47}$$

Define the parameters

$$\tilde{L}^{-1} = \left[\frac{1}{L} + \tilde{\chi}^2 E_J \cos(\phi_c + \phi'_x + \chi\phi_{Lc})\right] = \left[\frac{1}{L} + \tilde{\chi}^2 E_J u\right], \tag{3.48}$$

$$\omega = \frac{1}{\sqrt{\tilde{L}\tilde{C}}}, \tag{3.49}$$

$$\omega_q = \sqrt{\omega_C[\omega_L + (t+u)\omega_J]}. \tag{3.50}$$

Let $\hat{N} = \hat{q}/(2e)$ be the number of Cooper pairs tunneling through the junction with an effective charging energy $\tilde{E}_C = (2e)^2/\tilde{C}_J$. The Hamiltonian of the system is

$\hat{\mathcal{H}}_l = \hat{\mathcal{H}}_{rl} + \hat{\mathcal{H}}_{ql} + \hat{\mathcal{V}}_I$ where

$$\hat{H}_{rl} = \frac{\hat{q}_L^2}{2\tilde{C}} + \frac{\hat{\Phi}_L^2}{2\tilde{L}} \rightarrow \frac{\hat{q}_L^2}{2\tilde{C}} + \frac{1}{2}\tilde{C}\omega^2\hat{\Phi}_L^2, \tag{3.51}$$

$$\hat{H}_{ql} = \frac{\tilde{E}_C}{2}\hat{N}^2 + \frac{1}{2}\left[E_L + E_J(t+u)\right]\hat{\phi}^2, \tag{3.52}$$

$$\hat{H}_I = -\frac{\chi}{2\tilde{C}}\hat{q}\hat{q}_L + \tilde{\chi}uE_J\hat{\phi}\hat{\Phi}_L - \frac{\tilde{\chi}^2}{2}sE_J\hat{\phi}\hat{\Phi}_L^2. \tag{3.53}$$

I now introduce the operators $\{\hat{a}, \hat{a}^\dagger, \hat{b}, \hat{b}^\dagger\}$ satisfying $[\hat{a}, \hat{a}^\dagger] = 1 = [\hat{b}, \hat{b}^\dagger]$. Let

$$\hat{\Phi}_L = \sqrt{\frac{\tilde{L}\omega\hbar}{2}}(\hat{a} + \hat{a}^\dagger), \tag{3.54}$$

$$\hat{q}_L = -i\sqrt{\frac{\hbar}{2\tilde{L}\omega}}(\hat{a} - \hat{a}^\dagger), \tag{3.55}$$

$$\hat{\phi} = \sqrt{\frac{\tilde{\omega}_C}{2\omega_q}}(\hat{b} + \hat{b}^\dagger), \tag{3.56}$$

$$\hat{N} = -i\sqrt{\frac{\omega_q}{2\tilde{\omega}_C}}(\hat{b} - \hat{b}^\dagger). \tag{3.57}$$

The newly defined operators preserve the commutations relations $[\hat{\phi}, \hat{N}] = i$ and $[\hat{\Phi}, \hat{q}] = i\hbar$. This leads to the quantized Hamiltonians $\hat{H}_{rl} = \omega\hat{a}^\dagger\hat{a}$ and $\hat{\mathcal{H}}_{ql} = \omega_q\hat{b}^\dagger\hat{b}$. The linear part of the Hamiltonian is

$$\hat{H}_L = \hat{\mathcal{H}}_{rl} + \hat{\mathcal{H}}_{ql} - \frac{\chi}{2\tilde{C}}\hat{q}\hat{q}_L + \tilde{\chi}uE_J\hat{\phi}\hat{\Phi}_L. \tag{3.58}$$

The quantized nonlinear interaction term is

$$\hat{V}_{nl} = -\frac{\tilde{\chi}^2}{2}sE_J\hat{\phi}\hat{\Phi}_L^2. \tag{3.59}$$

Recall the dimensionless parameter $\mu = 2\pi\Phi_L^0/\Phi_0 \approx 2\pi/\Phi_0\sqrt{\tilde{L}\omega\hbar/2}$. I then define the energies

$$\eta_1 = \chi E_J\mu, \tag{3.60}$$

$$\eta_2 = \frac{\chi^2}{2}E_J\mu^2 = \frac{\eta_1^2}{2E_J}, \tag{3.61}$$

$$\eta_3 = \frac{\chi e}{\tilde{C}}\sqrt{\frac{\hbar}{2\tilde{L}\omega}} = \eta_1\frac{\hbar\omega}{2E_J}. \tag{3.62}$$

In terms of the creation and annihilation operators, the linear interaction term is

$$\begin{aligned}\hat{V}_l &= -\frac{\chi}{2\tilde{C}}\hat{q}\hat{q}_L + \tilde{\chi}uE_J\hat{\phi}\hat{\Phi}_L \\ &= -\frac{\chi}{2\tilde{C}}(2e)\hat{N}\hat{q}_L + \tilde{\chi}uE_J\hat{\phi}\hat{\Phi}_L \\ &= \eta_3\sqrt{\frac{\omega_q}{2\tilde{\omega}_C}}(\hat{a}-\hat{a}^\dagger)(\hat{b}-\hat{b}^\dagger) + \eta_1 u\sqrt{\frac{\tilde{\omega}_C}{2\omega_q}}(\hat{a}+\hat{a}^\dagger)(\hat{b}+\hat{b}^\dagger). \end{aligned} \tag{3.63}$$

I then make a rotating wave approximation to get

$$\hat{V}_l^{(RWA)} = g_1(\hat{a}\hat{b}^\dagger + \hat{a}^\dagger\hat{b}), \tag{3.64}$$

where the linear coupling is

$$g_1 = \eta_1 u\sqrt{\frac{\tilde{\omega}_C}{2\omega_q}} - \eta_3\sqrt{\frac{\omega_q}{2\tilde{\omega}_C}}. \tag{3.65}$$

Later it will be seen that the nonlinear phase shift operation will require g_1 to vanish. This is only possible if it changes sign. The term u varies as a function of the external fluxes but $|u| \leq 1$. g_1 vanishes when

$$\eta_1 u\sqrt{\frac{\tilde{\omega}_C}{2\omega_q}} = \eta_3\sqrt{\frac{\omega_q}{2\tilde{\omega}_C}} \implies u\sqrt{\frac{\tilde{\omega}_C}{2\omega_q}} = \frac{\hbar\omega}{2E_J}\sqrt{\frac{\omega_q}{2\tilde{\omega}_C}}. \tag{3.66}$$

Since $|u| \leq 1$, for g_1 to change sign, I require $\tilde{\omega}_C \leq \omega_q\omega/(2\omega_J)$. Note that ω_q also depends on the external fluxes. The non-linear coupling in terms of these operators is

$$\hat{V}_{nl} = -\eta_2 s\sqrt{\frac{\tilde{\omega}_C}{2\omega_q}}(\hat{a}+\hat{a}^\dagger)^2(\hat{b}+\hat{b}^\dagger) \xrightarrow{RWA} -\eta_2 s\sqrt{\frac{\tilde{\omega}_C}{2\omega_q}}(\hat{a}^2\hat{b}^\dagger + \hat{a}^{\dagger 2}\hat{b}). \tag{3.67}$$

3.5 Diagonalization of Linear Hamiltonian

I had the linear Hamiltonian

$$\hat{\mathcal{H}}_L = \omega\hat{a}^\dagger\hat{a} + \omega_q\hat{b}^\dagger\hat{b} + g_1(\hat{a}\hat{b}^\dagger + \hat{a}^\dagger\hat{b}). \tag{3.68}$$

To diagonalize $\hat{\mathcal{H}}_L$ I define new operators $\hat{c}$ and $\hat{d}$ with

$$\hat{a} = \mu_1 \hat{c} + \nu_1 \hat{d}, \tag{3.69}$$

$$\hat{b} = \mu_2 \hat{c} + \nu_2 \hat{d}, \tag{3.70}$$

such that $[\hat{c}, \hat{c}^\dagger] = 1 = [\hat{d}, \hat{d}^\dagger]$ and $[\hat{c}, \hat{d}^\dagger] = 0 = [\hat{c}, \hat{d}]$. This requires the conditions

$$|\mu_1|^2 + |\nu_1|^2 = 1 = |\mu_2|^2 + |\nu_2|^2, \tag{3.71}$$

$$\mu_1 \mu_2^\star + \nu_1 \nu_2^\star = 0. \tag{3.72}$$

The parametrization $\mu_1 = \cos\theta$, $\nu_1 = -\sin\theta$, $\mu_2 = \sin\theta$, $\nu_2 = \cos\theta$ satisfies the constraints (3.71), (3.72). Substituting the relations into $\hat{\mathcal{H}}_L$ and setting the diagonal terms to zero, I get a new Hamiltonian in the normal mode coordinates given by

$$\hat{\mathcal{H}}_N = \Omega_1 \hat{c}^\dagger \hat{c} + \Omega_2 \hat{d}^\dagger \hat{d}. \tag{3.73}$$

The dressed frequencies are

$$\Omega_1 = \omega + \frac{\Delta}{2}\left(1 - \sqrt{1 + \frac{4g_1^2}{\Delta^2}}\right), \tag{3.74}$$

$$\Omega_2 = \omega + \frac{\Delta}{2}\left(1 + \sqrt{1 + \frac{4g_1^2}{\Delta^2}}\right). \tag{3.75}$$

The detuning $\Delta = \omega_q - \omega$ is assumed to be positive. Note that for $\Delta \gg |g_1|$, $\Omega_1 \to \omega$, and $\Omega_2 \to \omega_q$.

In the following discussion, I denote the basis states of the resonator and qubit system by $|m\rangle \otimes |n\rangle \equiv |m\ n\rangle$, where the first and second labels refer to the quantum number of the resonator and qubit respectively. The eigenstates of the Hamiltonian in the new basis are number excitations of the $\hat{c}^\dagger \hat{c}$ and $\hat{d}^\dagger \hat{d}$ operators. Denoting these

kets as $\left|\bar{C}\bar{D}\right\rangle$,

$$|\bar{1}\bar{0}\rangle = \cos\theta\,|10\rangle + \sin\theta\,|01\rangle\,, \tag{3.76}$$

$$|\bar{0}\bar{1}\rangle = -\sin\theta\,|10\rangle + \cos\theta\,|01\rangle\,, \tag{3.77}$$

$$|\bar{2}\bar{0}\rangle = \cos^2\theta\,|20\rangle + \sqrt{2}\cos\theta\sin\theta\,|11\rangle + \sin^2\theta\,|02\rangle\,, \tag{3.78}$$

$$|\bar{1}\bar{1}\rangle = -\sqrt{2}\cos\theta\sin\theta\,|20\rangle + \cos 2\theta\,|11\rangle + \sqrt{2}\cos\theta\sin\theta\,|02\rangle\,, \tag{3.79}$$

$$|\bar{0}\bar{2}\rangle = \sin^2\theta\,|20\rangle - \sqrt{2}\cos\theta\sin\theta\,|11\rangle + \cos^2\theta\,|02\rangle\,. \tag{3.80}$$

Explicitly, the sines and cosines are

$$\sin\theta = \frac{1}{\sqrt{2}}\sqrt{1 - \frac{\Delta}{\sqrt{4g_1^2 + \Delta^2}}}, \tag{3.81}$$

$$\cos\theta = \frac{1}{\sqrt{2}}\sqrt{1 + \frac{\Delta}{\sqrt{4g_1^2 + \Delta^2}}}. \tag{3.82}$$

The parameter θ is also given by $\tan 2\theta = 2g_1\Delta^{-1}$. When $\Delta \gg |g_1|$, $\tan 2\theta \to 0$ or $\theta \to 0$. So $\sin\theta \to 0$ and $\cos\theta \to 1$. Thus, $|\bar{1}\bar{0}\rangle \to |10\rangle$, $|\bar{0}\bar{1}\rangle \to |01\rangle$, $|\bar{2}\bar{0}\rangle \to |20\rangle$, $|\bar{2}\bar{0}\rangle \to |20\rangle$. Similarly, when $\Delta \to 0$, $\theta \to \pi/4$. Hence, $\cos\theta \to 1/\sqrt{2}$ and $\sin\theta \to 1/\sqrt{2}$.

In terms of the normal mode operators,

$$\begin{aligned}\hat{\mathcal{V}}_{nl} = {} & \eta_2'(\cos^2\theta\sin\theta\hat{c}^{\dagger 2}\hat{c} - \cos^3\theta\hat{c}^{\dagger 2}\hat{d} - 2\cos\theta\sin^2\theta\hat{c}^\dagger\hat{c}\hat{d}^\dagger + 2\cos^2\theta\sin\theta\hat{c}^\dagger\hat{d}^\dagger\hat{d} \\ & + \sin^3\theta\hat{c}\hat{d}^{\dagger 2} - \sin^2\theta\cos\theta\hat{d}^{\dagger 2}\hat{d} + h.c.),\end{aligned} \tag{3.83}$$

where I have defined $\eta_2' \equiv \eta_2 s\sqrt{\frac{\tilde{\omega}_C}{2\omega_q}}$.

3.6 Subspace Hamiltonian and Two-Photon Nonlinearity

I will work in the subspace spanned by the states $\{|0\rangle \equiv |\bar{0}\bar{0}\rangle, |a\rangle \equiv |\bar{1}\bar{0}\rangle, |b\rangle \equiv |\bar{2}\bar{0}\rangle, |c\rangle \equiv |\bar{0}\bar{1}\rangle\}$. The Hamiltonian is

$$H = \begin{pmatrix} 0 & 0 & 0 & 0 \\ 0 & \Omega_1 & \lambda_1 & 0 \\ 0 & \lambda_1 & 2\Omega_1 & \lambda_2 \\ 0 & 0 & \lambda_2 & \Omega_2 \end{pmatrix}. \tag{3.84}$$

The parameters $\lambda_1 = (\sqrt{2}\cos^2\theta\sin\theta)\eta_2' \equiv r_1\eta_2'$ and $\lambda_2 = (-\sqrt{2}\cos^3\theta)\eta_2' \equiv r_2\eta_2'$. One can use a Schrieffer-Wolf transformation (Appendix A) to find an effective Hamiltonian

$$\tilde{H} = \begin{pmatrix} 0 & 0 & 0 & 0 \\ 0 & \Omega_1 - \dfrac{r_1^2\eta_2'^2}{\Omega_1} + O(\eta_2'^3) & O(\eta_2'^3) & O(\eta_2'^3) \\ 0 & O(\eta_2'^3) & 2\Omega_1 + \dfrac{r_1^2\eta_2'^2}{\Omega_1} + O(\eta_2'^3) & r_2\eta_2' + O(\eta_2'^3) \\ 0 & O(\eta_2'^3) & r_2\eta_2' + O(\eta_2'^3) & \Omega_2 + O(\eta_2'^3) \end{pmatrix}. \tag{3.85}$$

One can use this Hamiltonian to calculate the two-photon nonlinearity N_l. With $\delta' = \Omega_2 - 2\Omega_1 > 0$, I have

$$N_l = \eta_2'^2\left(\frac{3r_1^2}{\Omega_1} - \frac{r_2^2}{\delta'}\right) \approx -\frac{\eta_2'^2 r_2^2}{\delta'} = -\frac{g_2^2}{\delta'}, \tag{3.86}$$

where I have identified $\eta_2' r_2$ with g_2. With this nonlinearity and standard parameters, the two-photon π phase shift protocol can be implemented in a few hundred ns.

3.7 Numerical Results

In addition to my analytical model, I also diagonalize the Hamiltonian of the system numerically by working in the tensor product space $H = H_r \otimes H_q$ of the resonator and qubit. A basis state of H is written as $|n\rangle \otimes |q\rangle \equiv |n\ q\rangle$, a tensor product of the bases for the resonator and qubit spaces. The basis states in the resonator space are the number excitations $|n\rangle$ which are eigenstates of the number operator $\hat{n} = \hat{a}^\dagger \hat{a}$. The qubit space is written in the basis of qubit wavefunctions $\psi_q(\phi) = \langle \phi | \, q \rangle$. For this purpose, I start with the non-linearized Hamiltonians

$$\mathcal{H}_r = \frac{\hat{q}_L^2}{2\tilde{C}} + \frac{\hat{\Phi}_L^2}{2L}, \tag{3.87}$$

$$\mathcal{H}_q = \frac{\hat{q}^2}{2\tilde{C}_J} - E_J \cos(\hat{\phi} + \phi_x') - E_J \cos\hat{\phi} + \frac{1}{2} E_L (\hat{\phi} + \phi_x)^2, \tag{3.88}$$

$$\mathcal{V}_I = \chi E_J \sin(\hat{\phi} + \phi_x')\hat{\phi}_L + \frac{\chi^2}{2} E_J \cos(\hat{\phi} + \phi_x')\hat{\phi}_L^2 - \frac{\chi}{2\tilde{C}} \hat{q}\hat{q}_L. \tag{3.89}$$

Then I introduce creation and annihilation operators only for the resonator,

$$\hat{\Phi}_L = \sqrt{\frac{\tilde{L}\omega\hbar}{2}}(\hat{a} + \hat{a}^\dagger), \tag{3.90}$$

$$\hat{q}_L = -i\sqrt{\frac{\hbar}{2\tilde{L}\omega}}(\hat{a} - \hat{a}^\dagger). \tag{3.91}$$

In terms of these operators, the three interaction terms can be written as

$$V_1 = \eta_1(\hat{a} + \hat{a}^\dagger)\sin(\hat{\phi} + \phi_x'), \tag{3.92}$$

$$V_2 = \eta_2(\hat{a} + \hat{a}^\dagger)^2 \cos(\hat{\phi} + \phi_x'), \tag{3.93}$$

$$V_3 = i\eta_3(\hat{a} - \hat{a}^\dagger)\hat{N}. \tag{3.94}$$

From the potential V_2, the nonlinear coupling g_2 is seen to be

$$g_2 = \eta_2 \langle 20 | \, (\hat{a} + \hat{a}^\dagger)^2 \cos(\hat{\phi} + \phi_x') \, |01\rangle = \sqrt{2}\eta_2 \langle 0_q | \cos(\hat{\phi} + \phi_x') \, |1_q\rangle \, . \tag{3.95}$$

For my numerical analysis, I first remark that the dressed parameters like $\tilde{\omega}_C$ and $\tilde{C}$ are nearly equal to their corresponding bare counterparts ω_C and C. I let $\hbar = 1$ and choose $\omega_C/(2\pi) = 1$ GHz, $\omega_J/(2\pi) = 5$ GHz, $\omega_L = 3\omega_J$, and $\omega/(2\pi) = 2.225$ GHz. The characteristic impedance $Z \approx 449\,\Omega$. I choose a $\chi = 0.17$, representing an easily achievable mutual inductance, from which follow $\eta_1/(2\pi) =$ 400 MHz, $\eta_2/(2\pi) = 16$ MHz, and $\eta_3/(2\pi) = 89$ MHz.

I first plot g_1, g_2 and other parameters of the system as a function of the fluxes ϕ_x and ϕ'_x. The red marker in Figure 3.5 represents the starting point where the system is in the photon-like state and the green marker represents the parking point of the qubit. The starting point is chosen such that g_1 vanishes. The parking point is chosen so that the two-photon nonlinearity is still appreciable (at least a few MHz) but not to close to the avoided crossing (see more below). At this point, the system is still mostly photon-like and only marginally qubit-like. The detuning $\delta = \omega_q - 2\omega$ at this parking point is expected to be much larger than g_2.

I also plot the dressed energy levels of the system, along with the two-photon nonlinearity in Figure 3.7. Finally, I compare my numerical results with the analytical results derived previously. First, I test the accuracy of the nonlinear coupling $\eta'_2 r_2$ (3.86) which I associate with the numerical value derived from the expression $g_2 = \sqrt{2}\eta_2 \langle 0_q| \cos(\hat{\phi} + \phi'_x) |1_q\rangle$. I also compare the analytical and numerical values of $g_1 = \eta_1 \langle 0_q| \sin(\hat{\phi} + \phi'_x) |1_q\rangle$ in Figure 3.9. One can see that they are in good agreement.

3.8 Adiabatic and Non-Adiabatic Loss

Now I discuss the effect of loss on the gate. Throughout the operation of the gate the system remains mostly photon-like. Hence, loss is dominated by the cavity decay at a rate κ. Apart from κ, for the photon-like state $|\bar{2}\bar{0}\rangle$, there are two other decay channels due to the cavity-qubit coupling. In the limit $\Delta \gg |g_1|$, the linear coupling g_1 leads to a loss that is approximately

$$\gamma_1 \equiv \gamma g_1^2/\Delta^2 = \gamma g_1^2/(\delta+\omega)^2. \tag{3.96}$$

Similarly, for $|\delta| \gg |g_2|$, the nonlinear coupling leads to a loss

$$\gamma_2 \equiv \gamma g_2^2/\delta^2. \tag{3.97}$$

Including the cavity decay rate κ, the total decay rate of the two-photon-like state becomes

$$\Gamma(\delta) = \kappa + \gamma_1 + \gamma_2. \tag{3.98}$$

Assuming that g_2 is time independent for simplicity, adiabaticity of the state $|\bar{2}\bar{0}\rangle$ requires

$$g_2^2|\dot{\delta}|^2(\delta^2+4g_2^2)^{-3} \ll 1. \tag{3.99}$$

One can set this equal to some $\epsilon^2 \ll 1$ and solve for

$$\tau_h(\delta_m) \;=\; -\frac{1}{\epsilon}\int_{\delta_i}^{\delta_m} \frac{|g_2|}{(\delta^2+4g_2^2)^{\frac{3}{2}}}d\delta, \tag{3.100}$$

which is the time taken to go from $|\delta_i| \gg |g_2|$ at $t=0$ to smaller values of detuning with a minimum δ_m. The total dynamic loss during the process is given by

$$L_d(\delta_m) = \frac{2}{\epsilon}\int_{\delta_m}^{\delta_i} \Gamma(\delta)\frac{|g_2|}{(\delta^2+4g_2^2)^{\frac{3}{2}}}d\delta. \tag{3.101}$$

When the detuning is held at δ_m for a time $\tau_s = \pi\delta_m/g_2^2$, the static loss $L_s(\delta_m) = \tau_s\Gamma(\delta_m)$. Thus,

$$L_s(\delta_m) = \pi\left[\frac{\kappa\delta_m}{g_2^2} + \frac{\gamma\delta_m}{(\delta_m+\omega)^2}\left(\frac{g_1}{g_2}\right)^2 + \frac{\gamma}{\delta_m}\right], \tag{3.102}$$

and the total time of the protocol is $\tau_g = 2\tau_h + \tau_s$. Assuming $\delta_m \ll \omega$, $L_s(\delta_m)$ is minimized when $\delta_m \approx g_2\sqrt{\gamma/\kappa}$. However, the on-off ratio of the photon nonlinearity goes like $|\delta_i/\delta_m|$, and a value of δ_m that makes this ratio at least a hundred is desirable. For $\delta \sim \omega$, one can make $g_1 \approx g_2$ so that $L_s(\delta) < \kappa\delta/g_2^2 + 2\gamma/\delta$. In this regime L_s is limited by κ, as can be verified from Figure 3.11b. Thus, I optimize my protocol so that the loss $L = L_d + L_s \ll 1$. Note that one can minimize the static loss by increasing g_1, which has the effect of increasing g_2. However, to retrieve the photons with high fidelity, g_1 should vanish or be comparable to g_2 at large detuning. I note that my protection is only against qubit noise and loss, and comes at the cost of increased reliance on the cavity quality factor.

The protocol might also be limited by dephasing of the qubit due to flux noise [42,43,77]. The average slopes of the single and two-photon energy levels with respect to the reduced flux ϕ_x are approximately 50 MHz and 100 MHz respectively, while the slope of the qubit energy level is at most 1 GHz for the parameters chosen. However, the exact loss due to dephasing depends on the flux noise amplitude [46,78].

3.9 Conclusions and Outlook

In conclusion, I have demonstrated that by appropriately tuning two control fluxes, the nonlinear coupling in a system composed of photons in a resonator

coupled to a superconducting circuit enables a two-photon nonlinear phase shift operation, with loss at large detuning limited only by the cavity quality factor. The loss at large detuning can be further suppressed by increasing the strength of the linear coupling g_1, while at the same time assuring that it vanishes for large detuning. This is highly desirable compared to the self-Kerr nonlinearity which leads to more photon loss due to the noisy qubit at large detunings. Furthermore, my approach may be adaptable to recent ultra-high quality factor resonators enabling nonlinear optics quantum computing in a fully engineered system [70].

In the following chapter I consider the problem of simulating a system of bosons in a lattice in the presence of an artificial magnetic field and three-body on-site interactions. Again, I make use of the nonlinear nature of superconducting circuits to achieve this goal.

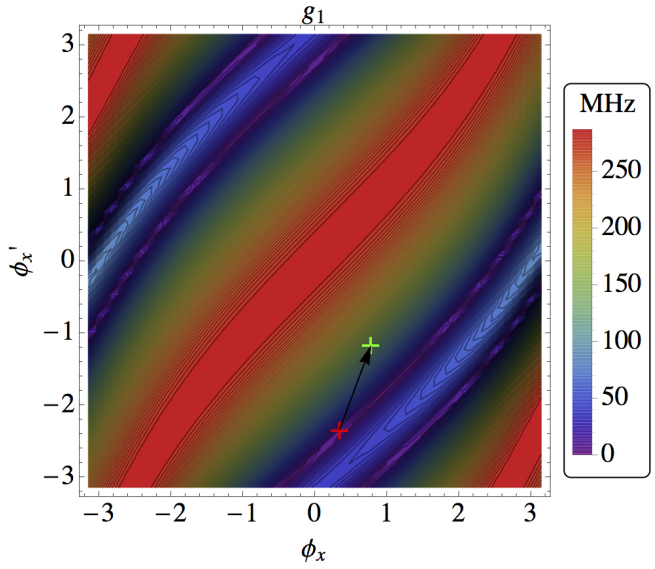

(a)

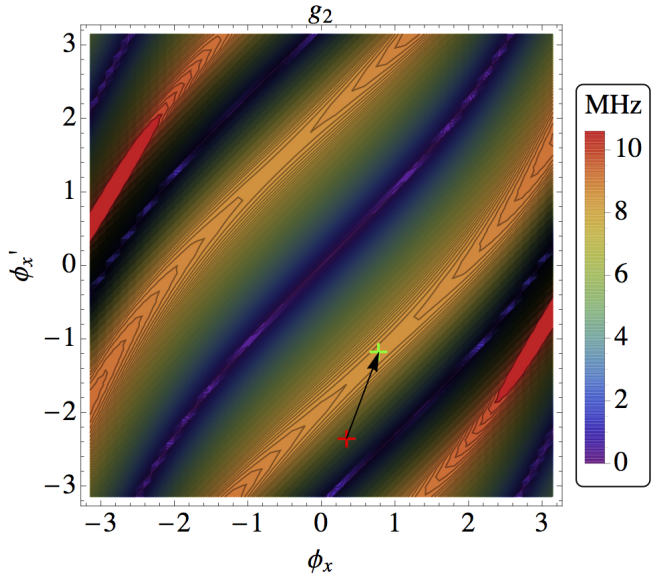

(b)

Figure 3.5: (a) Contour plot of g_1, and (b) g_2 as a function of the external fluxes.

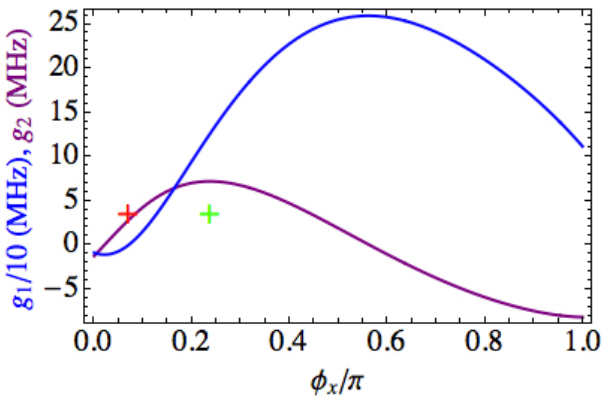

Figure 3.6: Variation of g_1 and g_2 along the trajectory defined by the arrows in Figure 3.5. Note that the starting point denoted by the red cross is chosen so that g_1 is close to zero.

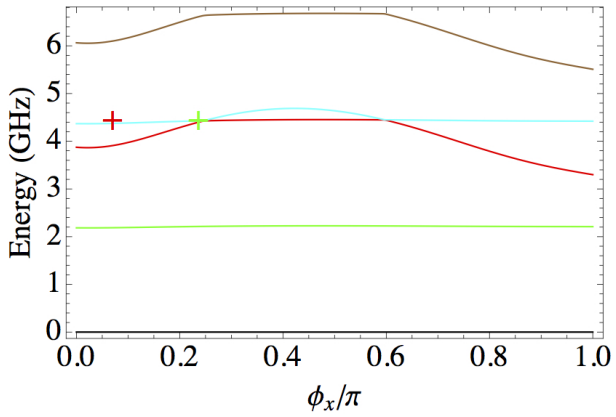

(a)

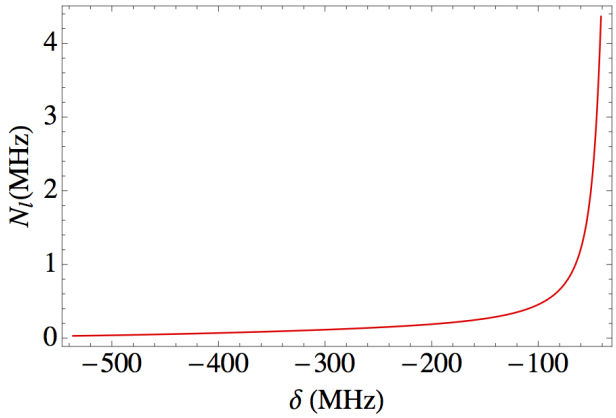

(b)

Figure 3.7: (a) The dressed energy levels of the coupled system. (b) The two-photon nonlinearity. The detuning on the horizontal axis is the detuning along the arrows from the red to the green markers. The minimum detuning δ_m is around -41 MHz.

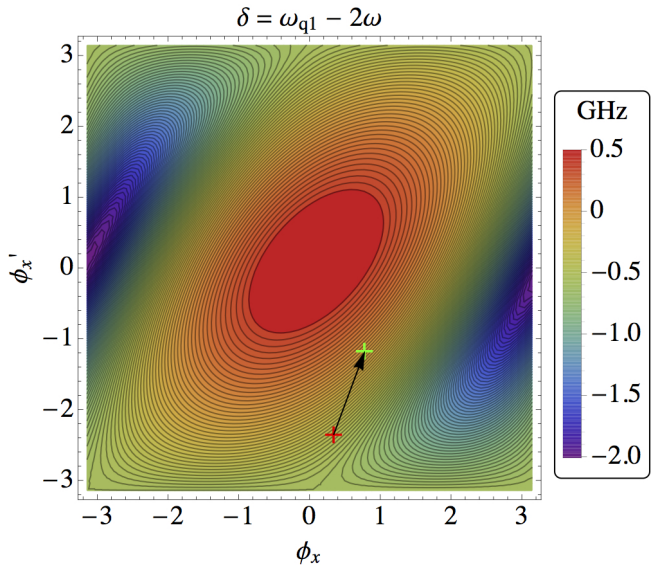

(a)

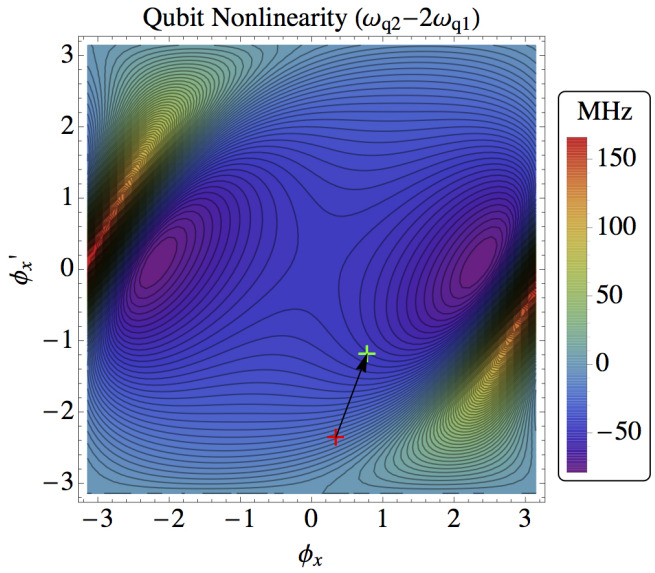

(b)

Figure 3.8: (a) The detuning $\delta = \omega_q - 2\omega$ with $\omega_{q1} \equiv \omega_q$. (b) The qubit nonlinearity $\omega_{q2} - 2\omega_{q1}$.

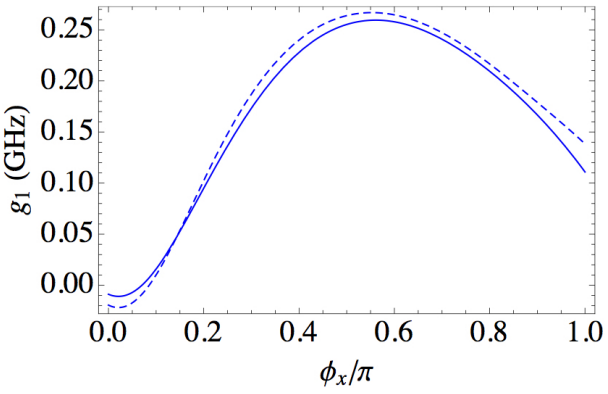

(a)

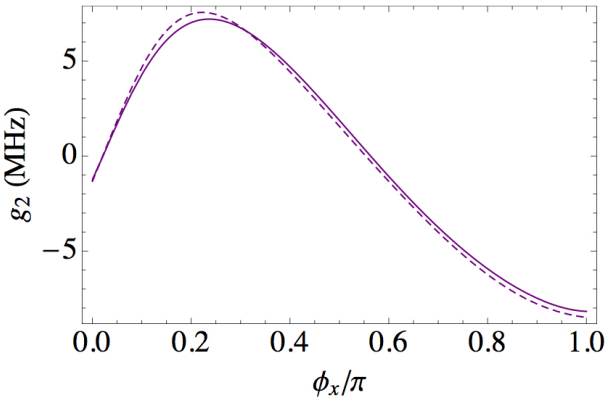

(b)

Figure 3.9: Comparison of the analytical (dashed) and numerical (solid) results. (a) Plot of $g_1 = \eta_1 \langle 0_q | \sin(\hat{\phi} + \phi'_x) | 1_q \rangle$ and the analytical value of the same coupling from (3.65). (b) Plot of $g_2 = \sqrt{2}\eta_2 \langle 0_q | \cos(\hat{\phi} + \phi'_x) | 1_q \rangle$ and $\eta'_2 r_2$ from (3.86).

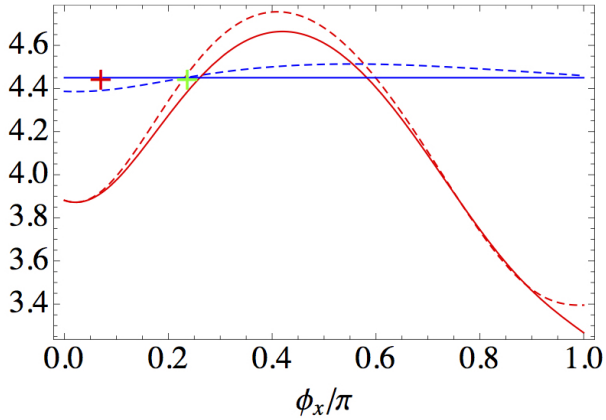

Figure 3.10: The frequencies (in GHz) 2ω in blue, and ω_q in red, with the analytical (dashed) expressions derived from (3.49) and (3.50) respectively.

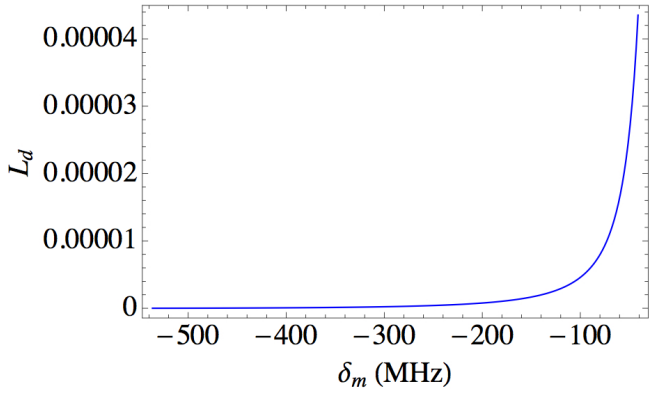

(a)

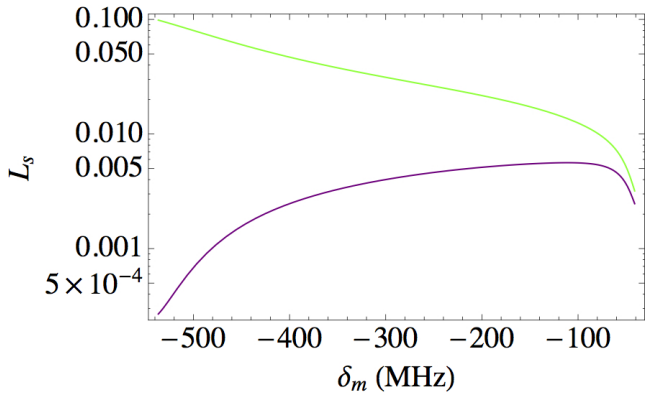

(b)

Figure 3.11: (a) A plot of the dimensionless dynamic loss L_d for $\kappa = 1$ kHZ, $\gamma = 100\kappa$ and $\epsilon^2 = 0.01$. The detuning -536 MHz $\leq \delta_{\rm m} \leq -41$ MHz. (b) The total static loss L_s in green, and the static loss without the effect of the cavity decay rate κ in purple.

Chapter 4

Circuit-QED Implementation of the Pfaffian State Parent Hamiltonian

4.1 Introduction

In nature fundamental particles are indistinguishable. For instance, all electrons in the universe are identical in all respects. One cannot put labels on different electrons to distinguish one electron from another. Therefore, exchanging any two identical particles in a system should leave all observables in the system invariant. If a system has n identical particles with positions $\mathbf{r}_1, \ldots \mathbf{r}_N$ and is described by a wavefunction $\psi(\mathbf{r}_1, \ldots, \mathbf{r}_k, \ldots, \mathbf{r}_l, \ldots, \mathbf{r}_N)$ (ignoring spin for now), exchanging particles at positions $\mathbf{r}_l$ and $\mathbf{r}_k$ should give

$$|\psi(\mathbf{r}_1, \ldots, \mathbf{r}_k, \ldots, \mathbf{r}_l, \ldots, \mathbf{r}_N)|^2 = |\psi(\mathbf{r}_1, \ldots, \mathbf{r}_l, \ldots, \mathbf{r}_k, \ldots, \mathbf{r}_N)|^2. \tag{4.1}$$

Hence, the wavefunctions can differ at most by an exchange phase,

$$\psi(\mathbf{r}_1, \ldots, \mathbf{r}_l, \ldots, \mathbf{r}_k, \ldots, \mathbf{r}_N) = e^{i\phi}\psi(\mathbf{r}_1, \ldots, \mathbf{r}_k, \ldots, \mathbf{r}_l, \ldots, \mathbf{r}_N). \tag{4.2}$$

It is taught in introductory quantum mechanics courses that the only allowable cases are $e^{i\phi} = \pm 1$, which refer to bosons and fermions respectively. But this is a naive viewpoint. While this is true in three and higher dimensions, in two dimensions, one can have any complex phase. This is because the topology of two dimensions is very different from that of higher dimensions. Exchanging two particles twice is equivalent to moving one around another in a closed loop and in three and higher dimensions, this loop can be deformed continuously to a point without ever crossing the stationary particle. However, in two dimensions it is not possible to do this without crossing the stationary particle. This leads to particle statistics which are neither bosonic, nor fermionic. Frank Wilczek coined the term "anyons" to refer to particles exhibiting these novel statistics [79].

Anyons exist as excitations in some condensed matter systems [80]. Such systems have highly non-trivial groundstates that are described as having *topological order*. The best studied example is the so called Laughlin state in the fractional quantum Hall system at filling factor $\nu = 1/3$ [81]. The filling factor $\nu = N/N_\phi$ is the ratio of the number of particles to the number of flux quanta in the system. It carries Abelian anyons with exchange phase $\phi = \pi/3$ and electric charge $\pm 1/3$. At filling factor $\nu = 1/5$, a different kind of state is observed. This state, also known as the Moore-Read state which has the form of a Pfaffian wave function [82] admits non-Abelian anyons with charge $\pm 1/4$. A good practical reason for interest in detecting and manipulating anyons is for their potential use in realization of quantum memory that is protected from decoherence. Furthermore, as shown by Freedman *et al.* [83] and Kitaev [84], certain types of non-Abelian anyons can be

manipulated for the purpose of universal quantum computation, also referred to as topological quantum computation.

Greiter *et al.* proposed a *parent* Hamiltonian with three-body interactions [85] which yields the so called Pfaffian state as its ground state, and excitations that are anyons with charge 1/4 and statistical parameter $\phi = \pi/8$. Specifically, they considered fermions in a magnetic field with repulsive three-body contact interactions of the form

$$V_{i;jk} = \sum_{\text{triples}} \delta^{(2)}(z_i - z_j)\delta^{(2)}(z_i - z_k), \tag{4.3}$$

where $z_i = x_i + iy_i$ is the complex representation of the position of particle i in two dimensions. Although the fractional quantum Hall effect occurs for fermions, bosonic systems with repulsive interactions can exhibit similar behaviors [86–88].

There have been several efforts to generate such Hamiltonians, using ultracold atomic systems, see for instance refs. [89, 90]. However, the elimination of two-body interactions while preserving the bosonic nature of excitations remains challenging [91–95], as expected for perturbatively generated three-body terms [96]. In this chapter, I propose a scheme that uses superconducting circuits to achieve this goal. In particular, I demonstrate how to engineer a three-body interaction and the synthetic magnetic field required to implement the parent Hamiltonian of Greiter *et al.* [85] on a lattice.

4.2 Parent Hamiltonian for the Pfaffian State

The parent Hamiltonian can be simulated on a discrete lattice [94]. An important question to ask is how the transition from the continuum to the discrete case modifies the ground state properties of the system. For example, a charged particle moving in a magnetic field in two dimensions has energies separated into Landau levels each of which is highly degenerate. However, in the presence of a discrete lattice, the spectrum becomes the well known Hofstadter butterfly [97].

Specifically, I want to simulate the parent Hamiltonian

$$H_p = -J\sum_{x,y}\left[\hat{a}^\dagger_{x+1,y}\hat{a}_{x,y}e^{-i\pi\alpha y} + \hat{a}^\dagger_{x,y+1}\hat{a}_{x,y}e^{+i\pi\alpha x} + \text{h.c.}\right] + \sum_{x,y}\frac{U_3}{6}\hat{a}^{\dagger 3}_{x,y}\hat{a}^3_{x,y}. \tag{4.4}$$

The indices x and y refer to different sites on a lattice where the bosons are located. There are two main ingredients in H_p. The first is the presence of the phase dependent hopping term analogous to that of a charged particle moving in a magnetic field. The flux acquired by a bosonic particle under the evolution of H_p in moving around a plaquette is $\alpha\Phi_0$ where α is a dimensionless parameter and Φ_0 is the superconducting flux quantum. One can equivalently say that the particle acquires a phase $2\pi\alpha$ when moving around a plaquette. The second main ingredient is the presence of a three-body repulsive on-site interaction of the form $\hat{a}^{\dagger 3}_{x,y}\hat{a}^3_{x,y}$.

In the discrete lattice case, there are two relevant length scales. The first is the lattice spacing a and the second is the magnetic length $l_B = \sqrt{\hbar/(qB)}$ in SI units, where q is the charge of the particle and B the magnetic field in the system.

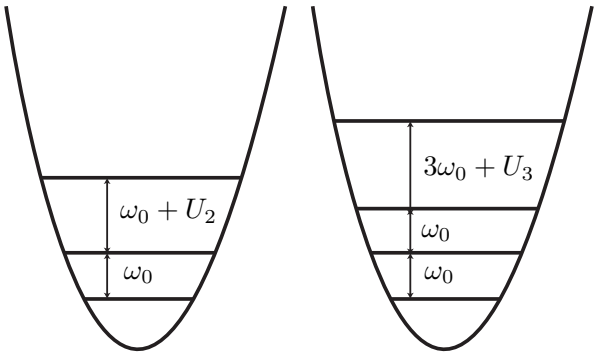

Figure 4.1: Energy levels of the system in the presence of a two and a three-body interaction.

For an electron with charge $q = e$, this reduces to $l_B = 1/\sqrt{\pi\alpha}$. In the limit where $l_B \gg a$, which corresponds to weak magnetic fields, the system is weakly sensitive to the discrete nature of the lattice.

In [86] it was argued that fractional quantum Hall physics persists until $\alpha \lesssim 0.3$ for a system of atoms in optical lattices with a similar Hamiltonian as Eq. (4.4) but with on-site two-body interactions. Their approach was to calculate the overlap of the numerically calculated ground state of the discrete Hamiltonian with the Laughlin state [81]. However, as shown in [98] the topological order in these systems can be characterized by topological invariants such as the Chern numbers even in the regime where α is larger. The study of topological invariants and topological order in these systems is beyond the scope of this thesis. Nevertheless, with the understanding that these Hamiltonians constitute a lot of interesting and important physics, in the remainder of the chapter, I will focus exclusively on the simulation of H_p [99].

4.3 Implementation of Magnetic Field

First I discuss the implementation of the magnetic hopping terms. There have been several proposals in the past to engineer such Hamiltonians in the context of circuit-QED systems [100, 101], and also proposals without breaking time reversal symmetry in photonic systems [102, 103]. Here, I follow the approach of [59]. I consider a lattice of three-body resonators coupled to each other using externally modulated squids, as depicted in Figure 4.2. The three-body resonators (to be discussed in the following section) are simply hybrid superconducting circuits biased appropriately, and with suitable parameters. The frequencies of the resonators are detuned from each other, the red denoting the one with lower frequency ω_r compared to the blue with frequency ω_b. On the horizontal connections at ordinates y, the modulations have phase $\phi_p = 2\pi\alpha y$ whereas the vertical connections have no phase difference. The modulation takes place at a frequency $\omega_p = \omega_b - \omega_r$ and amplitude $\delta\phi \ll 1$. That is

$$\phi_x(t) = \delta\phi(\cos\omega_p t + \phi_p(y)). \tag{4.5}$$

In the rotating frame with the rotating wave approximation, this induces a hopping Hamiltonian between two modes i and j of the form $\hat{a}_i^\dagger \hat{a}_j e^{i\phi_p} + \hat{a}_j^\dagger \hat{a}_i e^{-i\phi_p}$. The difference between the present case and Ref. [59] is that there the hopping was induced between two modes of the same waveguide, while here the hopping is induced between two modes of different sites.

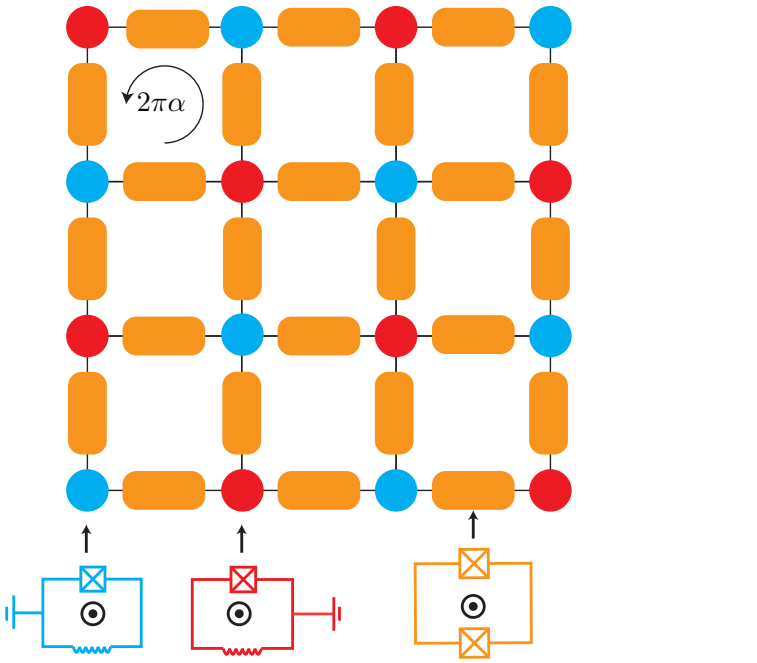

Figure 4.2: Implementation of H_p.

4.4 Three-Body Resonators

I will now consider a model for the three-body resonators occupying each site (x, y) in the lattice. Consider a Josephson junction with Josephson energy E_J, and charging energy $E_C = e^2/(2C_J)$, shunted by an inductance L in a superconducting loop as shown in Figure 4.3. This leads to an inductive energy $E_L = \Phi_0^2/(4\pi^2 L)$. Here, $\Phi_0 = h/(2e)$ is the superconducting flux quantum and h is Planck's constant. An external flux $\Phi_x \equiv \Phi_0/(2\pi)\phi_x$ threading through the superconducting loop can be used to control the energy levels of the system. The Hamiltonian of such an

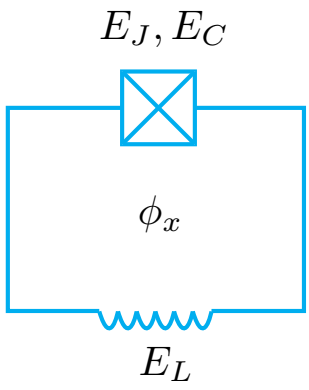

Figure 4.3: A Josephson junction shunted by an inductive loop.

inductively shunted Josephson junction can be written as

$$H = 4E_C\hat{N}^2 - E_J\cos(\hat{\phi} + \phi_x) + \frac{1}{2}E_L\hat{\phi}^2. \tag{4.6}$$

Here $\hat{\phi}$ is the operator corresponding to the phase across the junction and $\hat{N}$ is its conjugate momentum representing the number of Cooper pairs tunneling through the junction. They obey the commutation relation $[\hat{\phi}, \hat{N}] = i$. In the ϕ representation, $\hat{N} = -i\partial/\partial\phi$.

The regime considered in [104] with $E_J > E_C \gg E_L$, the so called fluxonium regime, leads to a situation where the first energy transition is different from the second transition and higher. Such nonlinearity leads to the isolation of the first transition and the system forms a qubit. In contrast, I choose a regime where the first and the second transitions are degenerate, while the third one is different as shown in the second of Figure 4.1. This happens when $E_L \approx E_J \gg E_C$, the so called hybrid regime [46].

If the Josephson term in Eq. (4.6) were ignored, one would simply have a

harmonic oscillator. A harmonic oscillator with frequency ω has a Hamiltonian

$$H = \hbar\omega\hat{c}^\dagger\hat{c}. \tag{4.7}$$

It has a linear spectrum of energy levels. However, the presence of the Josephson energy E_J induces a nonlinearity. This nonlinearity can be adjusted by tuning the strength of E_J relative to E_L. Depending on the ratio E_J/E_L, the potential well can have many minima like in the fluxonium regime. However, in the regime I am interested in, $E_L \approx E_J$ so that the potential has only one minimum. This is important since I want the first two excited states E_1 and E_2 to be linear and bosonic. Hence, the bottom of the potential cannot be too different from a harmonic potential.

In the presence of nonlinearity, the energy spectrum is no longer uniform. In the subspace consisting of the lowest states $\{|0\rangle, |1\rangle, |2\rangle, |3\rangle\}$, I define an operator $\hat{a}$ such that

$$\hat{a}\,|n\rangle = \sqrt{n}\,|n-1\rangle\,,\ n \in \{1,2,3\}, \tag{4.8}$$

$$\hat{a}\,|0\rangle = 0. \tag{4.9}$$

Similarly, $\hat{a}^\dagger$ is defined such that

$$\hat{a}^\dagger\,|n\rangle = \sqrt{n+1}\,|n+1\rangle\,,\ n \in \{0,1,2,3\}. \tag{4.10}$$

Then in this subspace $[\hat{a}, \hat{a}^\dagger] = 1$ and

$$H = \hbar\omega\hat{a}^\dagger\hat{a} + \frac{U_2}{2}\hat{a}^{\dagger 2}\hat{a}^2 + \frac{U_3}{6}\hat{a}^{\dagger 3}\hat{a}^3. \tag{4.11}$$

Alternately,

$$H = \hbar\omega\hat{n} + \frac{U_2}{2}\hat{n}(\hat{n}-1) + \frac{U_3}{6}\hat{n}(\hat{n}-1)(\hat{n}-2), \tag{4.12}$$

where $\hat{n} = \hat{a}^\dagger \hat{a}$ and $\hat{n}\,|n\rangle = n\,|n\rangle$. From this one can infer that the ground state energy $E_0 = 0$ and the energy of the first excited state is $E_1 = \hbar\omega$. The energy of the anharmonic second and third excited states are $E_2 = 2\hbar\omega + U_2$ and $E_3 = 3\hbar\omega + U_3 + 3U_2$. This leads to the expressions for the nonlinearities

$$U_2 = E_2 - 2E_1, \tag{4.13}$$

$$U_3 = E_3 - 3(E_2 - E_1). \tag{4.14}$$

I emphasize that these properties of the subspace are consistent with the observed numerical results which will be derived in the following sections.

4.5 Optimization of Parameters

Since I am working in the non-perturbative regime where $E_J \lesssim E_L$, optimization has to be done fully numerically. There are three external parameters available for tuning. The first two are the ratios $\alpha \equiv E_C/E_J$ and $\beta \equiv E_L/E_J$ which are fixed during fabrication. The third parameter is the external flux ϕ_x. I fix $\alpha = 0.05$ and vary β and ϕ_x. I then plot U_2 and U_3 as a function of these parameters in the regime where the potential of Eq. 4.6 has only a single well. The results are shown in Figure 4.4.

Recall that I am interested in a pure three-body interaction. Therefore, I seek points in these contours where U_2 vanishes. But due to numerical constraints arising from finite step size, I can only find those points for which $U_2 < 5 \times 10^{-4}$. At first thought, it might seem that all these points are valid bias points for the construction of a bosonic three-body resonator. After all, these are points where U_3

is significantly larger than U_2 which is close to zero. However, this is not sufficient. One still has to verify that the three lowest excitations behave bosonically. To do this, I adopt the following construction.

I couple two hybrid superconducting devices inductively with mutual inductance M as depicted in Figure 4.6. In the general case with devices corresponding to different parameters, the Hamiltonian of the system can be written as

$$H_C = H_1 + H_2 + V_I, \tag{4.15}$$

where for $i \in \{1, 2\}$, in the ϕ basis

$$H_i = -4E_{Ci}\frac{\partial^2}{\partial\phi^2} - E_{Ji}\cos\phi_i + \frac{1}{2}E_{Li}\left(\phi_i + \frac{\chi\sum_{j\in\{1,2\}}(1-\delta_{ij})\phi_{xj}}{2E_{Li}}\right)^2. \tag{4.16}$$

The interaction term is

$$V_I = \frac{1}{2}\chi\phi_1\phi_2. \tag{4.17}$$

The charging energy $E_{Ci} = e^2/(2C_{Ji})$. The inductive energies are given by $E_{Li} = \Phi_0^2/(4\pi^2 L_i)$, where L_i are the loop inductances, and the fluxes through the loops are denoted by ϕ_{xi}. χ is a coupling parameter with units of energy given by

$$\chi = \left(\frac{\Phi_0}{2\pi}\right)^2 \frac{M}{L_1 L_2}. \tag{4.18}$$

I let $J = \chi/2$ so that $V_I = J\phi_1\phi_2$ and from now on, assume that the two circuits are identical.

I label the three lowest eigenstates of circuit i by $\{|0_i\rangle, |1_i\rangle, |2_i\rangle\}$. The coupled Hamiltonian H_C can be written in the basis $|m\ n\rangle \equiv |m_1\ n_2\rangle$. The key idea is the following: if one initializes the system in the state $|m\ n\rangle$ where $m, n \in \{0, 1, 2\}$, then

the system evolves in such a way that m and n do not leak into the other excited manifolds $\{3, 4, \dots\}$. To check this, I analyze the system in the sub-manifolds with $m + n \in \{0, 1, 2, 3\}$. The basis states in the sub-manifolds are $\{|00\rangle\}$, $\{|01\rangle, |10\rangle\}$, $\{|02\rangle, |11\rangle, |20\rangle\}$, and $\{|03\rangle, |12\rangle, |21\rangle, |30\rangle\}$.

If the parameters are optimum, the Hamiltonian in the subspaces must have the following form. For the single excitation subspace,

$$H_1 = \begin{pmatrix} \omega_{01} & \Omega \\ \Omega & \omega_{10} \end{pmatrix}. \tag{4.19}$$

Obviously, by symmetry $\omega_{01} = \omega_{10}$. In the subspace consisting of the states with two excitations one must have a Hamiltonian of the form

$$H_2 = \begin{pmatrix} \omega_{02} & g_1 & \epsilon_1 \\ g_1 & \omega_{11} & g_1 \\ \epsilon_1 & g_1 & \omega_{20} \end{pmatrix}, \tag{4.20}$$

where $\epsilon_1 \ll g_1$. For the subspaces to be highly linear and bosonic, one must have $\omega_{02} = \omega_{20} \approx \omega_{11}$ (since $U_2 \approx 0$) and $g_1 \approx \sqrt{2}\Omega$, with $\sqrt{2}$ being the usual bosonic enhancement factor. However, the third subspace must be nonlinear. In the basis $\{|03\rangle, |12\rangle, |21\rangle, |30\rangle\}$, its Hamiltonian should look like

$$H_3 = \begin{pmatrix} \omega_{03} & g_2 & \epsilon_2 & \epsilon_3 \\ g_2 & \omega_{12} & g_3 & \epsilon_2 \\ \epsilon_2 & g_3 & \omega_{21} & g_2 \\ \epsilon_3 & \epsilon_2 & g_2 & \omega_{30} \end{pmatrix}, \tag{4.21}$$

with $\epsilon_2, \epsilon_3 \ll g_2, g_3$. The couplings $g_2 \approx \sqrt{3}\Omega$ and $g_3 \approx \sqrt{4}\Omega = 2\Omega$ are also enhanced by the usual bosonic factors. By symmetry, the energies $\omega_{03} = \omega_{30}$ and $\omega_{12} = \omega_{21}$

but crucially $\omega_{30} \neq \omega_{21}$. This is the result of the three body term U_3. If the coupled circuits are in the subspaces with two or less total excitations, they remain in these subspaces. Thus, each hybrid circuit effectively has energy levels $\{|0\rangle, |1\rangle, |2\rangle\}$ with bosonic characteristics, but separated from $|3\rangle$ with a three-body interaction.

With these additional conditions, it is revealed that the minimum value of β for which bosonic nature is retained is for $\beta = 1.4$ corresponding to $\phi_x \approx 2.683$ or $\phi_x/(2\pi) \approx 0.427$. Increasing β has the advantage that U_2 is suppressed. But at the same time U_3 gets smaller. First, I plot the energy levels and wavefunctions of the system corresponding to these parameters in Figure 4.9.

I claim that the three lowest energy states $\{|0\rangle, |1\rangle, |2\rangle\}$ are very close to the three lowest states of a harmonic oscillator. I first check this by confirming the linearity of these levels. In Figure 4.10(a), I have plotted the first few energy levels of the system as a function of ϕ_x. Then in Figure 4.10(b) I plot U_2 and U_3 as a function of ϕ_x. It is clear that U_2 changes sign at two values of ϕ_x and at these points $U_3 \approx 15E_J$ is non-zero, the first of which corresponds to our point of operation.

I also plot the matrix elements $|\langle 0|\phi|2\rangle / \langle 0|\phi|1\rangle|$ and $|\langle 1|\phi|2\rangle / (\sqrt{2}\langle 0|\phi|1\rangle)|$ in Figure 4.11. Near the optimum point where $U_2 = 0$, the matrix elements are close to the matrix elements of the harmonic oscillator operator $\hat{a} + \hat{a}^\dagger$. Therefore, one can guess that

$$\phi = \sqrt{\frac{1}{2m\hbar\omega}}(\hat{a} + \hat{a}^\dagger), \tag{4.22}$$

for some effective mass m and some frequency ω. Now the effective mass of the oscillator can only come from the charging energy E_C since it is the only energy

scale present in $\partial^2/\partial\phi^2$. Therefore, one can equate

$$-\frac{1}{2m}\frac{\partial^2}{\partial\phi^2} = -4E_C\frac{\partial^2}{\partial\phi^2} \tag{4.23}$$

to get $m = 1/(8E_C)$.

However, the variation of the frequency ω as a function of the energy scales is much more involved. That is because $V(\phi)$ is not necessarily quadratic at this point where U_2 vanishes. In fact, it has significant terms of $O(\phi^8)$. So to find ω, I rely on the numerical results (see Figure 4.9), and it shows that $\omega \approx 0.59$ GHz. Therefore, one can guess that

$$\phi = \sqrt{\frac{1}{2m\hbar\omega}}(\hat{a} + \hat{a}^\dagger) = 2\sqrt{\frac{\omega_C}{\omega}}(\hat{a} + \hat{a}^\dagger) \approx 0.58(\hat{a} + \hat{a}^\dagger), \tag{4.24}$$

and so $\langle 0|\,\phi\,|1\rangle \approx 0.58$. In Figure 4.12, I plot the matrix element $\langle 0|\,\phi\,|1\rangle$ around the optimum bias point. Therefore, in the subspace of the lowest three energy levels of the system, the operator ϕ behaves like $\hat{a} + \hat{a}^\dagger$.

Finally, I plot the wavefunctions for the states $|0\rangle$, $|1\rangle$, $|2\rangle$, and $|3\rangle$ and compare them to the eigenfunctions of a harmonic oscillator with an effective mass $m = 1/(8E_C)$ and frequency ω, but shifted to the left towards the minima of the potential $V(\phi)$ at $\phi_0 \approx -0.634$. Letting $\Lambda = \omega/(8\omega_C)$, the normalized harmonic oscillator eigenfunctions are given by

$$\psi_n(\phi) = \frac{1}{\sqrt{2^n n!}}\left(\frac{\Lambda}{\pi}\right)^{\frac{1}{4}} e^{-\Lambda\frac{(\phi-\phi_0)^2}{2}} H_n\left[\sqrt{\Lambda}(\phi - \phi_0)\right], \tag{4.25}$$

where H_n are the usual Hermite polynomials. I find that the ground, first, and second excited states are closer to the harmonic oscillator eigenfunctions than the third excited state as shown in Figure 4.13.

I now let $J/E_J = 8 \times 10^{-4} << U_3/E_J$ and study the dynamics of two coupled circuits in the subspaces with one, two, and three excitations as depicted in Figure 4.14. If one initializes the system in the states $|01\rangle$, it oscillates at frequency Ω until $|10\rangle$ is occupied. A coherent exchange of excitations takes place. Similarly, initialization in the state $|02\rangle$ results in the occupation of states $|11\rangle$ and $|20\rangle$. However, in the subspace of three excitations, the initial state $|12\rangle$ evolves into the state $|21\rangle$, but crucially, the states $|03\rangle$ and $|30\rangle$ do not get populated. This is because of the presence of U_3. Hence, the manifold of states $\{|0\rangle, |1\rangle, |2\rangle, |3\rangle\}$ can be described by the Hamiltonian

$$H = \hbar\omega\hat{a}^\dagger\hat{a} + \frac{U_3}{6}\hat{a}^{\dagger 3}\hat{a}^3. \tag{4.26}$$

4.6 Experimental Issues

Now I consider experimental issues involving the realization and detection of Pfaffian states in the proposed circuit-QED system. As discussed above the three-body interaction must be larger than the tunneling J. That is, one should make U_3 as large as possible and $J \ll U_3$. However, U_3 is bounded from above as a small fraction of the Josephson energy E_J. With a Josephson energy of tens of GHz, one can achieve U_3 of a few hundred MHz. Now J/h determines the frequency Ω at which the coherent oscillations take place. Hence, $J/h \gg T_1^{-1}, T_2^{-1}$ where T_1 and T_2 are the relaxation and decoherence times respectively. According to recent experiments, $T_1, T_2 \gg 10$ μs [25]. Therefore, having $J/h \approx 10$ MHz assures that many oscillations take place before coherence is lost.

The system is robust against charge noise. To understand the effect of charge noise in the system, I first plot the off diagonal matrix elements of $\hat{N}$ as a function of ϕ_x. The largest matrix elements are those between adjacent levels, *i.e.* $\langle n| \hat{N} |n+1\rangle$. The other matrix elements are non-zero but comparatively smaller. In fact, the matrix elements are not much more different that of a transmon as in Figure 7(a) of [41]. So one can expect the charge noise to be suppressed just as in the transmon. The diagonal matrix elements are suppressed significantly, which is expected since the eigenstates of the system are not eigenstates of $\hat{N}$ (or equivalently charge eigenstates). This is because $E_J \gg E_C$, *i.e.* one is not in the charge regime, and charge noise will not play a significant role.

The bias flux, however, needs to be controlled precisely. Recall the Hamiltonian in the two excitation subspace

$$H_2 = \begin{pmatrix} \omega_{02} & g_1 & \epsilon_1 \\ g_1 & \omega_{11} & g_1 \\ \epsilon_1 & g_1 & \omega_{20} \end{pmatrix}. \tag{4.27}$$

Preserving the bosonic nature of the system requires that $\epsilon_1 \ll g_1$. From further numerical analysis (not presented here), it is evident that U_2 being close to zero is not as strict a requirement as $\epsilon \ll g_1$. This second condition requires that one reduces U_3, which is possible by increasing β. However, as discussed before $J \ll U_3$ but $J/h \gg T_1^{-1}, T_2^{-1}$. Thus, either the flux has to be controlled precisely or the T_1 and T_2 times of the superconducting circuits have to be improved.

In experimental realizations, one needs to confirm that the system has nonlinear interactions. For this, I suggest a correlation function measurement. Specifically,

when a single site with the Hamiltonian (4.11) is driven by a weak coherent field, U_2 and U_3 can be obtained from measuring the output correlation functions

$$g^{(2)} = \frac{\langle \hat{a}^{\dagger 2} \hat{a}^2 \rangle}{\langle \hat{a}^\dagger \hat{a} \rangle^2}, \tag{4.28}$$

$$g^{(3)} = \frac{\langle \hat{a}^{\dagger 3} \hat{a}^3 \rangle}{\langle \hat{a}^\dagger \hat{a} \rangle^3}, \tag{4.29}$$

respectively. The details are in Appendix B. Such correlation function measurements have been successfully achieved in the microwave domain using quadrature amplitude measurements [105]. Alternatively, one can perform nonlinear spectroscopy to map out the anharmonicity in the energy levels [106].

4.7 Conclusions and Outlook

In conclusion, in this chapter I have demonstrated how one can implement the parent Hamiltonian for the Pfaffian state using a circuit-QED architecture. Specifically, I proposed techniques for implementation of magnetic hopping terms for bosons in a lattice, and the creation of strong pure three-body on-site interactions. This proposal for three-body interactions is notable for its simplicity, and I have argued that it is experimentally feasible.

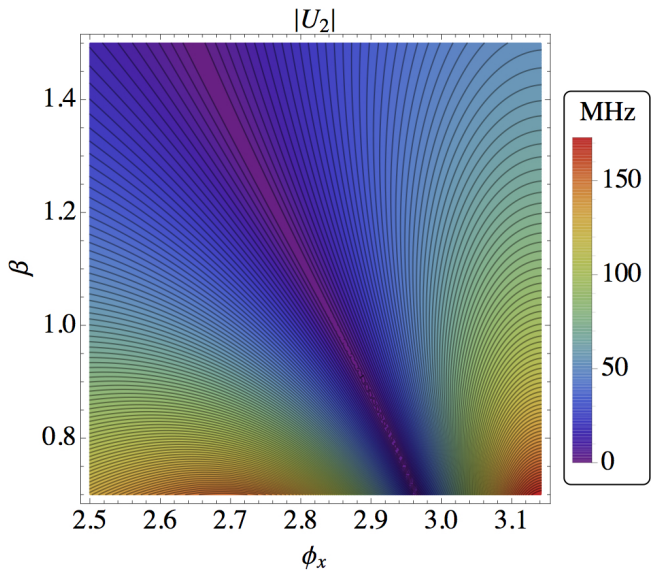

(a)

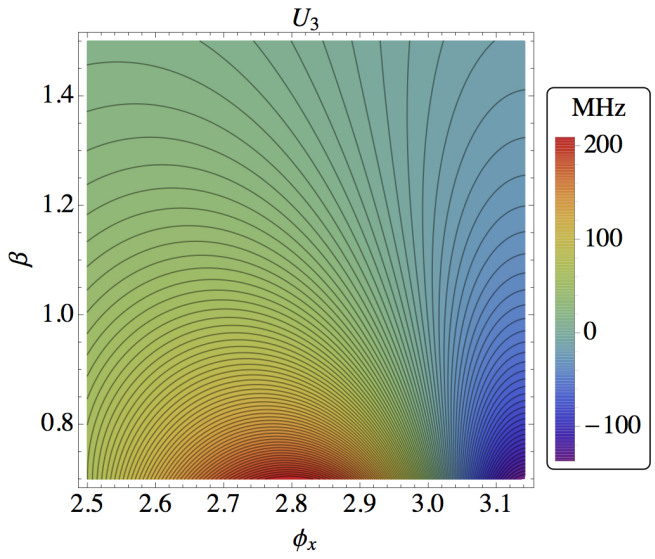

(b)

Figure 4.4: A plot of (a) $|U_2|$, and (b) U_3 as a function of ϕ_x and β.

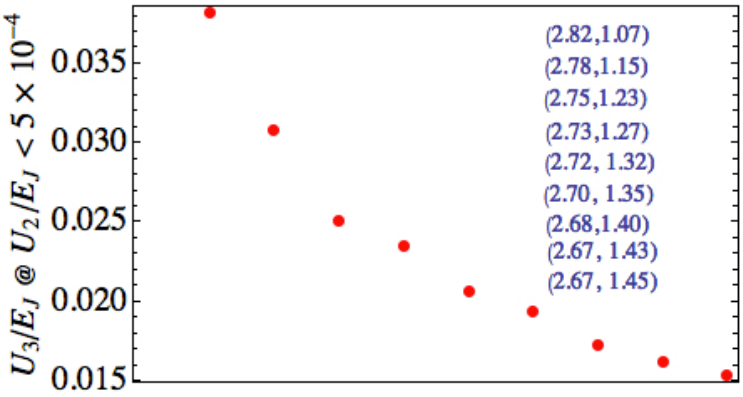

Figure 4.5: Plot of U_3 for those points where U_2 is optimized to be less than 5×10^{-4}. The coordinates refer to the pair (ϕ_x, β) at these points. Note that the plot is not meant to be continuous.

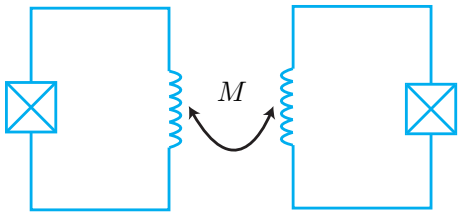

Figure 4.6: Two identical hybrid superconducting circuits coupled with mutual inductance M.

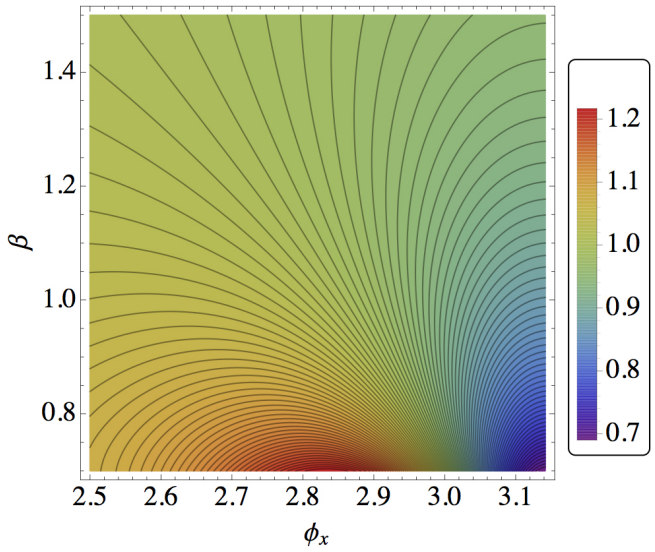

(a)

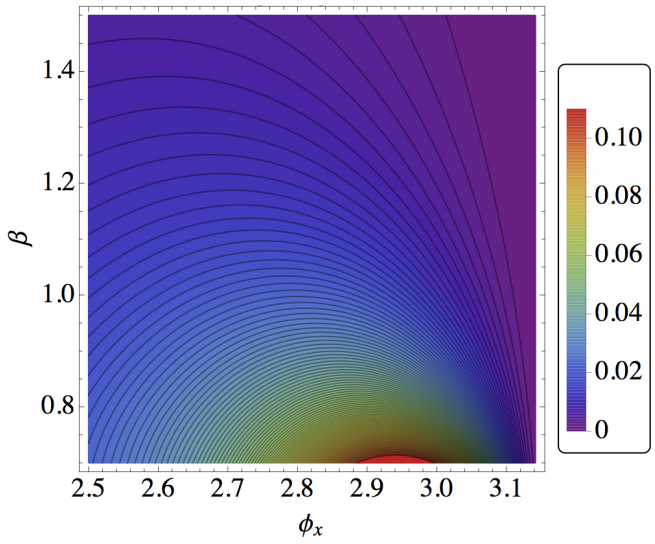

(b)

Figure 4.7: Contour plots of the norms of (a) $g_1/(\sqrt{2}\Omega)$, and (b) ϵ_1/g_1. The first needs to be close to unity and the second needs to be much smaller than unity.

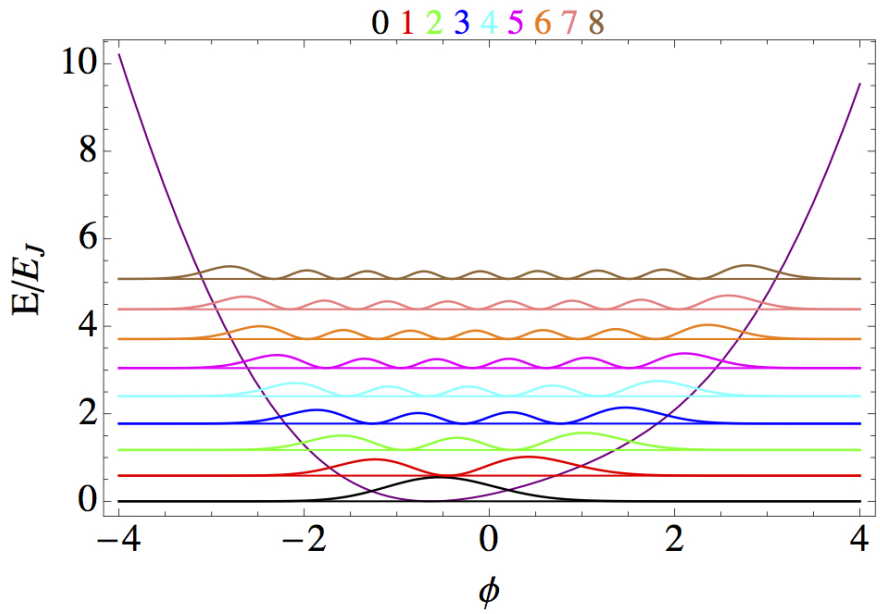

Figure 4.8: The first nine energy levels and modulus of the wavefunctions of the fluxonium circuit for $\alpha = 0.05$, $\beta = 1.4$, and $\phi_x \approx 2.683$. The purple curve represents the potential.

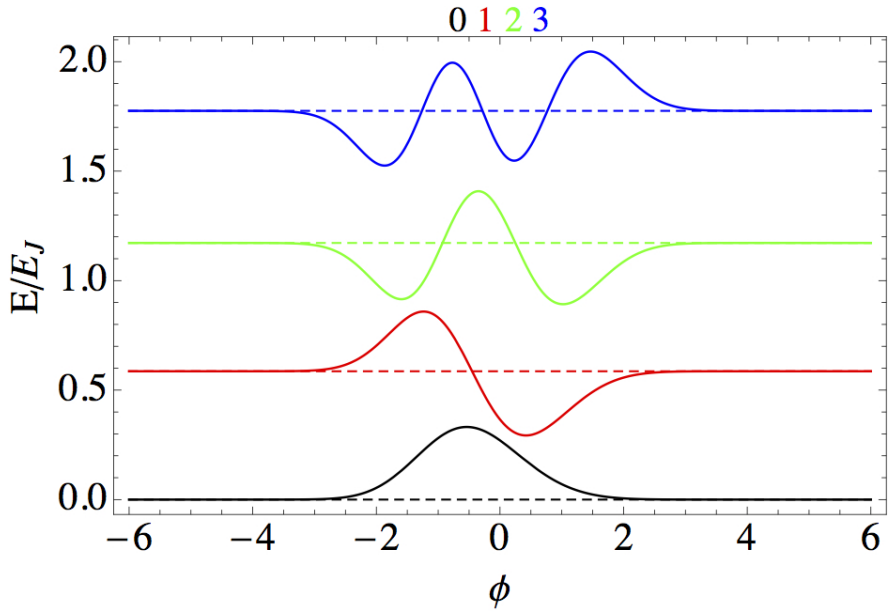

Figure 4.9: The first four energy levels and (unnormalized) wave functions.

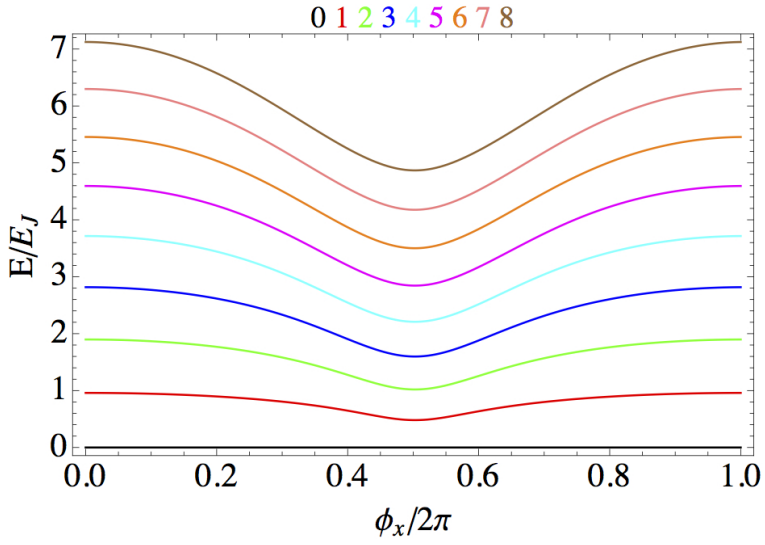

(a)

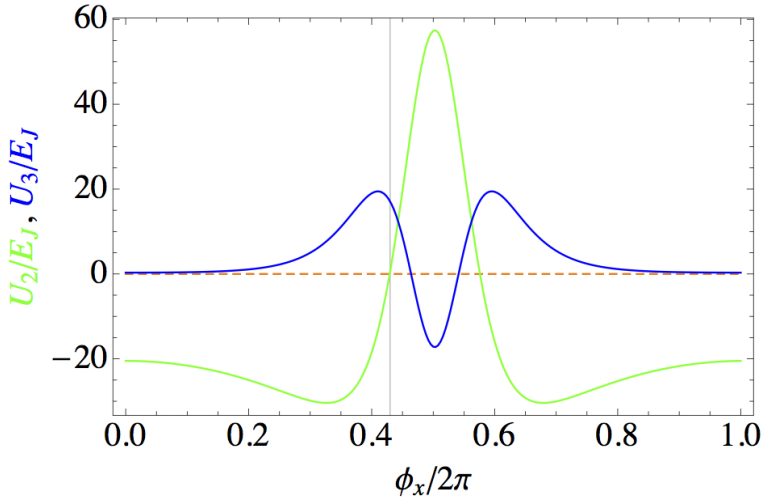

(b)

Figure 4.10: (a) The first nine energy levels of the system as a function of ϕ_x. (b) Variation of U_2 and U_3 with ϕ_x. The vertical line represents the operating point where $U_2 \approx 0$ but $U_3 > 0$, at $\phi_x \approx 2.683$.

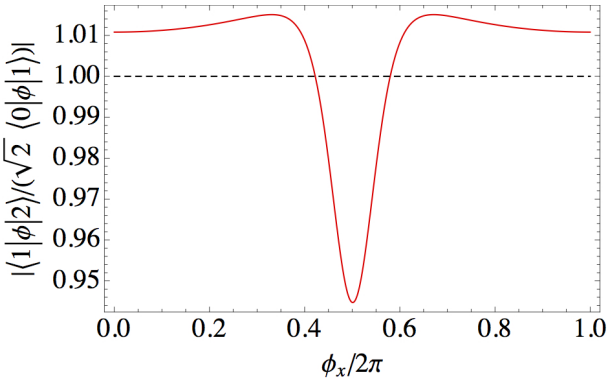

(a)

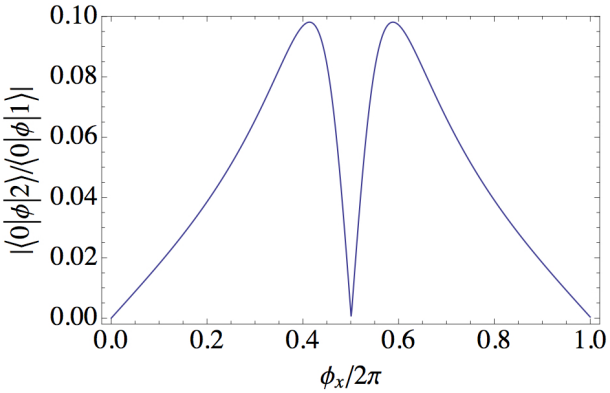

(b)

Figure 4.11: (a) The ratios $|\langle 1|\phi|2\rangle/(\sqrt{2}\langle 0|\phi|1\rangle)|$, and (b) $|\langle 0|\phi|2\rangle|/|\langle 0|\phi|1\rangle|$.

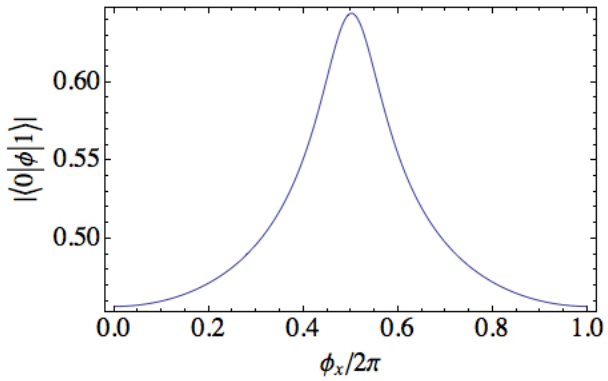

Figure 4.12: The matrix element $\langle 0|\,\phi\,|1\rangle$ whose value is close to the predicted value 0.58.

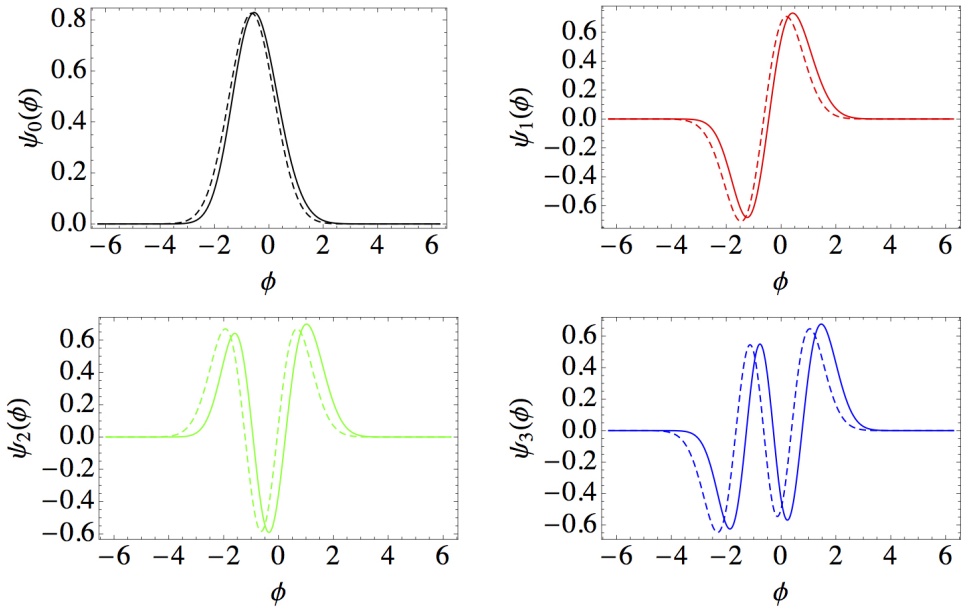

Figure 4.13: Comparison of the normalized eigenfuctions of the system (solid curves) with the harmonic oscillator eigenfunctions (dashed).

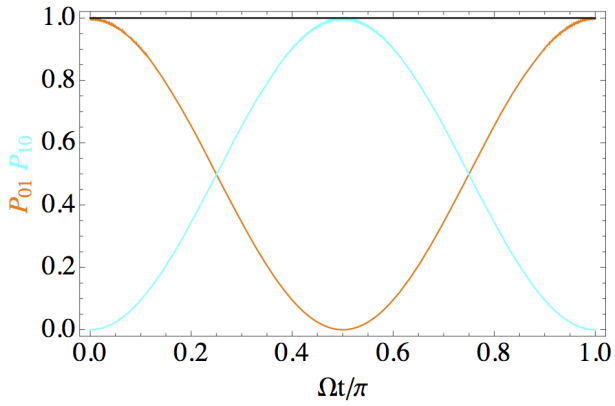

(a)

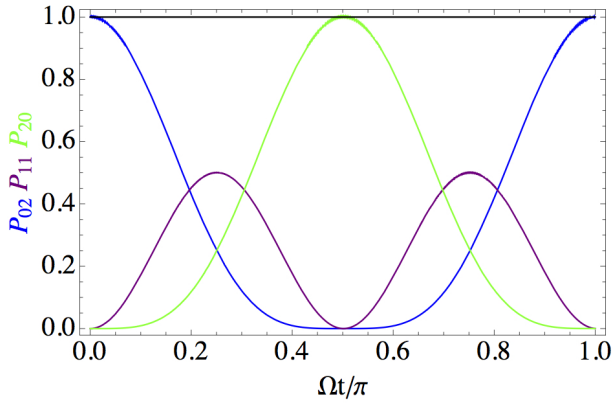

(b)

Figure 4.14: Dyamics of the (a) single, and (b) two excitation subspaces.

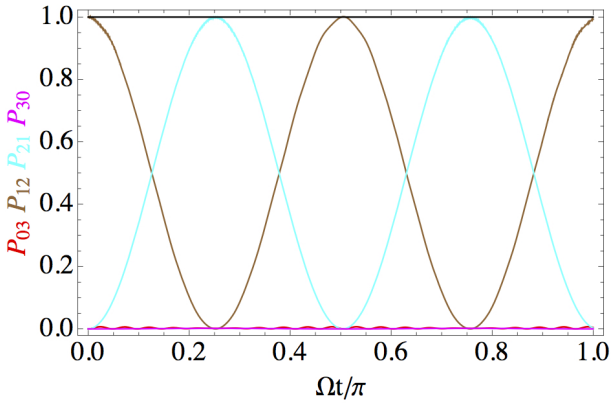

Figure 4.15: Oscillations in the three excitation manifold. Transition to $|03\rangle$ and $|30\rangle$ are suppressed due to the presence of U_3. This indicates the presence of a three-body interaction.

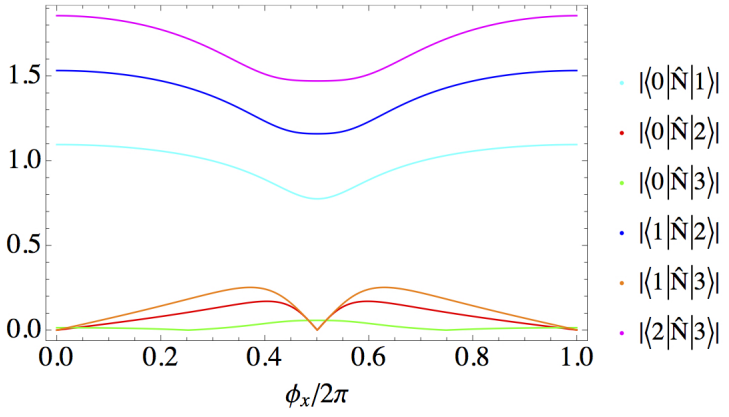

Figure 4.16: $\langle m|\,\hat{N}\,|n\rangle$ for $m \neq n$.

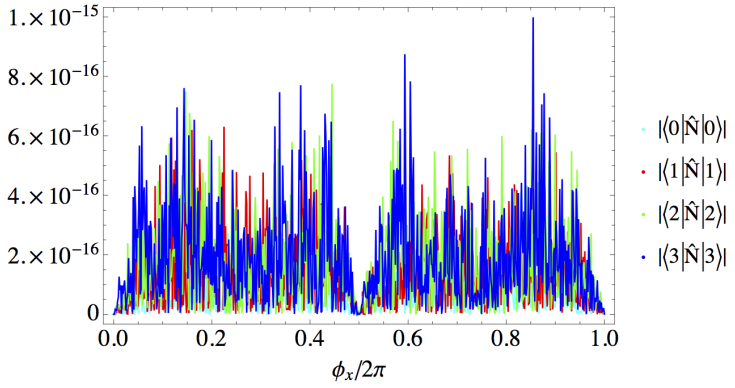

Figure 4.17: Plot of the first few diagonal matrix elements of $\hat{N}$ evaluated to machine precision.

Chapter 5

A Chemical Potential for Photons

5.1 Introduction

In statistical mechanics, a system of fixed volume V, which can exchange both energy and particles with a reservoir in equilibrium at temperature T can be described using the grand canonical ensemble [107]. The constraint on the total number of particles in the system plus reservoir gives rise to a Lagrange multiplier which is defined as the chemical potential μ. The partition function Z in the grand canonical ensemble is

$$Z(\mu, V, T) = \sum_{N=0}^{\infty} \sum_{j} e^{-\beta(E_j^{(N)} - \mu N)}, \tag{5.1}$$

where $E_j^{(N)}$ is the energy of a configuration of N particles in state j and $\beta = 1/k_B T$. In this system, the temperature and number of particles are independent variables. For an ideal Bose gas, this gives rise to an expected number of particles

$$\langle N \rangle = \sum_{\epsilon} \frac{1}{e^{\beta(\epsilon - \mu)} - 1}. \tag{5.2}$$

However, if one considers the thermodynamics of black-body radiation confined

in a cavity, one has

$$\langle N \rangle = \sum_{\epsilon} \frac{1}{e^{\beta\epsilon} - 1}, \tag{5.3}$$

i.e. the chemical potential is non-existent. This is because black body radiation confined in a cavity does not have a fixed number of excitations (photons). The average particle number does not follow a given conservation law but adjusts itself to the available thermal energy. This is the essence of the Stefan-Boltzmann law, *i.e.* the internal energy of photons per unit volume is given by

$$\frac{U}{V} = \frac{\pi^2}{15} \frac{(kT)^4}{(\hbar c)^3}, \tag{5.4}$$

and hence the specific heat is unbounded as $T \to \infty$,

$$c_V = \frac{\partial}{\partial T} \left(\frac{U}{V} \right) = \frac{4\pi^2 k^4 T^3}{15(\hbar c)^3}. \tag{5.5}$$

As one lowers the temperature of the system, the number of photons decreases to zero, as they are absorbed by the walls of the confining cavity. Hence, no macroscopic occupation of the ground state takes place.

Later, it was understood that in the absence of absorbing walls, photons can acquire a non-zero chemical potential, *e.g.* photon emission in semiconductor diodes (LED) [108]. Thus the useful concept of chemical potential started to be applied to these systems [109–111]. More recently, it was shown that photons can thermalize with a non-zero chemical potential and form a Bose-Einstein condensate [112–115] when interacting with a nonlinear medium. A Bose-Einstein condensate (BEC) [116] is a state of matter where a system comprising of bosons all collapse to the ground state. This happens when the interparticle separation becomes comparable to the

De-Broglie wavelength of the particles, which begin to overlap. The system can then be described by a single coherent macroscopic wave function. This overlap of wavefunctions can only happen if the particle number is fixed, and so photons cannot form a BEC under these conditions. What is required then is an appropriate method to keep the photon number fixed, and hence generate a chemical potential.

There have been several theoretical proposals for generating chemical potential of photons [117–119]. Here, I develop a simpler approach than these theories. In particular, by parametrically coupling a photonic system to a thermal bath, I show that a photonic system can equilibrate to the temperature of the bath, with a chemical potential given by the frequency of the parametric coupling. Although it is possible to apply this scheme to both circuit-QED and optomechanical systems, I focus on the circuit-QED part.

5.2 General Idea

Consider a system of choice with Hamiltonian H_S coupled via λH_{SB} to a bath with Hamiltonian H_B and initial state $\rho_B \propto e^{-\beta H_B}$ [120]. I will follow this approach with one small modification. I replace the coupling λ with a parametric coupling via $\lambda \to 2\lambda \cos \omega_p t$. That is, consider the Hamiltonian

$$H = H_S + 2\lambda \cos \omega_p t H_{SB} + H_B, \tag{5.6}$$

with initial conditions $\rho_B \propto e^{-\beta H_B}$. The parametric coupling will enable up and down-conversion of bath excitations to photons, which will lead to a controlled chemical potential.

To see this explicitly, I will assume that H_{SB} is bi-linear, of the form

$$H_{SB} = \sum_j (\hat{a}_j + \hat{a}_j^\dagger)\hat{B}_j, \tag{5.7}$$

where $\hat{B}_j$ is a bath operator and there exists $\hat{a}_j$, $\hat{n}_j$ such that $[\hat{a}_j, \hat{n}_j] = \hat{a}_j$, as occurs naturally for photons. This property defines particle numbers $\hat{n}_j$ and the total particle number $\hat{N} = \sum_j \hat{n}_j$.

I now consider what happens when the energy scales of the bath are small compared to ω_p, but the energy scales of the system are comparable to it. To do this, let $H_S = H_S' + H_{S,\perp}$ where $H_{S,\perp}$ includes all terms in H_S that do not commute with $\hat{N} = \sum_j \hat{n}_j$. In this regime, one can move to a rotating frame with the unitary transformation $U = e^{-it\omega_p \hat{N}}$. The transformed system Hamiltonian becomes

$$U^\dagger H_S U - i\hbar U^\dagger \frac{\partial U}{\partial t} \approx H_S' - \hbar\omega_p \hat{N}, \tag{5.8}$$

where I have neglected $U^\dagger H_{S,\perp} U$ by making the rotating wave approximation (RWA), requiring $\|H_{S,\perp}\| \ll \hbar\omega_p$.

Meanwhile, the bath Hamiltonian remains the same, while the system-bath coupling terms become

$$\left[\hat{a}_j + \hat{a}_j^\dagger + (e^{-2i\omega_p t}\hat{a}_j + e^{2i\omega_p t}\hat{a}_j^\dagger)\right]\hat{B}_j \approx \left[\hat{a}_j + \hat{a}_j^\dagger\right]\hat{B}_j. \tag{5.9}$$

The key approximation is again the RWA to neglect $e^{-2i\omega_p t}\hat{a}_j$-type terms, consistent for a bath whose two-point correlation function $\langle \hat{B}_i(t+\tau)\hat{B}_j(t)\rangle$ has a cutoff frequency $\omega_c < \omega_p$. Thus, the system bath coupling in the RWA becomes

$$H_{SB}' = \sum_j [\hat{a}_j + \hat{a}_j^\dagger]\hat{B}_j. \tag{5.10}$$

Through this set of transformations, and the rotating wave approximation, one has a new system-bath Hamiltonian which takes the traditional form

$$H = H'_S - \mu\hat{N} + \lambda H'_{SB} + H_B, \tag{5.11}$$

where one can identify $\mu \equiv \hbar\omega_p$ as the chemical potential. For weak coupling λ and an infinite bath at inverse temperature β, one can expect the system to thermalize in the long-time limit to a density matrix

$$\rho \approx e^{-\beta(H'_S - \mu\hat{N})}. \tag{5.12}$$

5.3 Circuit-QED Implementation of Parametric Hamiltonian

I now discuss a circuit-QED architecture to implement the Hamiltonian in (5.6). I model the thermal bath by a transmission line (TL) which is in thermal equilibrium at a temperature T by virtue of its interaction with some impedance $Z(\omega)$ which can be modeled by a resistor. For simplicity, I model the photonic system as a single mode bosonic oscillator. To derive an effective chemical potential for photons, I couple the photons parametrically to the thermal bath. This allows photons to exchange energy with the bath.

The parametric coupler consists of a Wheatstone configuration that acts as the right circuit (Figure 5.1) of the TL. It consists of four identical Josephson junctions in a Wheatstone bridge configuration [121]. I first derive the Hamiltonian of the coupler. For this purpose, I assume that each junction of the coupler has a large

area, and hence, a large capacitance, so that its charging energy can be ignored. In this approximation, the Hamiltonian of the Wheatstone bridge is

$$\begin{aligned} H_w &= -4E_J\left[\cos\left(\frac{\Phi_x}{4\varphi_0}\right)\cos\left(\frac{\Psi_X}{2\varphi_0}\right)\cos\left(\frac{\Psi_Y}{2\varphi_0}\right)\cos\left(\frac{\Psi_Z}{2\varphi_0}\right)\right] \\ &\quad -4E_J\left[\sin\left(\frac{\Phi_x}{4\varphi_0}\right)\sin\left(\frac{\Psi_X}{2\varphi_0}\right)\sin\left(\frac{\Psi_Y}{2\varphi_0}\right)\sin\left(\frac{\Psi_Z}{2\varphi_0}\right)\right]. \end{aligned} \tag{5.13}$$

Here $\varphi_0 = \Phi_0/(2\pi)$, $\Phi_0 = h/(2e)$ being the superconducting flux quantum. Let $\Phi_x = \Phi_0/2$ be the bias flux through the loop of the Wheatstone bridge. Furthermore, assume that the mode intensities $\Psi_X, \Psi_Y, \Psi_Z \ll \Phi_0$. Expanding H_w in $\psi_i = \Psi_i/\Phi_0$, $i \in \{X, Y, Z\}$ to third order, one gets

$$H_w = -2\sqrt{2}E_J + \mu\left(\psi_X^2 + \psi_Y^2 + \psi_Z^2\right) + \lambda\psi_X\psi_Y\psi_Z. \tag{5.14}$$

where $\mu = \sqrt{2}E_J\pi^2$ and $\lambda = -2\sqrt{2}E_J\pi^3$ have dimensions of energy.

I assume that the TL is coupled to the mode $\Psi_X = \Phi_1 - \Phi_2$ and the system is coupled to the mode $\Psi_Y = \Phi_4 - \Phi_3$. The driven mode is $\Psi_Z = \Phi_1 - \Phi_3 + \Phi_2 - \Phi_4$. The TL will be connected to an external impedance on the left at $z = 0$ via a capacitance C_L. The external impedance is in thermal equilibrium at temperature T.

The Lagrangian $\mathcal{L}_{tl}$ of the TL is derived in Appendix C. The mode Ψ_X can be written in terms of the TL modes as

$$\Psi_X = \sum_\nu \xi_\nu \varphi_{\nu L}, \tag{5.15}$$

where I have let $\varphi_{\nu L} \equiv \varphi_\nu(z = L)$, *i.e.* the boundary term. The Lagrangian of the system is

$$\mathcal{L} = \mathcal{L}_{tl} + \mathcal{L}_S - \mathcal{V}_C. \tag{5.16}$$

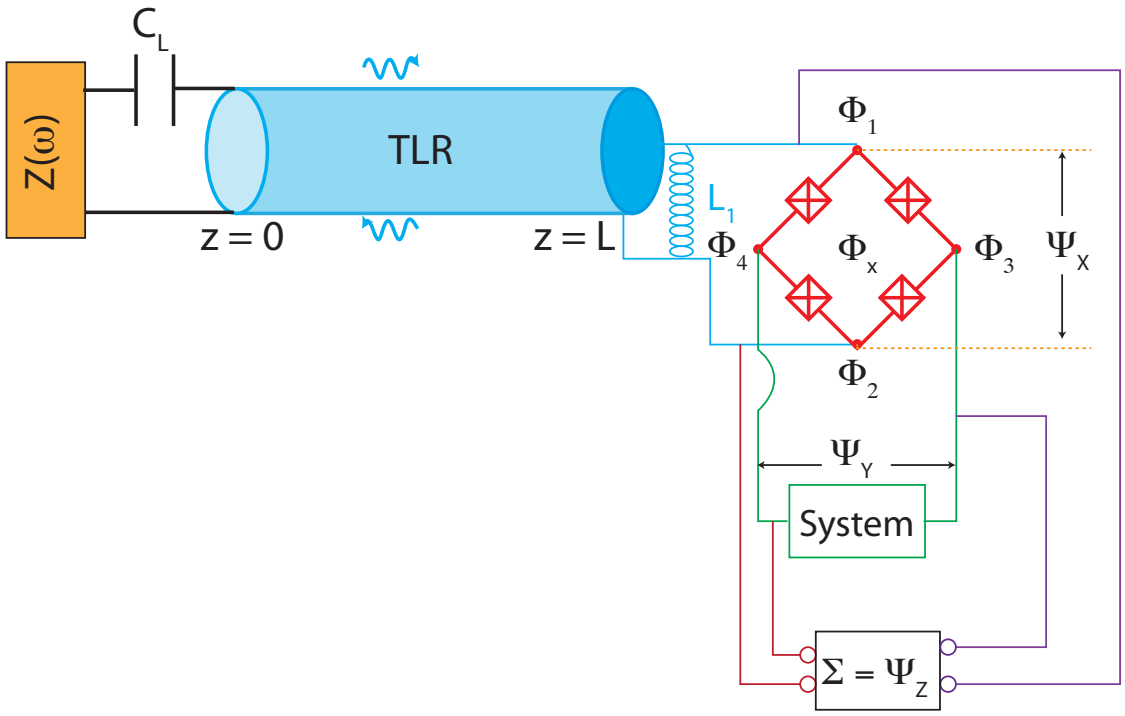

Figure 5.1: A transmission line (blue) is coupled to the mode Ψ_X. The system comprising the LC circuit is coupled to the mode Ψ_Y. The mode Ψ_Z is driven harmonically at frequency ω_p.

The individual terms are

$$\begin{aligned}
\mathcal{L}_{tl} &= \frac{1}{2}\sum_{\nu}\left[\dot{\xi}_\nu^2 - \omega_\nu^2\xi_\nu^2\right] - \frac{\mu}{\Phi_0^2}\,\Psi_X^2 \\
&= \frac{1}{2}\sum_{\nu}\left[\dot{\xi}_\nu^2 - \omega_\nu^2\xi_\nu^2\right] - \frac{\mu}{\Phi_0^2}\sum_{\mu,\nu}\xi_\mu\xi_\nu\varphi_{\mu L}\varphi_{\nu L}, \qquad (5.17)\\
\mathcal{L}_S &= \frac{1}{2}C\dot{\Psi}_Y^2 - \left(\frac{1}{2L} + \frac{\mu}{\Phi_0^2}\right)\Psi_Y^2, \qquad (5.18)\\
\mathcal{V}_C &= \frac{\lambda}{\Phi_0^3}\,\Psi_X\Psi_Y\Psi_Z. \qquad (5.19)
\end{aligned}$$

I assume that $\psi_Z = \Psi_Z/\Phi_0 = A\cos\omega_p t$ is a classical drive. I define another canoni-

cally conjugate momentum

$$q_Y = \frac{\partial \mathcal{L}}{\partial \dot{\Psi}_Y} = C\dot{\Psi}_Y. \tag{5.20}$$

Ignoring the coupling between different TLR modes, the system Hamiltonian is

$$\mathcal{H} = \mathcal{H}_{tl} + \mathcal{H}_S + \mathcal{V}, \tag{5.21}$$

where the individual Hamiltonians are

$$\begin{aligned}
\mathcal{H}_{tl} &= \sum_\nu \left[\hat{b}_\nu^\dagger \hat{b}_\nu + \frac{1}{2}\right] \hbar\omega_\nu, & (5.22)\\
\mathcal{H}_S &= \left[\frac{q_Y^2}{2C} + \left(\frac{1}{2L} + \frac{\mu}{\Phi_0^2}\right)\Psi_Y^2\right] \rightarrow \left[\hat{a}^\dagger \hat{a} + \frac{1}{2}\right]\hbar\omega_c, & (5.23)\\
\mathcal{V} &= \frac{\lambda A}{\Phi_0^2}\cos\omega_p t \sum_\nu F_\nu \psi_{\nu L}\Psi_Y \rightarrow (A\cos\omega_p t)\sum_\nu g_\nu(\hat{b}_\nu + \hat{b}_\nu^\dagger)(\hat{a}+\hat{a}^\dagger). & (5.24)
\end{aligned}$$

I have defined a coupling

$$g_\nu = \frac{\hbar\lambda}{2\Phi_0^2}\frac{\varphi_{\nu L}}{\sqrt{C\omega_c\omega_\nu}}, \tag{5.25}$$

which has dimensions of energy. I have also introduced quantum operators $\hat{a}$ and $\hat{a}^\dagger$ that satisfy $[\hat{a}, \hat{a}^\dagger] = 1$. In terms of these operators

$$\begin{aligned}
\Psi_Y &= \sqrt{\frac{\hbar}{2C\omega_c}}(\hat{a}+\hat{a}^\dagger), & (5.26)\\
q_Y &= -i\sqrt{\frac{C\omega_c\hbar}{2}}(\hat{a}-\hat{a}^\dagger), & (5.27)
\end{aligned}$$

where $\omega_c = 1/\sqrt{\tilde{L}C}$ with $1/\tilde{L} = 1/L + 2\mu/\Phi_0^2$.

One can now perform a unitary transformation $U = e^{-i\hat{a}^\dagger\hat{a}\omega_p t}$ to move into the frame moving at the pump frequency ω_p. The Hamiltonian then undergoes the

transformation

$$\begin{aligned}\tilde{H} &= U^\dagger H U - i\hbar U^\dagger \frac{\partial U}{\partial t} \\ &= \sum_\nu \left[\hat{b}_\nu^\dagger \hat{b}_\nu + \frac{1}{2}\right] \hbar\omega_\nu + \left[\hat{a}^\dagger \hat{a} + \frac{1}{2}\right] \hbar\Delta \\ &\quad + \frac{A}{2}(e^{i\omega_p t} + e^{-i\omega_p t}) \sum_\nu g_\nu (\hat{b}_\nu + \hat{b}_\nu^\dagger)(\hat{a}e^{-i\omega_p t} + \hat{a}^\dagger e^{i\omega_p t}), \end{aligned} \tag{5.28}$$

where the detuning $\Delta = \omega_c - \omega_p$. Ignoring terms oscillating rapidly with frequency ω_p in the rotated frame, and letting $G_\nu = Ag_\nu/2$, I arrive at a time independent Hamiltonian

$$\mathcal{H} = \sum_\nu \left[\hat{b}_\nu^\dagger \hat{b}_\nu + \frac{1}{2}\right] \hbar\omega_\nu + \left[\hat{a}^\dagger \hat{a} + \frac{1}{2}\right] \hbar\Delta + \sum_\nu G_\nu (\hat{b}_\nu + \hat{b}_\nu^\dagger)(\hat{a} + \hat{a}^\dagger). \tag{5.29}$$

I note that this Hamiltonian has the same form as the Hamiltonian that arises in optomechanics where a one-sided cavity with a mechanical oscillator is driven with a classical field [122]. In that case, the coupling is to a single mechanical mode μ so that

$$\mathcal{H} = \sum_\nu \left[\hat{b}_\nu^\dagger \hat{b}_\nu + \frac{1}{2}\right] \hbar\omega_\nu + \left[\hat{a}^\dagger \hat{a} + \frac{1}{2}\right] \hbar\Delta + G_\mu (\hat{b}_\mu + \hat{b}_\mu^\dagger)(\hat{a} + \hat{a}^\dagger). \tag{5.30}$$

5.4 Input-Output Formalism

Just as in the mechanical case, I assume coupling to a single TL mode μ, which is in turn coupled to a thermal bath. I also assume that the modes $\hat{a}$ and $\hat{b}_\mu$ have decay rates $\Gamma = \kappa + \kappa_i$ and γ_μ. The additional decay rate κ of $\hat{a}$ arises from coupling to the transmission line, while κ_i is the intrinsic decay rate due to other loss mechanisms in the absence of coupling to the transmission line. The decay rate

γ_μ arises from the coupling of the TL to the thermal bath. I now define the vectors

$$\mathbf{v}(t) = \begin{bmatrix} \hat{b}_\mu(t) \\ \hat{b}_\mu^\dagger(t) \\ \hat{a}(t) \\ \hat{a}^\dagger(t) \end{bmatrix}, \tag{5.31}$$

$$\xi_0(\omega) \equiv \xi_{in}(t = t_0, \omega) = \begin{bmatrix} \hat{b}_\mu(t = t_0, \omega) \\ \hat{b}_\mu^\dagger(t = t_0, \omega) \\ \hat{a}(t = t_0, \omega) \\ \hat{a}^\dagger(t = t_0, \omega) \end{bmatrix} \equiv \begin{bmatrix} \hat{b}_{\mu 0}(\omega) \\ \hat{b}_{\mu 0}^\dagger(\omega) \\ \hat{a}_0(\omega) \\ \hat{a}_0^\dagger(\omega) \end{bmatrix}. \tag{5.32}$$

I also define the matrices

$$\mathbf{A} = \begin{bmatrix} -i\omega_\mu - \gamma_\mu/2 & 0 & -iG_\mu & -iG_\mu \\ 0 & i\omega_\mu - \gamma_\mu/2 & iG_\mu & iG_\mu \\ -iG_\mu & -iG_\mu & -i\Delta - \Gamma/2 & 0 \\ iG_\mu & iG_\mu & 0 & i\Delta - \Gamma/2 \end{bmatrix}, \tag{5.33}$$

$$\mathbf{B} = \begin{bmatrix} \sqrt{\gamma_\mu} & 0 & 0 & 0 \\ 0 & \sqrt{\gamma_\mu} & 0 & 0 \\ 0 & 0 & \sqrt{\kappa} & 0 \\ 0 & 0 & 0 & \sqrt{\kappa} \end{bmatrix}, \tag{5.34}$$

$$\mathbf{C} = \begin{bmatrix} \sqrt{\gamma_\mu} & 0 & 0 & 0 \\ 0 & \sqrt{\gamma_\mu} & 0 & 0 \\ 0 & 0 & \Gamma/\sqrt{\kappa} & 0 \\ 0 & 0 & 0 & \Gamma/\sqrt{\kappa} \end{bmatrix}. \tag{5.35}$$

The Heisenberg equations of motion for the system with Hamiltonian $\mathcal{H}_S$ can be written as

$$\frac{d}{dt}\mathbf{v}(t) = \mathbf{A}\mathbf{v}(t) - \mathbf{B}\xi_{in}(t). \tag{5.36}$$

Let the input field column vector be

$$\xi_{in}(t) = \begin{bmatrix} \hat{b}_{\mu,in}(t) \\ \hat{b}^{\dagger}_{\mu,in}(t) \\ \hat{a}_{in}(t) \\ \hat{a}^{\dagger}_{in}(t) \end{bmatrix} = \frac{1}{\sqrt{2\pi}} \int_{-\infty}^{\infty} d\omega \; e^{-i\omega(t-t_0)} \xi_0(\omega), \tag{5.37}$$

where $t_0 < t$ is the initial time. This vector consists of components of the noise affecting the system. Define

$$\tilde{\mathbf{v}}(\omega) = \frac{1}{\sqrt{2\pi}} \int_{-\infty}^{\infty} e^{i\omega(t-t_0)} \; \mathbf{v}(t) \; d\omega. \tag{5.38}$$

The corresponding inverse relation is given by

$$\mathbf{v}(t) = \frac{1}{\sqrt{2\pi}} \int_{-\infty}^{\infty} e^{-i\omega(t-t_0)} \; \tilde{\mathbf{v}}(\omega) \; d\omega. \tag{5.39}$$

Equation (5.36) then becomes

$$\begin{aligned} & \frac{1}{\sqrt{2\pi}} \int_{-\infty}^{\infty} (-i\omega) e^{-i\omega(t-t_0)} \; \tilde{\mathbf{v}}(\omega) \; d\omega \\ = \; & \frac{1}{\sqrt{2\pi}} \int_{-\infty}^{\infty} e^{-i\omega(t-t_0)} \; \mathbf{A}\tilde{\mathbf{v}}(\omega) \; d\omega - \frac{1}{\sqrt{2\pi}} \int_{-\infty}^{\infty} e^{-i\omega(t-t_0)} \; \mathbf{B}\xi_0(\omega) \; d\omega. \end{aligned} \tag{5.40}$$

This implies that

$$\int_{-\infty}^{\infty} d\omega \; e^{-i\omega(t-t_0)} \left[(i\omega\mathbf{I} + \mathbf{A})\tilde{\mathbf{v}}(\omega) - \mathbf{B}\xi_0(\omega) \right] = 0. \tag{5.41}$$

Thus, $(i\omega\mathbf{I} + \mathbf{A})\tilde{\mathbf{v}}(\omega) - \mathbf{B}\xi_0(\omega) = 0$ or $\tilde{\mathbf{v}}(\omega) = (i\omega\mathbf{I} + \mathbf{A})^{-1}\mathbf{B}\xi_0(\omega) \equiv \mathbf{M}\mathbf{B}\xi_0(\omega)$, where $\mathbf{M} = (i\omega\mathbf{I} + \mathbf{A})^{-1}$.

Let the output field column vector be

$$\xi_{out}(t) = \begin{bmatrix} \hat{b}_{\mu,out}(t) \\ \hat{b}^{\dagger}_{\mu,out}(t) \\ \hat{a}_{out}(t) \\ \hat{a}^{\dagger}_{out}(t) \end{bmatrix} = \frac{1}{\sqrt{2\pi}} \int_{-\infty}^{\infty} \tilde{\xi}_{out}(\omega) e^{-i\omega(t-t_0)} d\omega. \tag{5.42}$$

The input-output relations for $\hat{a}$ and $\hat{b}_\mu$ are

$$\hat{a}_{out}(t) - \hat{a}_{in}(t) = \frac{\Gamma}{\sqrt{\kappa}} \hat{a}(t), \tag{5.43}$$

$$\hat{b}_{\mu,out}(t) - \hat{b}_{\mu,in}(t) = \sqrt{\gamma_\mu} \hat{b}_\mu(t). \tag{5.44}$$

I therefore have the input output relations in matrix form as

$$\begin{aligned} \tilde{\xi}_{out}(\omega) &= \xi_0(\omega) + \mathbf{C}\tilde{\mathbf{v}}(\omega) \\ &= \xi_0(\omega) + \mathbf{CMB}\xi_0(\omega) \\ &= (\mathbf{I} + \mathbf{CMB})\, \xi_0(\omega) \\ &\equiv \mathbf{S}\xi_0(\omega). \end{aligned} \tag{5.45}$$

Using this result, one can write the output operators $\hat{a}_{out}$ and $\hat{a}^{\dagger}_{out}$ as

$$\begin{bmatrix} \hat{a}_{out}(\omega) \\ \hat{a}^{\dagger}_{out}(\omega) \end{bmatrix} = \begin{bmatrix} \bar{\zeta}_\mu(\omega) & \bar{\eta}_\mu(\omega) \\ \bar{\eta}^*_\mu(-\omega) & \bar{\zeta}^*_\mu(-\omega) \end{bmatrix} \begin{bmatrix} \hat{b}_{\mu 0}(\omega) \\ \hat{b}^{\dagger}_{\mu 0}(\omega) \end{bmatrix} + \begin{bmatrix} \bar{\alpha}(\omega) & \bar{\beta}(\omega) \\ \bar{\beta}^*(-\omega) & \bar{\alpha}^*(-\omega) \end{bmatrix} \begin{bmatrix} \hat{a}_0(\omega) \\ \hat{a}^{\dagger}_0(\omega) \end{bmatrix}, \tag{5.46}$$

where the frequency dependent parameters are given by

$$\begin{aligned}
\bar{\zeta}_\mu(\omega) &= \frac{4\Gamma\sqrt{\gamma_\mu}G_\mu\left(2\left(\omega+\omega_\mu\right)-i\gamma_\mu\right)\left(\Gamma+2i(\Delta+\omega)\right)}{D_1(\omega)}, \\
\bar{\eta}_\mu(\omega) &= \frac{4\Gamma\sqrt{\gamma_\mu}G_\mu\left(2(\omega-\omega_\mu)-i\gamma_\mu\right)\left(\Gamma+2i(\Delta+\omega)\right)}{D_1(\omega)}, \\
\bar{\alpha}(\omega) &= -\frac{[(\Gamma-2i\Delta)^2+4\omega^2]+32G_\mu^2\omega_\mu(i\Gamma+2\Delta)+4\omega_\mu^2[(\Gamma-2i\Delta)^2+4\omega^2]}{D_2(\omega)/(\gamma_\mu-2i\omega)^2}, \\
\bar{\beta}(\omega) &= -\frac{32iG_\mu^2\Gamma\omega_\mu}{D_2(\omega)},
\end{aligned} \tag{5.47}$$

with $D_1(\omega)$ and $D_2(\omega)$ given by

$$\begin{aligned}
D_1(\omega) &= \sqrt{\kappa}[(\gamma_\mu+2i\omega)^2\left(4\Delta^2+(\Gamma+2i\omega)^2\right)+4\omega_\mu^2\left(4\Delta^2+(\Gamma+2i\omega)^2\right) \\
&\quad -64\Delta G_\mu^2\omega_\mu], \qquad (5.48) \\
D_2(\omega) &= [4\Delta^2+(\Gamma-2i\omega)^2](\gamma_\mu-2i\omega)^2-64G_\mu^2\Delta\omega_\mu \\
&\quad +4\omega_\mu^2[4\Delta^2+(\Gamma-2i\omega)^2]. \qquad (5.49)
\end{aligned}$$

I am interested in the field inside the cavity and can write

$$\begin{bmatrix} \hat{a}(\omega) \\ \hat{a}^\dagger(\omega) \end{bmatrix} = \begin{bmatrix} \zeta_\mu(\omega) & \eta_\mu(\omega) \\ \eta_\mu^*(-\omega) & \zeta_\mu^*(-\omega) \end{bmatrix} \begin{bmatrix} \hat{b}_{\mu 0}(\omega) \\ \hat{b}_{\mu 0}^\dagger(\omega) \end{bmatrix} + \begin{bmatrix} \alpha(\omega) & \beta(\omega) \\ \beta^*(-\omega) & \alpha^*(-\omega) \end{bmatrix} \begin{bmatrix} \hat{a}_0(\omega) \\ \hat{a}_0^\dagger(\omega) \end{bmatrix}. \tag{5.50}$$

The corresponding frequency dependent parameters for the intracavity field are

$$\begin{aligned}
\zeta_\mu(\omega) &= \frac{4G_\mu\sqrt{\gamma_\mu}[\Gamma-2i(\Delta+\omega)][i\gamma_\mu+2(\omega+\omega_\mu)]}{[4\Delta^2+(\Gamma-2i\omega)^2](\gamma_\mu-2i\omega)^2-64G_\mu^2\Delta\omega_\mu+4\omega_\mu^2[4\Delta^2+(\Gamma-2i\omega)^2]}, \\
\eta_\mu(\omega) &= \frac{4G_\mu\sqrt{\gamma_\mu}[\Gamma-2i(\Delta+\omega)][i\gamma_\mu+2(\omega-\omega_\mu)]}{[4\Delta^2+(\Gamma-2i\omega)^2](\gamma_\mu-2i\omega)^2-64G_\mu^2\Delta\omega_\mu+4\omega_\mu^2[4\Delta^2+(\Gamma-2i\omega)^2]}.
\end{aligned} \tag{5.51}$$

Similarly,

$$\begin{aligned}\alpha(\omega) &= \frac{2i\sqrt{\kappa}[-16G_\mu^2\omega_\mu + (i\Gamma + 2(\Delta+\omega))(\gamma_\mu - 2i(\omega-\omega_\mu)(\gamma_\mu - 2i(\omega+\omega_\mu))]}{[4\Delta^2 + (\Gamma - 2i\omega)^2](\gamma_\mu - 2i\omega)^2 - 64G_\mu^2\Delta\omega_\mu + 4\omega_\mu^2[4\Delta^2 + (\Gamma-2i\omega)^2]}, \\ \beta(\omega) &= -\frac{32iG_\mu^2\sqrt{\kappa}\omega_\mu}{[4\Delta^2 + (\Gamma - 2i\omega)^2](\gamma_\mu - 2i\omega)^2 - 64G_\mu^2\Delta\omega_\mu + 4\omega_\mu^2[4\Delta^2 + (\Gamma-2i\omega)^2]}.\end{aligned} \tag{5.52}$$

5.5 Correlation Functions and Thermal Spectrum

Now I calculate the correlation functions for the photon intracavity field. One can write the input field operators in terms of their Fourier components as

$$\hat{a}_{in}(t) = \frac{1}{\sqrt{2\pi}}\int_{-\infty}^{\infty} d\omega\ e^{-i\omega(t-t_0)}\hat{a}_0(\omega), \tag{5.53}$$

$$\hat{a}_{in}^\dagger(t) = \frac{1}{\sqrt{2\pi}}\int_{-\infty}^{\infty} d\omega\ e^{-i\omega(t-t_0)}\hat{a}_0^\dagger(\omega) = \frac{1}{\sqrt{2\pi}}\int_{-\infty}^{\infty} d\omega\ e^{i\omega(t-t_0)}\hat{a}_0^\dagger(-\omega). \tag{5.54}$$

Note that

$$[\hat{a}_0(-\omega)]^\dagger = \frac{1}{\sqrt{2\pi}}\int_{-\infty}^{\infty} dt\ e^{i\omega(t-t_0)}\hat{a}_{in}^\dagger(t) = \hat{a}_0^\dagger(\omega). \tag{5.55}$$

The commutator $[\hat{a}_{in}(t), \hat{a}_{in}^\dagger(t')] = \delta(t-t')$ gives $[\hat{a}_0(\omega), \hat{a}_0^\dagger(-\omega')] = \delta(\omega-\omega')$. Hence, $\hat{a}_0^\dagger(-\omega')$ and $\hat{a}_0(\omega)$ are the relevant Bose operators. One can similarly define $\hat{b}_{\mu 0}^\dagger(-\omega')$ and $\hat{b}_{\mu 0}(\omega)$.

One has the correlations

$$\langle \hat{b}_{\mu 0}^\dagger(-\omega')\hat{b}_{\mu 0}(\omega)\rangle = \delta_{\mu\mu}\delta(\omega'-\omega)n_1(\hbar\omega'), \tag{5.56}$$

$$\langle \hat{b}_{\mu 0}(-\omega')\hat{b}_{\mu 0}^\dagger(\omega)\rangle = \delta_{\mu\mu}\delta(\omega'-\omega)(1+n_1(\hbar\omega')), \tag{5.57}$$

$$\langle \hat{a}_0^\dagger(-\omega')\hat{a}_0(\omega)\rangle = \delta(\omega'-\omega)n_2(\hbar\omega'), \tag{5.58}$$

$$\langle \hat{a}_0(-\omega')\hat{a}_0^\dagger(\omega)\rangle = \delta(\omega'-\omega)(1+n_2(\hbar\omega')). \tag{5.59}$$

where $n_i(\hbar\omega) = (e^{\beta_i\hbar\omega} - 1)^{-1}$, $\beta_i = 1/k_B T_i$. All other commutators vanish. The spectrum for the intracavity field can then be calculated to be

$$\begin{aligned}
&\left\langle \hat{a}^\dagger(-\omega')\hat{a}(\omega)\right\rangle \\
= \;& \eta_\mu^*(\omega')\zeta_\mu(\omega)\langle \hat{b}_{\mu 0}(-\omega')\hat{b}_{\mu 0}(\omega)\rangle + \eta_\mu^*(\omega')\eta_\mu(\omega)\langle \hat{b}_{\mu 0}(-\omega')\hat{b}_{\mu 0}^\dagger(\omega)\rangle \\
&+\zeta_\mu^*(\omega')\zeta_\mu(\omega)\langle \hat{b}_{\mu 0}^\dagger(-\omega')\hat{b}_{\mu 0}(\omega)\rangle + \zeta_\mu^*(\omega')\eta_\mu(\omega)\langle \hat{b}_{\mu 0}^\dagger(-\omega')\hat{b}_{\mu 0}^\dagger(\omega)\rangle \\
&+\beta^*(\omega')\alpha(\omega)\langle \hat{a}_0(-\omega')\hat{a}_0(\omega)\rangle + \beta^*(\omega')\beta(\omega)\langle \hat{a}_0(-\omega')\hat{a}_0^\dagger(\omega)\rangle \\
&+\alpha^*(\omega')\alpha(\omega)\langle \hat{a}_0^\dagger(-\omega')\hat{a}_0(\omega)\rangle + \alpha^*(\omega')\beta(\omega)\langle \hat{a}_0^\dagger(-\omega')\hat{a}_0^\dagger(\omega)\rangle. \qquad (5.60)
\end{aligned}$$

I will now assume that the noise influencing the system is at zero temperature so that $n_2 = 0$, *i.e.* it is vacuum noise. Then

$$\begin{aligned}
&\left\langle \hat{a}^\dagger(-\omega')\hat{a}(\omega)\right\rangle \\
= \;& \eta_\mu^*(\omega')\eta_\mu(\omega)\langle \hat{b}_{\mu 0}(-\omega')\hat{b}_{\mu 0}^\dagger(\omega)\rangle + \zeta_\mu^*(\omega')\zeta_\mu(\omega)\langle \hat{b}_{\mu 0}^\dagger(-\omega')\hat{b}_{\mu 0}(\omega)\rangle \\
&+\beta^*(\omega')\beta(\omega)\langle \hat{a}_0(-\omega')\hat{a}_0^\dagger(\omega)\rangle \\
= \;& \eta_\mu^*(\omega')\eta_\mu(\omega)\delta(\omega'-\omega)(1 + n_1(\hbar\omega')) + \zeta_\mu^*(\omega')\zeta_\mu(\omega)\delta(\omega'-\omega)n_1(\hbar\omega') \\
&+\beta^*(\omega')\beta(\omega)\delta(\omega'-\omega). \qquad (5.61)
\end{aligned}$$

Since one wants the system to be in thermal equilibrium with the bath in the steady state, this means that energy will have to be extracted from the bath by the system and vice versa. Note that the coupling in the Hamiltonian (5.29) has terms like $\hat{a}\hat{b}_\mu^\dagger + \hat{a}^\dagger\hat{b}_\mu$ and $\hat{a}\hat{b}_\mu + \hat{a}^\dagger\hat{b}_\mu^\dagger$. The first leads to energy exchange with the conservation of the total number of photons and phonons, while the second leads to squeezing. It is well known from optomechanics that if $\Delta = \omega_\mu$ for some μ, the former interaction will dominate [122]. Note that my definition of Δ here is different

from the definition in the literature in the sign. For frequencies $\omega = \omega_\mu \pm \delta$ with $\delta \ll \omega_\mu$, one can make further simplifications to $\left\langle \hat{a}^\dagger(-\omega')\hat{a}(\omega)\right\rangle$. First, I impose the constraint that

$$\left[\frac{|\eta_\mu(\omega)|^2}{|\zeta_\mu(\omega)|^2}\right]_{\omega=\omega_\mu} = \frac{\gamma_\mu^2}{\gamma_\mu^2 + 16\omega_\mu^2} \ll 1. \tag{5.62}$$

Similarly, I require

$$\left[\frac{|\beta_\mu(\omega)|^2}{|\zeta_\mu(\omega)|^2}\right]_{\omega=\omega_\mu} = \frac{64G_\mu^2\kappa\omega_\mu^2}{(\Gamma^2 + 16\omega_\mu^2)(\gamma_\mu^3 + 16\gamma_\mu\omega_\mu^2)} \ll 1. \tag{5.63}$$

Then in this limit, considering coupling to a single mode μ, I get

$$\left\langle \hat{a}^\dagger(-\omega')\hat{a}(\omega)\right\rangle = \zeta_\mu^*(\omega')\zeta_\mu(\omega)\delta(\omega' - \omega)n_1(\hbar\omega'). \tag{5.64}$$

In this regime, approximately

$$\begin{aligned} \zeta_\mu(\omega) &\approx \frac{4iG_\mu\sqrt{\gamma_\mu}}{4G_\mu^2 + [\Gamma + 2i(\omega_\mu - \omega)][\gamma_\mu - 2i(\omega - \omega_\mu)]}, \\ \alpha(\omega) &\approx -\frac{2\sqrt{\kappa}(\gamma - 2i(\omega - \omega_\mu))}{4G_\mu^2 + [\Gamma + 2i(\omega_\mu - \omega)][\gamma_\mu - 2i(\omega - \omega_\mu)]}. \end{aligned} \tag{5.65}$$

The relevant quantity is $|\zeta_\mu(\omega)|^2$ which I plot in Figure 5.2 with the choice of parameters $\omega_\mu/\kappa = 300$, $G_\mu/\kappa = 20$, $\kappa_i/\kappa = 0.1$, $\gamma_\mu/\kappa = 80$. This is the regime where the constraints (5.62) and (5.63) are satisfied. There is a peak in the approximate value of $|\zeta_\mu(\omega)|^2$ at $\omega = \omega_\mu$ as can be evaluated from (5.65), provided $8G_\mu^2 < \gamma_\mu^2 + \Gamma^2$ as depicted in Figure 5.3(a).

The approximate bandwidth B_w of $|\zeta_\mu(\omega)|^2$ is shown in Figure 5.4. Over this bandwidth, $|\zeta_\mu(\omega)|^2$ is approximately constant and

$$\left\langle \hat{a}^\dagger(-\omega)\hat{a}(\omega)\right\rangle \approx \frac{16G_\mu^2\gamma_\mu}{(4G_\mu^2 + \gamma_\mu\Gamma)^2}\left(\frac{1}{e^{\beta\hbar\omega} - 1}\right). \tag{5.66}$$

Rotating back to the lab frame I get,

$$\left\langle \hat{a}^{\dagger}(-\omega)\hat{a}(\omega)\right\rangle \approx \frac{16G_{\mu}^{2}\gamma_{\mu}}{(4G_{\mu}^{2}+\gamma_{\mu}\Gamma)^{2}}\left(\frac{1}{e^{\beta\hbar(\omega-\omega_{p})}-1}\right). \tag{5.67}$$

Thus, the system has an effective chemical potential $\mu = \hbar\omega_p$ over the bandwidth B_w.

5.6 Conclusions and Outlook

In this chapter I showed that parametrically modulating the coupling between a generic system and a thermal bath leads to thermalization of the system. In particular, for a photonic system, this leads to thermalization with a chemical potential equal to the frequency of the parametric coupling. A similar analysis for photons coupled to an optomechanical system in thermal equilibrium leads to the same conclusions.

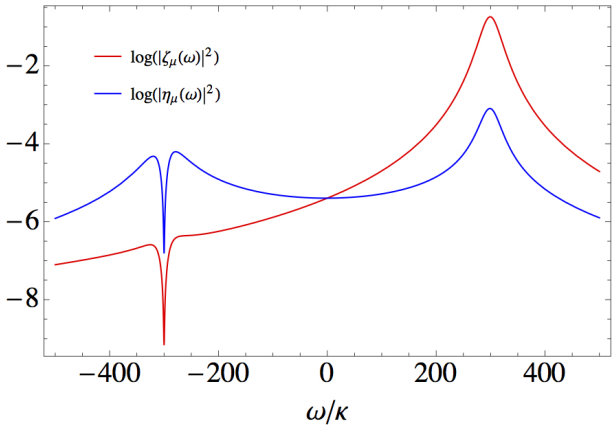

(a) $(\omega_\mu, G_\mu, \kappa_i, \gamma_\mu)/\kappa = (300, 20, 0.1, 80)$.

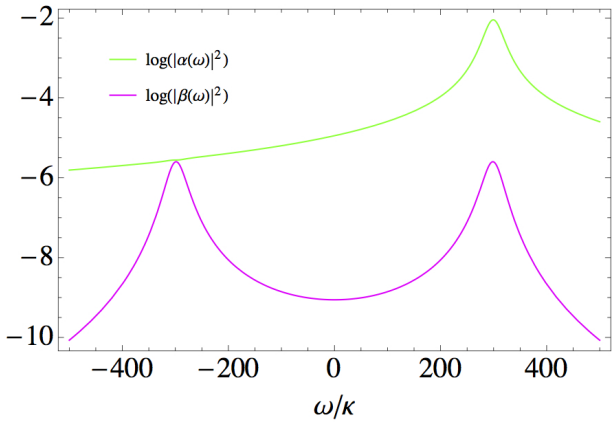

(b) $(\omega_\mu, G_\mu, \kappa_i, \gamma_\mu)/\kappa = (300, 20, 0.1, 80)$.

Figure 5.2: Plot of the logarithm of the spectral coefficients for $\Delta = \omega_\mu = 300\kappa$.

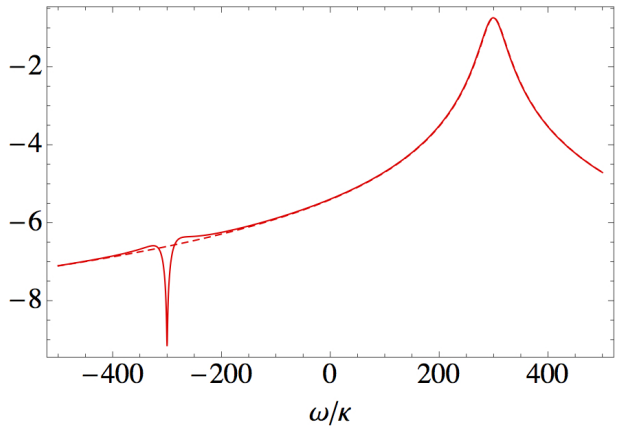

(a) $(\omega_\mu, G_\mu, \kappa_i, \gamma_\mu)/\kappa = (300, 20, 0.1, 80)$.

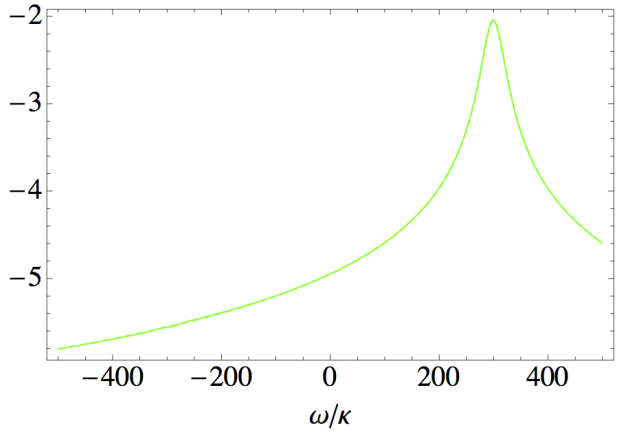

(b) $(\omega_\mu, G_\mu, \kappa_i, \gamma_\mu)/\kappa = (300, 20, 0.1, 80)$.

Figure 5.3: Plot of the approximate values (dotted) of $\log(|\zeta_\mu(\omega)|^2)$ and $\log(|\alpha(\omega)|^2)$ for $\Delta = \omega_\mu = 300\kappa$. For positive frequencies, the results are in good agreement.

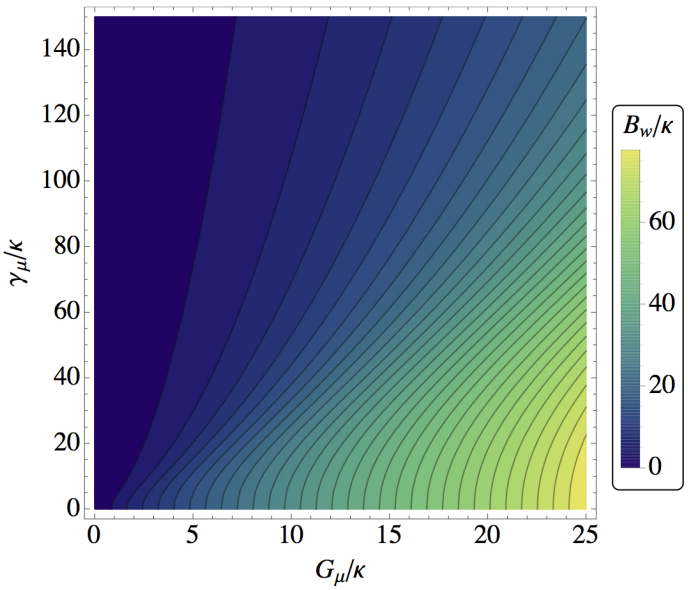

Figure 5.4: Approximate bandwidth B_w of $|\zeta_\mu(\omega)|^2$.

Chapter 6

Dynamics of an Ion Coupled to a Superconducting Circuit

6.1 Introduction

We have already seen that superconducting circuits are promising candidates for the implementation of quantum information processing and the study of quantum phenomena. They have been used to demonstrate strong coupling to a single photon [30], for the realization of quantum error correction [123], and for the generation of single-photon Fock states [59] among others. They also form an important aspect of hybrid quantum systems. In Chapter 3 a flux qubit was used to generate two-photon nonlinearities for the construction of a two-qubit phase gate with microwave photons (see also [57]).

Similarly, atomic systems like ions traps have been used to generate and manipulate entanglement [124] and to implement multi-qubit gates [125]. It is therefore natural to attempt to construct hybrid systems comprising these two architectures.

Although the couplings of the dipoles generated by the motion of trapped ions to the electric field of an LC circuit can be several hundred kHz, this coupling is far off resonance. This is because the motional frequencies of ions are on the order of MHz whereas the superconducting circuits are in the GHz (microwave) regime. Therefore, implementation of a practical quantum device requires something additional.

Parametric processes are useful in this end, and they are common to many physical systems. In the field of quantum optics, they are widely used in the frequency conversion of photons using nonlinear media [21, 126]. In the realm of superconducting quantum devices, one class of parametric amplifiers called Josephson bifurcation amplifiers have been used to amplify signals, and also to perform very sensitive quantum measurements, while adding very little noise [127]. Parametric processes have also been used to generate controllable interactions between superconducting qubits and microwave resonators [128].

In [129] a successful attempt was made to generate a resonant coupling scheme between ions and LC circuits. The ion, confined in a trap with frequency ω_i, was coupled to the driven sidebands of a high quality factor parametric LC circuit whose capacitance was modulated at frequency $\nu = \omega_{LC} - \omega_i$. This gave rise to a coupling strength $g/2\pi = 60$ kHz. Here I try a different approach. I drive a superconducting loop comprising a Josephson junction and a capacitor confining a trapped ion, using a time dependent external flux. This causes the system to act as a parametric oscillator with a tunable inductance, and hence a tunable resonant frequency. In the presence of a small nonlinearity in the junction, the parametric oscillator develops sidebands and the ion can be resonantly coupled to these sidebands. However, one

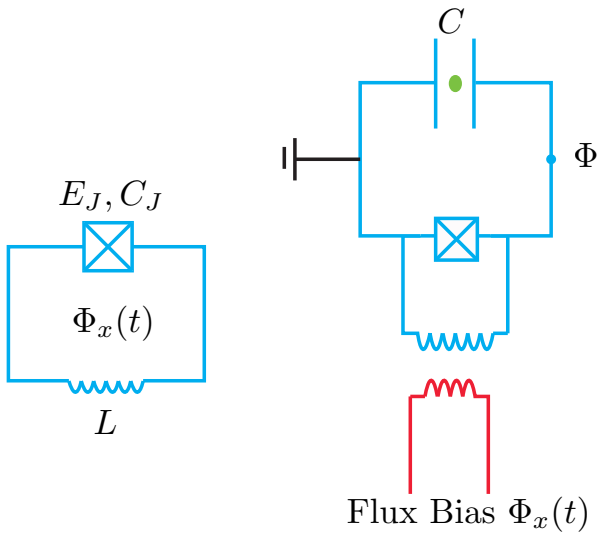

Figure 6.1: Depiction of an rf-SQUID with Josephson energy E_J and junction capacitance C_J driven by a time-dependent external flux $\Phi_x(t)$. The outer loop with inductance L contributes an energy E_L. The rf-SQUID is connected in parallel to a capacitor C that confines an ion (green).

will see that the coupling strength cannot be made very large.

6.2 Model and Hamiltonian

I consider an ion in an ion-trap that generates a harmonic potential with frequency ω_z along the z-direction. However, the confinement of an ion in a trap also leads to motion in the x and y directions. This is referred to as ion micromotion [130]. These motions correspond to a parametrically driven harmonic oscillator at parametric frequencies $\omega_x(t)$ and $\omega_y(t)$ respectively. I will ignore such x-y micromotion here.

The ion motion in the z-direction interacts with the electric field of a capacitor

C of a circuit containing an rf-SQUID (Fig. 6.1) [37, 75]. The SQUID is driven using a time-dependent magnetic flux $\Phi_x(t)$. I will show below that this SQUID and capacitor system will act as a parametric LC circuit. For the purpose of the following discussion, I define the dimensionlesss flux $\phi_x = 2\pi(\Phi_x/\Phi_0)$ and the phase $\phi = 2\pi(\Phi/\Phi_0)$, where $\Phi_0 = h/(2e)$ is the superconducting flux quantum.

I first construct the classical Lagrangian $\mathcal{L} = T - V$ of the system [50], so that with the usual Legendre transformation prescription, one can determine the Hamiltonian. The kinetic energy of the system is

$$T = \frac{1}{2}(C + C_J)\dot{\Phi}^2 + \frac{1}{2}m\dot{z}^2, \tag{6.1}$$

where Φ denotes the node flux for the circuit and z describes the longitudinal ion position. The potential energy is

$$V = -E_J \cos\phi + \frac{1}{2}E_L(\phi + \phi_x)^2 + \frac{1}{2}m\omega_z^2 z^2 + V_I. \tag{6.2}$$

The parameters E_J and $E_L = \Phi_0^2(4\pi^2 L)^{-1}$ are the Josephson energy and the inductive energy of the rf-SQUID respectively. The interaction potential V_I between the ion with charge Q and the capacitor is given in the dipole approximation by

$$V_I = QE_z z = Q\frac{V}{d}z = -\frac{Q}{d}z\dot{\Phi}. \tag{6.3}$$

Let $C_\Sigma = C + C_J$. The canonical coordinates are

$$q = \frac{\partial \mathcal{L}}{\partial \dot{\Phi}} = C_\Sigma \dot{\Phi} + \frac{Q}{d}z, \tag{6.4}$$

$$p_z = \frac{\partial \mathcal{L}}{\partial \dot{z}} = m\dot{z}. \tag{6.5}$$

Let the effective ion harmonic frequency be

$$\omega_i = \left(\omega_z^2 + \frac{Q^2}{d^2 C_\Sigma m}\right)^{\frac{1}{2}}. \tag{6.6}$$

The quantum Hamiltonian of the system can be written as

$$\hat{H}(t) = \hat{H}_{ion} + \hat{H}_q(t) + \hat{H}_I, \tag{6.7}$$

corresponding to the ion, qubit, and interaction Hamiltonians respectively, where

$$\hat{H}_{ion} = \frac{\hat{p}_z^2}{2m} + \frac{1}{2}m\omega_i^2\hat{z}^2 \rightarrow \left(\hat{b}^\dagger\hat{b} + \frac{1}{2}\right)\hbar\omega_i, \tag{6.8}$$

$$\hat{H}_q(t) = \frac{\hat{q}^2}{2C_\Sigma} - E_J\cos\hat{\phi} + \frac{1}{2}E_L(\hat{\phi} + \phi_x(t))^2, \tag{6.9}$$

$$\hat{H}_I = -\frac{Q\hat{q}}{C_\Sigma}\frac{\hat{z}}{d} \rightarrow -\frac{Q}{C_\Sigma}\left(\frac{z_p}{d}\right)\hat{q}(\hat{b} + \hat{b}^\dagger). \tag{6.10}$$

Here I introduced ionic operators $\hat{b}$ and $\hat{b}^\dagger$ satisfying $[\hat{b}, \hat{b}^\dagger] = 1$ and zero-point fluctuations of the ion motion $z_p = \sqrt{\hbar/(2m\omega_i)}$. This ensures that $[\hat{z}, \hat{p}_z] = i\hbar$ with

$$\hat{z} = \sqrt{\frac{\hbar}{2m\omega_i}}(\hat{b} + \hat{b}^\dagger) \equiv z_p(\hat{b} + \hat{b}^\dagger), \tag{6.11}$$

$$\hat{p}_z = -i\sqrt{\frac{m\omega_i\hbar}{2}}(\hat{b} - \hat{b}^\dagger). \tag{6.12}$$

The canonical coordinates of the SQUID satisfy $[\hat{\phi}, \hat{q}] = 2ei$.

If E_J and $\Phi_x(t)$ where zero, one could quantize the SQUID just like the ion motion, say with operators $\hat{a}$ and $\hat{a}^\dagger$ satisfying $[\hat{a}, \hat{a}^\dagger] = 1$. In that case, the interaction would be proportional to $(\hat{a} - \hat{a}^\dagger)(\hat{b} + \hat{b}^\dagger)$. However, in the frame rotating at the frequencies of the SQUID (say ω_0) and ion (ω_i), one would get something like

$$H_I = (\hat{a}e^{-i\omega_0 t} - \hat{a}^\dagger e^{i\omega_0 t})(\hat{b}e^{-i\omega_i t} + \hat{b}^\dagger e^{i\omega_i t}). \tag{6.13}$$

One is interested in interactions of the form $\hat{a}\hat{b}^\dagger + \hat{a}^\dagger\hat{b}$ where a resonant exchange of energy takes place between the two systems. However, since $\omega_0 \gg \omega_i$, $\omega_0 - \omega_i$ is comparable to $\omega_0 + \omega_i$, and so a rotating-wave approximation is not possible in (6.13). My goal is then the following: by tuning E_J and $\phi_x(t)$ adjust the spectrum of $\hat{q}(t)$ so that $\hat{a}\hat{b}^\dagger$ contains a time independent component, whereas $\hat{a}\hat{b}$ does not.

6.3 Linearization of the Parametric Oscillator

In the presence of E_J, $\hat{H}_q(t)$ is nonlinear and so $\hat{a}$ and $\hat{a}^\dagger$ are ill-defined. Therefore, the first task is to linearize $\hat{H}_q(t)$ and to find the operators corresponding to the the superconducting charge and flux variables. I let $\eta = E_J/E_L$ denote the strength of nonlinearity. Linearization is possible in the regime where $\eta/(1-\eta) \ll 1$ and when the quantum fluctuations of flux are much less than Φ_0.

Let the time-dependent classical values of the reduced flux $\hat{\phi}$ and the charge $\hat{q}$ be denoted by $\phi_c(t)$ and $q_c(t)$ respectively. Recall that they satisfy the commutation relation $[\hat{\Phi}, \hat{q}] = i\hbar$ or $[\hat{\phi}, \hat{N}] = i$ with $\hat{q} = 2e\hat{N}$. Let the time-dependent generators of charge and flux translations be denoted by

$$U_1(t) = e^{-i\hat{\Phi}q_c(t)/\hbar}, \tag{6.14}$$

$$U_2(t) = e^{i\hat{q}\Phi_c(t)/\hbar}, \tag{6.15}$$

and let

$$\hat{V}_q(\hat{\phi}) = -E_J \cos\hat{\phi} + \frac{1}{2}E_L(\hat{\phi} + \phi_x)^2. \tag{6.16}$$

Under $U_1(t)$ the Hamiltonian transforms to

$$\begin{aligned} \hat{H}_1 &= U_1^\dagger \hat{H} U_1 - i\hbar U_1^\dagger \frac{\partial U_1}{\partial t} \\ &= \hat{H}_{ion} + \frac{(\hat{q} - q_c)^2}{2C_\Sigma} + \hat{V}_q(\hat{\phi}) - \frac{Q}{dC_\Sigma}\hat{z}(\hat{q} - q_c) \\ &\quad -\hat{\Phi}\dot{q}_c. \end{aligned} \tag{6.17}$$

Now under $U_2(t)$, H_1 transforms to

$$\begin{aligned}\hat{H}_2 &= U_2^\dagger \hat{H}_1 U_2 - i\hbar U_2^\dagger \frac{\partial U_2}{\partial t} \\ &= \hat{H}_{ion} + \frac{(\hat{q}-q_c)^2}{2C_J} + \hat{V}_q(\hat{\phi}-\phi_c) \\ &\quad -\frac{Q}{dC_\Sigma}\hat{z}(\hat{q}-q_c) - (\hat{\Phi}-\Phi_c)\dot{q}_c + \hat{q}\dot{\Phi}_c. \end{aligned} \tag{6.18}$$

I approximate

$$\hat{V}_q(\hat{\phi}-\phi_c) = \hat{V}_q(-\phi_c) + \hat{V}_q'(-\phi_c)\hat{\phi} + \frac{\hat{V}_q''(-\phi_c)}{2}\hat{\phi}^2 + O(\hat{\phi}^3). \tag{6.19}$$

One can then set the terms linear in $\hat{q}$ and $\hat{\phi}$ in $\hat{H}_2$ to be zero. This gives

$$\dot{\phi}_c - \frac{2e}{\hbar}\frac{q_c}{C_J} = 0; \;\; \hat{V}_q'(-\phi_c) - \frac{\hbar}{2e}\dot{q}_c = 0. \tag{6.20}$$

These can be solved for $\phi_c(t)$ and $q_c(t)$. Let the effective charging energy be $E_C = (2e)^2/(2C_\Sigma)$. The linearized Hamiltonian can then be written as

$$\hat{H}_L = \hat{H}_{ion} + \left[\frac{\hat{N}^2}{2M} + \frac{1}{2}M\hbar^2\omega(t)^2\hat{\phi}^2\right] - \frac{Q\hat{z}}{dC_\Sigma}(\hat{q}-q_c), \tag{6.21}$$

the interaction term being

$$\hat{V}_L = -\frac{Q\hat{z}}{dC_\Sigma}(\hat{q}-q_c). \tag{6.22}$$

The parametric frequency is denoted by $\omega(t)^2 = \omega_0^2(1+\eta\cos\phi_c(t))$ with $\omega_0 = \sqrt{2E_L E_C}/\hbar$. I have also defined an effective mass $M \equiv 1/(2E_C)$. One can modulate $\phi_x(t)$ such that $\cos\phi_c(t) = \cos\omega_d t$ for some frequency ω_d. For instance, this can be done by modulating $\phi_x(t)$ as a saw-tooth wave. With this approximation,

$$\omega(t)^2 = \omega_0^2(1+\eta\cos\omega_d t), \tag{6.23}$$

and my stated goal is now achieved.

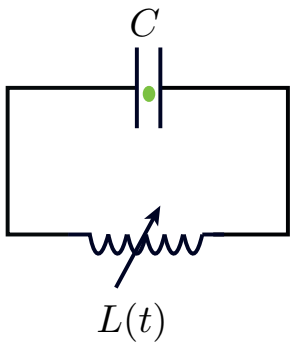

Figure 6.2: After linearization, the effective picture consists of an ion confined between the capacitance C of an LC circuit with parametric inductance $L(t)$.

6.4 Time-Dependent Quantum Harmonic Oscillator

I now follow the approach in [131] to quantize the parametric Hamiltonian

$$\hat{H}_P = \frac{\hat{N}^2}{2M} + \frac{1}{2}M\hbar^2\omega(t)^2\hat{\phi}^2, \tag{6.24}$$

the details being provided in Appendix D. The parametric frequency $\omega(t)$ has period $\tau = 2\pi/\omega_d$. The classical equation of motion for ϕ is

$$\ddot{\phi}(t) + \omega(t)^2\phi(t) = 0. \tag{6.25}$$

Suppose some function $f(t)$ is a solution of Equation (6.25). Then $f^*(t)$ is also a linearly independent solution. Since $f(t)$ is periodic, $f(t+\tau) = e^{i\varphi}f(t)$ for some real φ. It is helpful to write

$$f(t) = r(t)e^{i\theta(t)}, \tag{6.26}$$

with $r(t) > 0$ and $\theta(t)$ real-valued. The Wronskian corresponding to these solutions is

$$W = \frac{1}{2i}\begin{vmatrix} f(t) & f^*(t) \\ \dot{f}(t) & \dot{f}^*(t) \end{vmatrix} = -r(t)^2\dot{\theta}(t). \tag{6.27}$$

However, it can be shown that the time derivative of the Wronskian is zero and so is a constant of the motion. Then apart from a time dependent factor $|f(t)|^{-2}$, the Hamiltonian (6.24) can be written as the Hamiltonian of a time-independent harmonic oscillator with frequency W. One can write $\hat{\phi}$ and $\hat{N}$ in terms of creation and annihilation operators $\hat{a}^\dagger$ and $\hat{a}$ satisfying $[\hat{a}, \hat{a}^\dagger] = 1$ as

$$\hat{\phi} = \sqrt{\frac{1}{2M\hbar W}}(\hat{a} + \hat{a}^\dagger), \tag{6.28}$$

$$\hat{N} = -i\sqrt{\frac{M\hbar W}{2}}(\hat{a} - \hat{a}^\dagger). \tag{6.29}$$

and get a quantized Hamiltonian

$$\begin{aligned} \hat{H}_P &= \frac{1}{|f(t)|^2}\left(\hat{a}^\dagger\hat{a} + \frac{1}{2}\right)\hbar W \\ &= \hbar\omega_a(t)\left(\hat{a}^\dagger\hat{a} + \frac{1}{2}\right), \end{aligned} \tag{6.30}$$

where $\omega_a(t) = W/|f(t)|^2 = -\dot{\theta}(t)$ plays the role as a time-dependent oscillator frequency.

6.5 Classical Solutions

To find the classical solutions, one can transform (6.25) with the substitution $2z = \omega_d t$ into

$$\frac{d^2\phi}{dz^2} + (a - 2q\cos 2z)\phi = 0, \tag{6.31}$$

where $a = 4\omega_0^2/\omega_d^2$ and $q = -\eta a/2 = -2\eta\omega_0^2/\omega_d^2$. This equation is known as the Mathieu equation [132]. I am interested in solutions of Mathieu's equation of the form $f(z+\pi) = e^{i\mu\pi} f(z)$, where μ is a real number. μ can in general be complex, but that leads to solutions which decay in time, or to solutions which are unstable. If μ is a rational or irrational, but positive number, then the Mathieu equation admits solutions of fractional order [132]. These are solutions which reduce to $\sin \mu z$ or $\cos \mu z$ when $q = 0$. They are

$$\begin{aligned} ce_\mu(z,q) &= \cos \mu z + \sum_{i=1}^{\infty} q^i c_i(z), && (6.32) \\ se_\mu(z,q) &= \sin \mu z + \sum_{i=1}^{\infty} q^i s_i(z), && (6.33) \\ a &= \mu^2 + \sum_{i=1}^{\infty} \alpha_i q^i, && (6.34) \end{aligned}$$

where $c_i(z)$, $s_i(z)$ are functions to be determined, and α_i are constants to be determined. The parameter a has the same value for both solutions for any q. So (6.32) and (6.33) coexist and are linearly independent. Thus, the general solution to (6.31) with two arbitrary constants is

$$\phi(z) = A\ ce_\mu(z,q) + B\ se_\mu(z,q). \tag{6.35}$$

When $\mu > 0$ and $q^2(\mu^2 - 1)/2 \ll \mu^2$, one approximately has $\mu^2 = a$. Additionally, if $|q| \ll 1$ one can ignore terms of $O(q^2)$. Then I get

$$\begin{aligned} ce_\mu(z,q) &= \cos \mu z - \frac{q}{4}\left[\frac{\cos(\mu+2)z}{\mu+1} - \frac{\cos(\mu-2)z}{\mu-1}\right], \\ se_\mu(z,q) &= \sin \mu z - \frac{q}{4}\left[\frac{\sin(\mu+2)z}{\mu+1} - \frac{\sin(\mu-2)z}{\mu-1}\right], \end{aligned} \tag{6.36}$$

Switching back to the original notation with $2z = \omega_d t$, the linearly independent

solutions become

$$\begin{aligned} f_1(t) &= \cos\omega_0 t + \frac{\eta\omega_0^2}{2\omega_d}\left[\frac{\cos(\omega_0+\omega_d)t}{\omega_d+2\omega_0} + \frac{\cos(\omega_0-\omega_d)t}{\omega_d-2\omega_0}\right], \\ f_2(t) &= \sin\omega_0 t + \frac{\eta\omega_0^2}{2\omega_d}\left[\frac{\sin(\omega_0+\omega_d)t}{\omega_d+2\omega_0} + \frac{\sin(\omega_0-\omega_d)t}{\omega_d-2\omega_0}\right]. \end{aligned} \tag{6.37}$$

These solutions are valid when

$$K_1 \equiv \frac{\eta^2\omega_0^2}{2\omega_d^2}\left(\frac{4\omega_0^2}{\omega_d^2}-1\right) \ll 1. \tag{6.38}$$

The time-independent Wronskian corresponding to $f_1(t)$ and $f_2(t)$ is

$$W = \omega_0 + O(\eta^2). \tag{6.39}$$

Note that the Wronskian acts as an effective frequency. The general solution can be written in terms of two real constants C and φ as

$$f(t) = Ce^{-i(\omega_0 t+\varphi)} + \frac{C\eta\omega_0^2 e^{-i\varphi}}{2\omega_d}\left[\frac{e^{-i(\omega_0+\omega_d)t}}{\omega_d+2\omega_0} + \frac{e^{-i(\omega_0-\omega_d)t}}{\omega_d-2\omega_0}\right]. \tag{6.40}$$

6.6 Derivation of the Interaction

As shown before, the time derivative of the Wronskian is zero and the only time dependence is in $f(t)$, the classical solution. Once again following the approach in [131], one can show that the interaction potential (6.22) of the linearized Hamiltonian under the relevant unitary transformations becomes

$$H_I = -\frac{2Qe}{dC_\Sigma} z\left(\frac{N}{|f(t)|} - 2\chi|f(t)|\phi - N_c(t)\right),$$

where χ is a dimensionless parameters that satisfies

$$\chi = -\frac{\hbar M}{4}\frac{d}{dt}\ln|f|^2. \tag{6.41}$$

Define the energies

$$\Omega_1(t) = \alpha \frac{d|f(t)|}{dt} = \hbar\alpha\dot{r}(t), \tag{6.42}$$

$$\Omega_2(t) = \beta \frac{1}{|f(t)|} = \frac{\beta}{r(t)}, \tag{6.43}$$

$$\Lambda(t) = \frac{2Qe}{dC_\Sigma} z_p N_c(t), \tag{6.44}$$

with the parameters

$$\alpha = -\frac{\sqrt{2}Qe}{C_\Sigma}\left(\frac{z_p}{d}\right)\sqrt{\frac{M}{\hbar W}}, \tag{6.45}$$

$$\beta = \frac{\sqrt{2}Qe}{C_\Sigma}\left(\frac{z_p}{d}\right)\sqrt{M\hbar W}, \tag{6.46}$$

where α is dimensionless and β has units of energy. The full quantized Hamiltonian is $\hat{H} = \hat{H}_0 + \hat{V}$, where

$$\hat{H}_0 = \hbar\omega_a(t)\hat{a}^\dagger\hat{a} + \hbar\omega_i\hat{b}^\dagger\hat{b}, \tag{6.47}$$

$$\hat{V} = \left(\Omega(t)\hat{a} + \Omega^*(t)\hat{a}^\dagger\right)(\hat{b} + \hat{b}^\dagger) + \Lambda(t)(\hat{b} + \hat{b}^\dagger), \tag{6.48}$$

with coupling $\Omega(t) = \Omega_1(t) + i\Omega_2(t)$.

6.7 Sideband Coupling

I now examine the coupling to the ion motion in the z-direction. Coupling to the ion micromotion can be done in a similar manner albeit much more involved. Define the unitary operator

$$U = \exp\left[-i\left(G_a(t)\hat{a}^\dagger\hat{a} + \omega_i t\ \hat{b}^\dagger\hat{b}\right)\right] \tag{6.49}$$

where

$$G_a(t) = \int_0^t dt'\ \omega_a(t') = -\int_0^t dt'\ \dot{\theta}(t') = -\theta(t). \tag{6.50}$$

Under this transformation, the original Hamiltonian

$$\begin{aligned}\hat{H} \quad \rightarrow \quad & \left[\Omega(t)\hat{a}e^{i\theta(t)} + \Omega^*(t)\hat{a}^\dagger e^{-i\theta(t)}\right](\hat{b}e^{-i\omega_i t} + \hat{b}^\dagger e^{i\omega_i t}) \\ & +\Lambda(t)(\hat{b}e^{-i\omega_i t} + \hat{b}^\dagger e^{i\omega_i t}). \end{aligned} \tag{6.51}$$

To find the coupling to the ion motion in the z-direction, one first needs to evaluate the coefficient of $\hat{a}\hat{b}$ which is $\Omega(t)e^{i\theta(t)}e^{-i\omega_i t}$. Similarly, the coefficient of $\hat{a}\hat{b}^\dagger$ is $\Omega(t)e^{i\theta(t)}e^{i\omega_i t}$. Note that

$$\frac{df(t)}{dt} = \frac{d}{dt}(r(t)e^{i\theta(t)}) = \dot{r}(t)e^{i\theta(t)} + i\dot{\theta}(t)r(t)e^{i\theta(t)}. \tag{6.52}$$

Then,

$$\begin{aligned}\Omega_1(t)e^{i\theta(t)} &= \hbar\alpha\dot{r}(t)e^{i\theta(t)} \\ &= \hbar\alpha\frac{df(t)}{dt} - i\hbar\alpha\dot{\theta}(t)r(t)e^{i\theta(t)} \\ &= \hbar\alpha\frac{df(t)}{dt} + i\hbar\alpha\frac{W}{r(t)}e^{i\theta(t)}, \end{aligned} \tag{6.53}$$

$$\begin{aligned}i\Omega_2(t)e^{i\theta(t)} &= i\frac{\beta}{r(t)}e^{i\theta(t)} \\ &= -i\hbar\alpha\frac{W}{r(t)}e^{i\theta(t)}. \end{aligned} \tag{6.54}$$

Therefore,

$$\Omega e^{i\theta(t)} = (\Omega_1(t) + i\Omega_2(t))e^{i\theta(t)} = \hbar\alpha\frac{df(t)}{dt}. \tag{6.55}$$

Let $C = 1$ and $\varphi = 0$ for simplicity. The time derivative of $f(t)$ is

$$\frac{df(t)}{dt} = -i\omega_0 e^{-i\omega_0 t} - \frac{i\eta\omega_0^2}{2\omega_d}\left[\frac{(\omega_0+\omega_d)e^{-i(\omega_0+\omega_d)t}}{\omega_d+2\omega_0} + \frac{(\omega_0-\omega_d)e^{-i(\omega_0-\omega_d)t}}{\omega_d-2\omega_0}\right]. \tag{6.56}$$

Therefore, the time dependent coefficient of $\hat{a}\hat{b}$ is

$$-i\omega_0 e^{-i(\omega_0+\omega_i)t} - \frac{i\eta\omega_0^2}{2\omega_d}\left[\frac{(\omega_0+\omega_d)e^{-i(\omega_0+\omega_d+\omega_i)t}}{\omega_d+2\omega_0} + \frac{(\omega_0-\omega_d)e^{-i(\omega_0-\omega_d+\omega_i)t}}{\omega_d-2\omega_0}\right]. \tag{6.57}$$

Similarly the coefficient of $\hat{a}\hat{b}^\dagger$ is

$$-i\omega_0 e^{-i(\omega_0-\omega_i)t} - \frac{i\eta\omega_0^2}{2\omega_d}\left[\frac{(\omega_0+\omega_d)e^{-i(\omega_0+\omega_d-\omega_i)t}}{\omega_d+2\omega_0} + \frac{(\omega_0-\omega_d)e^{-i(\omega_0-\omega_d-\omega_i)t}}{\omega_d-2\omega_0}\right]. \quad (6.58)$$

If one assumes that $\omega_d = \omega_0 - \omega_i$, then only $\hat{a}\hat{b}^\dagger$ has a time independent term given by

$$\lambda = \hbar\alpha\left(-\frac{i\eta\omega_0^2}{2\omega_d}\right)\frac{\omega_0-\omega_d}{\omega_d-2\omega_0} = \hbar\alpha\left(\frac{i\eta\omega_0^2}{2}\right)\frac{\omega_i}{(\omega_0+\omega_i)(\omega_0-\omega_i)} \approx \frac{i\hbar\alpha\eta}{2}\omega_i. \quad (6.59)$$

where the approximation arises from the fact that $\omega_0 \gg \omega_i$.

Ignoring all the coupling terms which oscillate rapidly compared to time scales of the ion motion leads to a resonant coupling

$$\hat{V}_R = \lambda(\hat{a}\hat{b}^\dagger + \hat{a}^\dagger\hat{b}). \quad (6.60)$$

Linearization requires $\eta \ll 1$, and the quantum fluctuations in $\hat{\phi}$

$$\hat{\phi}_{zp} = \frac{1}{\sqrt{2M\hbar W}} \ll 1. \quad (6.61)$$

Since $W \approx \omega_0$,

$$\alpha = -\frac{\sqrt{2}Qe}{C_\Sigma}\left(\frac{z_p}{d}\right)\sqrt{\frac{M}{\hbar W}} \approx -\frac{\sqrt{2}Qe}{C_\Sigma}\left(\frac{z_p}{d}\right)\frac{1}{(2E_C)^{\frac{3}{4}}E_L^{\frac{1}{4}}}. \quad (6.62)$$

Because the parameters η and α are small, λ is also small. With these constraints, the coupling strength λ is much smaller than even a kHz.

6.8 Conclusions and Outlook

My analysis reveals that coupling a single trapped ion to a superconducting circuit resonantly has limitations. It is the geometry which creates a severe limiting factor, and not the dynamics. Therefore, a novel approach is required. Early

proposals for realizing a hybrid system comprising atoms or trapped ions coupled to solid state systems include [133] and [134] respectively. However, these proposals have yet to be realized experimentally. Other approaches involve coupling solid state systems to an ensemble of polar molecules with large dipole moments to enhance the coupling as proposed in [135], or using Rydberg atoms with large dipole moments [136].

Chapter 7

Conclusions

Superconducting circuits may be used to implement many other interesting Hamiltonians, and are an integral part of hybrid quantum sytems. In this thesis I showed how to generate two-photon nonlinearities by coupling microwave photons to a flux superconducting circuit. I also considered the implementation of a parent Hamiltonian for the Pfaffian state using circuit-QED. Then I described a Hamiltonian that can emulate a chemical potential for light. I believe that these proposals can be implemented experimentally, although the quantum control of these systems will present challenges. Superconducting systems combined with other architectures have already been used to demonstrate strong coupling to a single photon [30], and to implement quantum error correcting codes [123]. They have also been used to generate Fock states of photons [64], and in the creation of low noise amplifiers [127]. The lifetime and quality of superconducting quantum circuits have increased by many orders of magnitude over the past decade and the trend continues [25]. Therefore, it is reasonable to hope that they may eventually form scalable quantum simulation and quantum information architectures in the future. As I discussed in the introduc-

tion, classical computation will encounter increasing challenges due to fundamental laws of nature. By stepping into a domain where quantum processes occur, one can cross these barriers [137].

Chapter 8

Appendix

8.1 Appendix A

In this appendix, I present a derivation of the effective Hamiltonian (3.85) using a unitary transformation. I will ignore the state $|0\rangle \equiv |\bar{0}\bar{0}\rangle$ and focus on the nontrivial subspace for this part. The starting Hamiltonian is

$$H = \begin{pmatrix} \Omega_1 & \lambda_1 & 0 \\ \lambda_1 & 2\Omega_1 & \lambda_2 \\ 0 & \lambda_2 & \Omega_2 \end{pmatrix}. \tag{8.1}$$

Let $P = |b\rangle\langle b| + |c\rangle\langle c|$ denote the projector onto the two-dimensional subspace and $Q = |a\rangle\langle a|$ be the projector onto the one dimensional subspace. I will find a Hermitian matrix S such that the unitary transformation $U = e^{iS}$ generated by S, renders H block diagonal in the respective subspaces P and Q [138]. That is

$$\tilde{H} \equiv UHU^\dagger = P \oplus Q. \tag{8.2}$$

Let S have the most general form

$$S = \begin{pmatrix} d_1 & q & r \\ q^* & d_2 & u \\ r^* & u^* & d_3 \end{pmatrix}. \tag{8.3}$$

One can impose the constraints, $PSP = QSQ = 0$ [138]. This implies that $d_1 = d_2 = d_3 = u = u^* = 0$. Thus, S reduces to

$$S = \begin{pmatrix} 0 & q & r \\ q^* & 0 & 0 \\ r^* & 0 & 0 \end{pmatrix}. \tag{8.4}$$

S can be diagonalized with the unitary transformation

$$W = \frac{1}{\sqrt{|q|^2 + |r|^2}} \begin{pmatrix} 0 & -\frac{\sqrt{|q|^2 + |r|^2}}{\sqrt{2}} & \frac{\sqrt{|q|^2 + |r|^2}}{\sqrt{2}} \\ -r & \frac{q^*}{\sqrt{2}} & \frac{q^*}{\sqrt{2}} \\ q & \frac{r^*}{\sqrt{2}} & \frac{r^*}{\sqrt{2}} \end{pmatrix}, \tag{8.5}$$

to a matrix $S_d = W^\dagger S W = \text{Diagonal}(0, -\sqrt{|q|^2 + |r|^2}, \sqrt{|q|^2 + |r|^2})$. W simply consists of normalized eigenvectors of S as its columns.

After finding S one needs to evaluate $U = e^{iS}$ which can be expanded as

$$U = e^{iS} = \sum_{n=0}^{\infty} \frac{(iS)^n}{n!}. \tag{8.6}$$

One can apply W to U to get

$$W^\dagger U W = \sum_{n=0}^{\infty} \frac{(i)^n}{n!} W^\dagger S^n W = \sum_{n=0}^{\infty} \frac{(i)^n}{n!} \left(W^\dagger S W\right)^n = \sum_{n=0}^{\infty} \frac{(i)^n}{n!} (S_d)^n, \tag{8.7}$$

since $W^\dagger W = WW^\dagger = 1$. Define the matrices

$$M_1 = \begin{pmatrix} 0 & 0 & 0 \\ 0 & -1 & 0 \\ 0 & 0 & 1 \end{pmatrix}; \; M_2 = \begin{pmatrix} 0 & 0 & 0 \\ 0 & 1 & 0 \\ 0 & 0 & 1 \end{pmatrix}, \tag{8.8}$$

and let $z = \sqrt{|q|^2 + |r|^2}$. Therefore,

$$\begin{aligned} W^\dagger U W &= \sum_{n=0}^{\infty} \frac{(i)^n}{n!} (S_d)^n \\ &= I + \sum_{n=1}^{\infty} \frac{(i)^n}{n!} (zM_1)^n \\ &= I + M_1 \sum_{n=1,3,\ldots} \frac{(iz)^n}{n!} + M_2 \sum_{n=2,4\ldots} \frac{(iz)^n}{n!} \\ &= I + iM_1 \sum_{n=0}^{\infty} (-1)^n \frac{z^{2n+1}}{(2n+1)!} + M_2 \sum_{n=1}^{\infty} (-1)^n \frac{z^{2n}}{(2n)!} \\ &= I + iM_1 \sum_{n=0}^{\infty} (-1)^n \frac{z^{2n+1}}{(2n+1)!} + M_2 \left[-1 + \sum_{n=0}^{\infty} (-1)^n \frac{z^{2n}}{(2n)!} \right] \\ &= I + iM_1 \sin z - M_2 (1 - \cos z). \end{aligned} \tag{8.9}$$

Hence,

$$U = I + iWM_1W^\dagger \sin z - WM_2W^\dagger (1 - \cos z). \tag{8.10}$$

One can find the elements of the matrix S and that of U perturbatively in η_2' by ensuring that $\tilde{H}_{12} = \tilde{H}_{13} = 0$. One then gets the effective Hamiltonian

$$\tilde{H} = UHU^\dagger = \begin{pmatrix} \Omega_1 - \dfrac{r_1^2 \eta_2'^2}{\Omega_1} + O(\eta_2'^3) & O(\eta_2'^3) & O(\eta_2'^3) \\ O(\eta_2'^3) & 2\Omega_1 + \dfrac{r_1^2 \eta_2'^2}{\Omega_1} + O(\eta_2'^3) & r_2\eta_2' + O(\eta_2'^3) \\ O(\eta_2'^3) & r_2\eta_2' + O(\eta_2'^3) & \Omega_2 + O(\eta_2'^3) \end{pmatrix}. \tag{8.11}$$

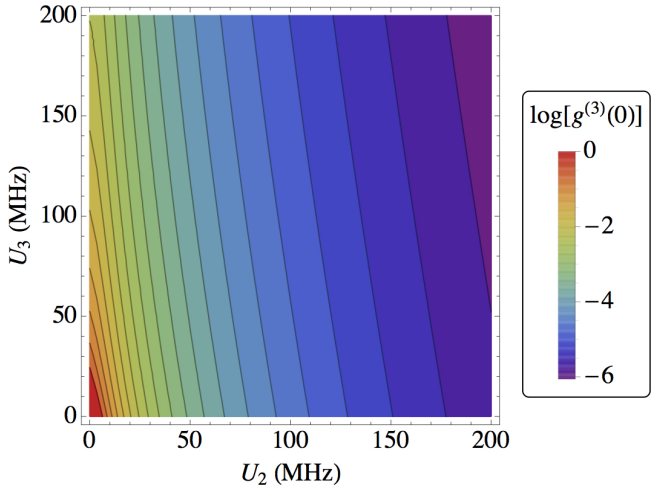

Figure 8.1: A plot of $\log_{10}[g^{(3)}(0)]$ as a function of U_2 and U_3 for $\Delta = 0$.

8.2 Appendix B

I briefly review the method to measure U_2 and U_3 using correlation functions. I start with the system Hamiltonian $\hat{H}$ and input-ouput equations for a one-sided driven system with a loss rate κ in a frame rotating at a frequency ω_L of the input field $\hat{b}_{in} = \mathcal{E}e^{-i\omega_L t}$.

$$\hat{H} = \left(\Delta - i\frac{\kappa}{2}\right)\hat{a}^\dagger\hat{a} + \left(\frac{U_2}{2}\hat{a}^{\dagger 2}\hat{a}^2 + \frac{U_3}{6}\hat{a}^{\dagger 3}\hat{a}^3\right) - i\sqrt{\kappa}(\mathcal{E}\hat{a}^\dagger - \mathcal{E}^*\hat{a}). \tag{8.12}$$

$$\dot{\hat{a}} = -i[\hat{a}, \hat{H}]; \quad \hat{b}_{out} = \hat{b}_{in} + \sqrt{\kappa}\hat{a}. \tag{8.13}$$

I will assume that the field is on resonance, that is $\Delta = \omega - \omega_L = 0$ and $\beta = \mathcal{E}/\sqrt{\kappa} \ll 1$. For numerical analysis, I let $\kappa = 10$ MHz and $\Delta = 0$.

I want to solve for $|\psi\rangle$ in

$$i\frac{\partial|\psi\rangle}{\partial t} = \hat{H}|\psi\rangle. \tag{8.14}$$

I start with the ansatz $|\psi\rangle = c_0|0\rangle + c_1|1\rangle + c_2|2\rangle + c_3|3\rangle + O(\beta^4)$, where I assume that c_0 is $O(1)$ and c_i is of $O(\beta^i)$. I want to solve for the steady state of the system and calculate the correlation functions. One can show that the second order correlation function is

$$g^{(2)}(0) = \frac{\langle \hat{a}^\dagger \hat{a}^\dagger \hat{a}\hat{a}\rangle}{\langle \hat{a}^\dagger \hat{a}\rangle^2} \approx \frac{2|c_2|^2}{|c_1|^4} = \frac{4\Delta^2 + \kappa^2}{(U_2 + 2\Delta)^2 + \kappa^2} \xrightarrow{\Delta=0} \frac{\kappa^2}{U_2^2 + \kappa^2}, \tag{8.15}$$

where the mean is taken in the steady state $|\psi\rangle$. When $U_2 = 0$, one has $g^{(2)}(0) \approx 1$. However, in the presence of U_2, $g_2(0) < 1$. Similarly, in the presence of both U_2 and U_3, one can show that the third order correlation function is

$$\begin{aligned} g^{(3)}(0) &= \frac{\langle \hat{a}^\dagger \hat{a}^\dagger \hat{a}^\dagger \hat{a}\hat{a}\hat{a}\rangle}{\langle \hat{a}^\dagger \hat{a}\rangle^3} \\ &\approx \frac{6|c_3|^2}{|c_1|^6} \\ &= \frac{9(4\Delta^2 + \kappa^2)^2}{[(U_2 + 2\Delta)^2 + \kappa^2]\,[4(3U_2 + U_3 + 3\Delta)^2 + 9\kappa^2]} \\ &\xrightarrow{\Delta=0} \frac{9\kappa^4}{(U_2^2 + \kappa^2)\,[4(3U_2 + U_3)^2 + 9\kappa^2]}. \end{aligned} \tag{8.16}$$

Note that when both $U_2, U_3 \to 0$, $g^{(3)}(0) \to 1$. The result is plotted in Figure 8.1.

8.3 Appendix C

In this appendix, I derive the Hamiltonian of a transmission line coupled to external circuits following the approach in [100]. I assume that the left end of the TL is connected to a left circuit via a capacitor C_L, and the right end of the TL is connected to a right circuit via an inductor L_1. I also assume that the energies associated with the capacitive coupling to the right Wheatstone circuit is small compared to other energies in the system, and can be ignored.

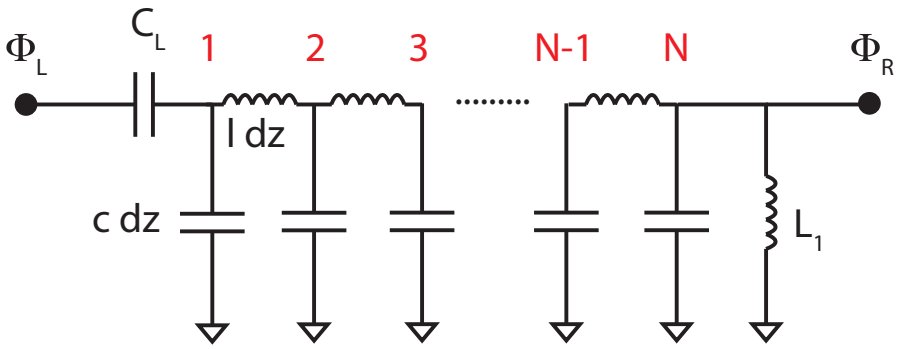

Figure 8.2: A schematic of a transmission line. A left circuit is connected to its left end via a capacitor C_L, and a right circuit is connected to its right end via an inductor L_1.

In the discrete case where the TL is modeled by a series of inductors and capacitors (Figure 8.2). The TL Lagrangian is

$$\mathcal{L}_{tl} = \frac{1}{2}C_L\dot{\eta}_1^2 + \frac{1}{2}\sum_{i=1}^{N}(cdz)\dot{\eta}_i^2 - \frac{1}{2(ldz)}\sum_{i=2}^{N}(\eta_i - \eta_{i-1})^2 + \frac{\eta_N^2}{2L_1}. \tag{8.17}$$

I define a column vector η as $\tilde{\eta} = (\eta_1, \ldots, \eta_N) = \eta^T$. The Lagrangian can then be written as

$$\mathcal{L}_{tl} = \mathcal{T} - \mathcal{V} = \frac{1}{2}\tilde{\dot{\eta}}\mathbf{T}\dot{\eta} - \frac{1}{2}\tilde{\eta}\mathbf{V}\eta, \tag{8.18}$$

where the kinetic energy matrix $\mathbf{T}$ has components

$$\mathbf{T}_{ij} = \delta_{ij}(cdz + C_L\delta_{i1}). \tag{8.19}$$

The potential energy matrix is

$$\mathbf{V} = \frac{1}{ldz}\begin{bmatrix} 1 & -1 & 0 & 0 & \dots & 0 \\ -1 & 2 & -1 & 0 & \dots & 0 \\ 0 & -1 & 2 & -1 & \dots & 0 \\ \vdots & \vdots & \vdots & \ddots & \ddots & \vdots \\ 0 & 0 & 0 & -1 & 2 & -1 \\ 0 & 0 & 0 & 0 & -1 & 1-\frac{ldz}{L_1} \end{bmatrix}. \tag{8.20}$$

In the continuum limit, the flux along the TL can be represented by a function $\eta(z)$ with $0 \leq z \leq L$. In terms of the eigenmodes $\varphi_\nu(z) = 0, 1, \dots$ of the TL,

$$\eta(z) = \sum_\nu \xi_\nu \varphi_\nu(z), \tag{8.21}$$

where the coefficients ξ_ν satisfy

$$\ddot{\xi}_\nu + \omega_\nu^2 \xi_\nu = 0. \tag{8.22}$$

The functions $\varphi_\nu(z)$ satisfy

$$\frac{\partial^2 \varphi_\nu(z)}{\partial z^2} = -(\omega_\nu \sqrt{lc})^2 \varphi_\nu(z). \tag{8.23}$$

It has the solution

$$\varphi_\nu(z) = A_\nu \cos(\omega_\nu \sqrt{lc} z) + B_\nu \sin(\omega_\nu \sqrt{lc} z). \tag{8.24}$$

Letting $k_\nu = \omega_\nu \sqrt{lc}$, the solution can also be written as

$$\varphi_\nu(z) = C_\nu \cos(k_\nu z + \phi_\nu) = \Re[C_\nu e^{i(k_\nu z + \phi_\nu)}]. \tag{8.25}$$

On the left, there is a boundary condition,

$$-\left[\frac{\partial \varphi_\nu(z)}{\partial z}\right]_{z=0} = lC_L\omega_\nu^2 \left[\varphi_\nu(z)\right]_{z=0}, \tag{8.26}$$

and on the right, there is a boundary condition

$$\left[\frac{\partial\varphi_\nu(z)}{\partial z}\right]_{z=L} = -\frac{l}{L_1}\left[\varphi_\nu(z)\right]_{z=L}. \tag{8.27}$$

In the discrete picture, the orthonormalization condition is

$$(cdz + C_L)\varphi_\nu(z_1)\varphi_\mu(z_1) + cdz\varphi_\nu(z_2)\varphi_\mu(z_2) + \cdots + cdz\varphi_\nu(z_{N-1})\varphi_\mu(z_{N-1})$$

$$+cdz\varphi_\nu(z_N)\varphi_\mu(z_N) = \delta_{\mu\nu}. \tag{8.28}$$

In the continuum limit, this becomes

$$C_L\left[\varphi_\nu(z)\varphi_\mu(z)\right]_{z=0} + c\int_0^L dz\ \varphi_\nu(z)\varphi_\mu(z) = \delta_{\mu\nu}. \tag{8.29}$$

Note that the normal modes $\varphi_\nu(z)$ have units of $1/\sqrt{C}$ where C has units of capacitance. With these results,

$$\begin{aligned}
\mathcal{L}_{tl} &= \frac{1}{2}\sum_{\mu,\nu}\left[\dot\xi_\mu\dot\xi_\nu\varphi_\mu^* T\varphi_\nu - \xi_\mu\xi_\nu\varphi_\mu^* V\varphi_\nu\right] \\
&= \frac{1}{2}\sum_{\mu,\nu}\left[\dot\xi_\mu\dot\xi_\nu\varphi_\mu^* T\varphi_\nu - \xi_\mu\xi_\nu\varphi_\mu^*\omega_\nu^2 T\varphi_\nu\right] \\
&= \frac{1}{2}\sum_{\mu,\nu}\left[\dot\xi_\mu\dot\xi_\nu - \omega_\nu^2\xi_\mu\xi_\nu\right]\underbrace{\varphi_\mu^* T\varphi_\nu}_{\delta_{\mu\nu}} \\
&= \frac{1}{2}\sum_{\nu}\left[\dot\xi_\nu^2 - \omega_\nu^2\xi_\nu^2\right].
\end{aligned} \tag{8.30}$$

For convenience, one can let $\xi_\nu = \sqrt{C_{tl}}F_\nu$ with $C_{tl} = cL$, and F_ν has units of flux. One can also define the dimensionless $\psi_\nu = \sqrt{C_{tl}}\varphi_\nu$. The canonically conjugate momentum is

$$q_\nu = \frac{\partial\mathcal{L}}{\partial\dot F_\nu}. \tag{8.31}$$

The Hamiltonian is then

$$\mathcal{H}_{tl} = \sum_\nu\left[\frac{q_\nu^2}{2C_{tl}} + \frac{1}{2}C_{tl}\omega_\nu^2 F_\nu^2\right]. \tag{8.32}$$

Introducing quantum operators $\hat{b}_\nu$ that satisfy $[\hat{b}_\mu, \hat{b}_\nu^\dagger] = \delta_{\mu\nu}$, and letting

$$F_\nu = \sqrt{\frac{\hbar}{2C_{tl}\omega_\nu}}(\hat{b}_\nu + \hat{b}_\nu^\dagger), \tag{8.33}$$

$$q_\nu = -i\sqrt{\frac{C_{tl}\omega_\nu\hbar}{2}}(\hat{b}_\nu - \hat{b}_\nu^\dagger), \tag{8.34}$$

one gets a quantized Hamiltonian

$$H = \sum_\nu \left[\hat{b}_\nu^\dagger \hat{b}_\nu + \frac{1}{2}\right] \hbar\omega_\nu. \tag{8.35}$$

The flux along the TL is

$$\eta(z) = \sum_\nu F_\nu \psi_\nu(z) = \sum_\nu \sqrt{\frac{\hbar}{2Lc\omega_\nu}}(\hat{b}_\nu + \hat{b}_\nu^\dagger)\psi_\nu(z). \tag{8.36}$$

The time dependence of this flux comes from the normal mode operators $\hat{b}_\nu$ and $\hat{b}_\nu^\dagger$.

Hence,

$$\eta(z,t) = \sum_\nu F_\nu \psi_\nu(z) = \sum_\nu \sqrt{\frac{\hbar}{2Lc\omega_\nu}}(\hat{b}_\nu e^{-i\omega_\nu t} + \hat{b}_\nu^\dagger e^{i\omega_\nu t})\psi_\nu(z). \tag{8.37}$$

Hence, the voltage $V(z,t) = -\dot{\eta}(z,t)$ along the TL is

$$V(z,t) = i\sqrt{\frac{1}{2Lc}}\sum_\nu \sqrt{\hbar\omega_\nu}(\hat{b}_\nu e^{-i\omega_\nu t} - \hat{b}_\nu^\dagger e^{i\omega_\nu t})\psi_\nu(z). \tag{8.38}$$

Alternately,

$$\begin{aligned} V(z,t) &= i\frac{1}{\sqrt{2}}\sum_\nu \sqrt{\hbar\omega_\nu}(\hat{b}_\nu e^{-i\omega_\nu t} - \hat{b}_\nu^\dagger e^{i\omega_\nu t})\varphi_\nu(z), \\ &= i\frac{1}{\sqrt{2}}\sum_\nu \sqrt{\hbar\omega_\nu}(\hat{b}_\nu e^{-i\omega_\nu t} - \hat{b}_\nu^\dagger e^{i\omega_\nu t})\Re[C_\nu e^{i(k_\nu z+\phi_\nu)}]. \end{aligned} \tag{8.39}$$

One can decompose $V(z,t)$ into left and right moving components

$$V^{\leftarrow}(z,t) = \frac{1}{\sqrt{2}}\sum_\nu \sqrt{\hbar\omega_\nu}\ \hat{b}_\nu^\dagger C_\nu e^{i(k_\nu z+\omega_\nu t+\phi_\nu-\pi/2)}, \tag{8.40}$$

$$V^{\rightarrow}(z,t) = \frac{1}{\sqrt{2}}\sum_\nu \sqrt{\hbar\omega_\nu}\ \hat{b}_\nu C_\nu e^{i(k_\nu z-\omega_\nu t+\phi_\nu+\pi/2)}, \tag{8.41}$$

so that $V(z,t) = V^{\rightarrow}(z,t) + V^{\leftarrow}(z,t)$.

8.4 Appendix D

In this appendix, I show in more detail how one can quantize a time-dependent harmonic oscillator, following the approach of [131]. The Hamiltonian of a particle in a Paul trap is given by

$$H(t) = \frac{p^2}{2m} + \frac{1}{2}k(t)q^2. \tag{8.42}$$

The parameter $k(t)$ has period τ. In experiments $k(t) = a + b\cos(2\pi t/\tau)$. But in general, $k(t+\tau) = k(t)$. The classical equation of motion is

$$m\ddot{q}(t) + k(t)q(t) = 0. \tag{8.43}$$

Suppose some function $f(t)$ is a solution to the classical equation. Since $f(t)$ is periodic, $f(t+\tau) = e^{i\theta}f(t)$. Note that $f^*(t)$ is also a linearly independent solution. The Wronskian is

$$W = \begin{vmatrix} f(t) & f^*(t) \\ \dot{f}(t) & \dot{f}^*(t) \end{vmatrix}. \tag{8.44}$$

The time derivative of the Wronskian is zero. That is

$$\begin{aligned} \frac{d}{dt}W &= \frac{d}{dt}\left[(f\dot{f}^* - f^*\dot{f})\right] \\ &= (\dot{f}\dot{f}^* + f\ddot{f}^*) - (\dot{f}^*\dot{f} + f^*\ddot{f}) \\ &= f\ddot{f}^* - f^*\ddot{f} \\ &= -\frac{k}{m}ff^* + \frac{k}{m}f^*f \\ &= 0. \end{aligned} \tag{8.45}$$

Henceforth, I will let $(f\dot{f}^* - f^*\dot{f}) = 2iW$ with $W > 0$.

Let

$$\chi(t) = -\frac{m}{4}\left(\frac{\dot{f}}{f}+\frac{\dot{f}^*}{f^*}\right) = -\frac{m}{4}\frac{d}{dt}\ln|f|^2. \tag{8.46}$$

In a new basis $|\Psi'\rangle = U_1|\Psi\rangle$ with $U_1 = e^{-i\chi(t)q^2}$, the coordinate and momentum transform as

$$q \rightarrow U_1^\dagger q U_1 = q, \tag{8.47}$$

$$p \rightarrow U_1^\dagger p U_1 = p + i\chi[q^2,p] + \frac{i^2\chi^2}{2!}[q^2,[q^2,p]] + ... = p - 2\chi q. \tag{8.48}$$

I have used the commutation relation $[q^2,p] = i\frac{\partial q^2}{\partial q} = 2iq$. Under U_1 the Hamiltonian transforms as $H \rightarrow \bar{H}$ where

$$\begin{aligned}\bar{H} &= U_1^\dagger H U_1 - iU_1^\dagger\frac{dU}{dt},\\ &= \frac{(p-2\chi q)^2}{2m} + \frac{1}{2}k(t)q^2 - \dot{\chi}(t)q^2,\\ &= \frac{p^2}{2m} - \frac{\chi}{m}(qp+pq) + \frac{2\chi^2q^2}{m} + \frac{1}{2}k(t)q^2 - \dot{\chi}(t)q^2.\end{aligned} \tag{8.49}$$

Now

$$\begin{aligned}\dot{\chi} &= -\frac{m}{4}\left(\frac{f\ddot{f}-\dot{f}\dot{f}}{f^2} + \frac{f^*\ddot{f}^*-\dot{f}^*\dot{f}^*}{f^{*2}}\right)\\ &= -\frac{m}{4}\left(\frac{\ddot{f}}{f} - \frac{\dot{f}^2}{f^2} + \frac{\ddot{f}^*}{f^*} - \frac{\dot{f}^{*2}}{f^{*2}}\right)\\ &= -\frac{m}{4}\left(-\frac{2k}{m}\right) + \frac{m}{4}\left(\frac{\dot{f}^2}{f^2}+\frac{\dot{f}^{*2}}{f^{*2}}\right)\\ &= \frac{k}{2} + \frac{m}{4}\left(\frac{\dot{f}^2}{f^2}+\frac{\dot{f}^{*2}}{f^{*2}}\right).\end{aligned} \tag{8.50}$$

There is also the relation

$$\left(\frac{\dot{f}^2}{f^2}+\frac{\dot{f}^{*2}}{f^{*2}}\right) = 2\frac{|\dot{f}|^2}{|f|^2} - \frac{4W^2}{|f|^4}. \tag{8.51}$$

So,

$$\begin{aligned}\dot{\chi} &= \frac{k}{2}+\frac{m}{4}\left(2\frac{|\dot{f}|^2}{|f|^2}-\frac{4W^2}{|f|^4}\right)\\ &= \frac{k}{2}+\frac{m}{2}\frac{|\dot{f}|^2}{|f|^2}-\frac{mW^2}{|f|^4}.\end{aligned} \tag{8.52}$$

Thus,

$$\frac{1}{2}kq^2-\dot{\chi}q^2 = -\frac{m}{2}\frac{|\dot{f}|^2}{|f|^2}q^2+\frac{mW^2}{|f|^4}. \tag{8.53}$$

There is one final term. That is

$$\begin{aligned}\frac{2\chi^2q^2}{m} &= \frac{2}{m}\frac{m^2}{16}\left(\frac{\dot{f}}{f}+\frac{\dot{f}^*}{f^*}\right)^2q^2\\ &= \frac{m}{8}\left[\left(\frac{\dot{f}}{f}\right)^2+2\left|\frac{\dot{f}}{f}\right|^2+\left(\frac{\dot{f}^*}{f^*}\right)^2\right]q^2\\ &= \frac{m}{8}q^2\left[4\left|\frac{\dot{f}}{f}\right|^2-4\frac{W^2}{|f|^4}\right]\\ &= \frac{mq^2}{2}\left|\frac{\dot{f}}{f}\right|^2-\frac{mq^2}{2}\frac{W^2}{|f|^4}.\end{aligned} \tag{8.54}$$

Adding all three terms together, one gets

$$\frac{2\chi^2q^2}{m}+\frac{1}{2}kq^2-\dot{\chi}q^2=\frac{mW^2}{2|f|^4}q^2. \tag{8.55}$$

Thus, the transformed Hamiltonian is

$$\bar{H} = \frac{p^2}{2m}-\frac{\chi}{m}(pq+qp)+\frac{mW^2}{2|f|^4}q^2. \tag{8.56}$$

Now let $\lambda=\ln|f|^2/4$, and $U_2=e^{-i\lambda(pq+qp)}$. Using the commutation relations $[pq+qp,p]=2ip$, $[pq+qp,q]=-2iq$

$$U_2^\dagger pU_2 = p\sum_{n=0}^{\infty}\frac{(2i)^n(i\lambda)^n}{n!}=pe^{(2i)(i\lambda)}=pe^{-2\lambda}=pe^{-\ln|f|}=\frac{p}{|f|}, \tag{8.57}$$

$$U_2^\dagger qU_2 = q\sum_{n=0}^{\infty}\frac{(-2i)^n(i\lambda)^n}{n!}=qe^{(-2i)(i\lambda)}=qe^{2\lambda}=pe^{\ln|f|}=|f|q. \tag{8.58}$$

Note that $\chi = -m\dot{\lambda}$. Then the Hamiltonian $\bar{H}$ transforms again as

$$\begin{aligned}
\bar{H} &= \frac{1}{|f|^2}\frac{p^2}{2m} - \frac{\chi}{m}(pq+qp) + \frac{mW^2}{2|f|^2}q^2 - i(-i\dot{\lambda})(pq+qp) \\
&= \frac{1}{|f|^2}\frac{p^2}{2m} + \dot{\lambda}(pq+qp) + \frac{mW^2}{2|f|^2}q^2 - \dot{\lambda}(pq+qp) \\
&= \frac{1}{|f|^2}\frac{p^2}{2m} + \frac{mW^2}{2|f|^2}q^2 \\
&= \frac{1}{|f|^2}\left(\frac{p^2}{2m} + \frac{1}{2}mWq^2\right). \qquad (8.59)
\end{aligned}$$

Apart from a time dependent factor $|f(t)|^{-2}$ one now has a simple harmonic oscillator Hamiltonian with frequency W. One can finally write q and p in terms of the usual creation and annihilation operators $\hat{a}^\dagger$ and $\hat{a}$ to get

$$H = \frac{1}{|f(t)|^2}\left(\hat{a}^\dagger\hat{a} + \frac{1}{2}\right)W. \qquad (8.60)$$

Bibliography

[1] M. A. Nielsen and I. Chuang, *Quantum Computation and Quantum Information*. Cambridge University Press, 2000.

[2] A. M. Turing, "On computable numbers with an application to the entscheidungsproblem," 1936.

[3] A. M. Turing, "Computability and λ-definability," *Journal of Symbolic Logic*, vol. 2, no. 04, pp. 153–163, 1937.

[4] J. von Neumann, "First draft of a report on the EDVAC," tech. rep., Moore School of Electrical Engineering, University of Pennsylvania, 1945.

[5] W. Shockley, "The theory of p-n junctions in semiconductors and p-n junction transistors," *Bell System Technical Journal*, vol. 28, pp. 435–489, 1949.

[6] M. Riordan, L. Hoddeson, and C. Herring, "The invention of the transistor," *Rev. Mod. Phys.*, vol. 71, pp. S336–S345, Mar. 1999.

[7] W. H. Zurek, "Thermodynamic cost of computation, algorithmic complexity and the information metric," *Nature*, vol. 341, pp. 119–124, Sept. 1989.

[8] R. Landauer, "Irreversibility and heat generation in the computing process," *IBM Journal of Research and Development*, vol. 5, pp. 183–191, July 1961.

[9] E. L. Wolf, *Nanophysics of Solar and Renewable Energy*. Wiley-VCH, 2012.

[10] R. Feynman, "Simulating physics with computers," *International Journal of Theoretical Physics*, vol. 21, no. 6-7, pp. 467–488, 1982.

[11] S. P. Jordan, "Quantum algorithm zoo."

[12] L. K. Grover, "A fast quantum mechanical algorithm for database search," in *Proceedings of the Twenty-eighth Annual ACM Symposium on Theory of Computing*, STOC '96, (New York, NY, USA), pp. 212–219, ACM, 1996.

[13] P. W. Shor, "Polynomial-time algorithms for prime factorization and discrete logarithms on a quantum computer," *SIAM J. Comput.*, vol. 26, pp. 1484–1509, Oct. 1997.

[14] A. Kitaev, S. A. H. Yu, and M. N. Vyalyi, *Classical and Quantum Computation*. American Mathematical Society, 2002.

[15] D. P. DiVincenzo, "Two-bit gates are universal for quantum computation," *Phys. Rev. A*, vol. 51, pp. 1015–1022, Feb 1995.

[16] S. Lloyd, "Almost any quantum logic gate is universal," *Phys. Rev. Lett.*, vol. 75, pp. 346–349, Jul 1995.

[17] S. X. Wang, J. Labaziewicz, Y. Ge, R. Shewmon, and I. L. Chuang, "Demonstration of a quantum logic gate in a cryogenic surface-electrode ion trap," *Phys. Rev. A*, vol. 81, p. 062332, June 2010.

[18] G. S. Buller and R. J. Collins, "Single-photon generation and detection," *Measurement Science and Technology*, vol. 21, no. 1, p. 012002, 2010.

[19] G. J. Milburn, "Quantum optical Fredkin gates," *Phys. Rev. Lett.*, vol. 62, pp. 2124–2127, May 1989.

[20] R. W. Boyd, *Nonlinear Optics*. Academic Press, Amsterdam, 2003.

[21] L. Mandel and E. Wolf, *Optical Coherence and Quantum Optics*. Cambridge University Press, September 29, 1995.

[22] J. I. Cirac and P. Zoller, "Quantum computations with cold trapped ions," *Phys. Rev. Lett.*, vol. 74, pp. 4091–4094, May 1995.

[23] D. Loss and D. P. DiVincenzo, "Quantum computation with quantum dots," *Phys. Rev. A*, vol. 57, pp. 120–126, Jan. 1998.

[24] J. Wrachtrup, S. Kilin, and A. Nizovtsev, "Quantum computation using the 13c nuclear spins near the single nv defect center in diamond," *Optics and Spectroscopy*, vol. 91, no. 3, pp. 429–437–, 2001.

[25] M. H. Devoret and R. J. Schoelkopf, "Superconducting circuits for quantum information: An outlook," *Science*, vol. 339, pp. 1169–1174, Mar. 2013.

[26] D. P. DiVincenzo, "The physical implementation of quantum computation," *Fortschr. Phys.*, vol. 48, pp. 771–783, Sept. 2000.

[27] S. Lloyd, "Universal quantum simulators," *Science*, vol. 273, pp. 1073–1078, Aug. 1996.

[28] I. M. Georgescu, S. Ashhab, and F. Nori, "Quantum simulation," *Rev. Mod. Phys.*, vol. 86, pp. 153–185, Mar. 2014.

[29] Z.-L. Xiang, S. Ashhab, J. Q. You, and F. Nori, "Hybrid quantum circuits: Superconducting circuits interacting with other quantum systems," *Rev. Mod. Phys.*, vol. 85, pp. 623–653, Apr. 2013.

[30] A. Blais, R.-S. Huang, A. Wallraff, S. M. Girvin, and R. J. Schoelkopf, "Cavity quantum electrodynamics for superconducting electrical circuits: An architecture for quantum computation," *Phys. Rev. A*, vol. 69, p. 062320, Jun 2004.

[31] P. Rabl, P. Cappellaro, M. V. G. Dutt, L. Jiang, J. R. Maze, and M. D. Lukin, "Strong magnetic coupling between an electronic spin qubit and a mechanical resonator," *Phys. Rev. B*, vol. 79, p. 041302, Jan. 2009.

[32] K. H. Onnes *Leiden Communications*, vol. 120b, 1911.

[33] M. Tinkham, *Introduction to Superconductivity*. Dover, 2004.

[34] "30 - On the theory of superconductivity," in *Collected Papers of L.D. Landau* (D. T. HAAR, ed.), pp. 217–225, Pergamon, 1965.

[35] J. Bardeen, L. N. Cooper, and J. R. Schrieffer, "Theory of superconductivity," *Phys. Rev.*, vol. 108, pp. 1175–1204, Dec. 1957.

[36] B. Josephson, "Possible new effects in superconductive tunnelling," *Physics Letters*, vol. 1, pp. 251–253, July 1962.

[37] K. K. Likharev, *Dynamics of Josephson Junctions and Circuits*. CRC Press, 1986.

[38] C. P. Slichter, *Principles of Nuclear Magnetic Resonance*. Springer, 3rd ed., 1990.

[39] Y. Makhlin, G. Schön, and A. Shnirman, "Quantum-state engineering with Josephson-junction devices," *Rev. Mod. Phys.*, vol. 73, pp. 357–400, May 2001.

[40] J. Clarke and F. K. Wilhelm, "Superconducting quantum bits," *Nature*, vol. 453, pp. 1031–1042, June 2008.

[41] J. Koch, T. M. Yu, J. Gambetta, A. A. Houck, D. I. Schuster, J. Majer, A. Blais, M. H. Devoret, S. M. Girvin, and R. J. Schoelkopf, "Charge-insensitive qubit design derived from the Cooper pair box," *Phys. Rev. A*, vol. 76, p. 042319, Oct 2007.

[42] R. C. Bialczak, R. McDermott, M. Ansmann, M. Hofheinz, N. Katz, E. Lucero, M. Neeley, A. D. OConnell, H. Wang, A. N. Cleland, and J. M. Martinis, "Flux noise in josephson phase qubits," *Phys. Rev. Lett.*, vol. 99, p. 187006, Nov. 2007.

[43] J. M. Martinis, S. Nam, J. Aumentado, K. M. Lang, and C. Urbina, "Decoherence of a superconducting qubit due to bias noise," *Phys. Rev. B*, vol. 67, p. 094510, Mar. 2003.

[44] J. Bylander, S. Gustavsson, F. Yan, F. Yoshihara, K. Harrabi, G. Fitch, D. G. Cory, Y. Nakamura, J.-S. Tsai, and W. D. Oliver, "Noise spectroscopy through dynamical decoupling with a superconducting flux qubit," *Nat Phys*, vol. 7, pp. 565–570, July 2011.

[45] L. Faoro and L. B. Ioffe, "Quantum two level systems and Kondo-like traps as possible sources of decoherence in superconducting qubits," *Phys. Rev. Lett.*, vol. 96, p. 047001, Jan. 2006.

[46] M. Steffen, S. Kumar, D. P. DiVincenzo, J. R. Rozen, G. A. Keefe, M. B. Rothwell, and M. B. Ketchen, "High-coherence hybrid superconducting qubit," *Phys. Rev. Lett.*, vol. 105, p. 100502, Sept. 2010.

[47] R. J. Schoelkopf and S. M. Girvin, "Wiring up quantum systems," *Nature*, vol. 451, pp. 664–669, Feb. 2008.

[48] H. Walther, B. T. H. Varcoe, B.-G. Englert, and T. Becker, "Cavity quantum electrodynamics," *Reports on Progress in Physics*, vol. 69, no. 5, p. 1325, 2006.

[49] D. Kleppner, "Inhibited spontaneous emission," *Phys. Rev. Lett.*, vol. 47, pp. 233–236, July 1981.

[50] M. Devoret, "Quantum fluctuations in electrical circuits," *Les Houches Session LXIII, Elsevier Science B. V.*, 1995.

[51] G. Burkard, R. H. Koch, and D. P. DiVincenzo, "Multilevel quantum description of decoherence in superconducting qubits," *Phys. Rev. B*, vol. 69, p. 064503, Feb 2004.

[52] E. Knill, R. Laflamme, and G. J. Milburn, "A scheme for efficient quantum computation with linear optics," *Nature*, vol. 409, pp. 46–52, Jan. 2001.

[53] P. Kok, W. J. Munro, K. Nemoto, T. C. Ralph, J. P. Dowling, and G. J. Milburn, "Linear optical quantum computing with photonic qubits," *Rev. Mod. Phys.*, vol. 79, pp. 135–174, Jan. 2007.

[54] M. A. Nielsen, "Optical quantum computation using cluster states," *Phys. Rev. Lett.*, vol. 93, p. 040503, July 2004.

[55] D. E. Browne and T. Rudolph, "Resource-efficient linear optical quantum computation," *Phys. Rev. Lett.*, vol. 95, p. 010501, June 2005.

[56] D. I. Schuster, A. A. Houck, J. A. Schreier, A. Wallraff, J. M. Gambetta, A. Blais, L. Frunzio, J. Majer, B. Johnson, M. H. Devoret, S. M. Girvin, and R. J. Schoelkopf, "Resolving photon number states in a superconducting circuit," *Nature*, vol. 445, pp. 515–518, Feb. 2007.

[57] P. Adhikari, M. Hafezi, and J. M. Taylor, "Nonlinear optics quantum computing with circuit QED," *Phys. Rev. Lett.*, vol. 110, p. 060503, Feb 2013.

[58] A. Wallraff, D. I. Schuster, A. Blais, L. Frunzio, R.-S. Huang, J. Majer, S. Kumar, S. M. Girvin, and R. J. Schoelkopf, "Strong coupling of a single photon to a superconducting qubit using circuit quantum electrodynamics," *Nature*, vol. 431, pp. 162–167, Sept. 2004.

[59] E. Zakka-Bajjani, F. Nguyen, M. Lee, L. R. Vale, R. W. Simmonds, and J. Aumentado, "Quantum superposition of a single microwave photon in two different "colour" states," *Nat Phys*, vol. 7, pp. 599–603, Aug. 2011.

[60] J. M. Martinis and O. Kevin, "Superconducting qubits and the physics of Josephson junctions," 2004.

[61] M. Boissonneault, J. M. Gambetta, and A. Blais, "Improved qubit bifurcation readout in the straddling regime of circuit QED," *Phys. Rev. A*, vol. 86, p. 022326, Aug. 2012.

[62] C. Eichler, D. Bozyigit, C. Lang, L. Steffen, J. Fink, and A. Wallraff, "Experimental state tomography of itinerant single microwave photons," *Phys. Rev. Lett.*, vol. 106, p. 220503, June 2011.

[63] A. A. Houck, D. I. Schuster, J. M. Gambetta, J. A. Schreier, B. R. Johnson, J. M. Chow, L. Frunzio, J. Majer, M. H. Devoret, S. M. Girvin, and R. J. Schoelkopf, "Generating single microwave photons in a circuit," *Nature*, vol. 449, pp. 328–331, Sept. 2007.

[64] M. Hofheinz, E. M. Weig, M. Ansmann, R. C. Bialczak, E. Lucero, M. Neeley, A. D. O'Connell, H. Wang, J. M. Martinis, and A. N. Cleland, "Generation of Fock states in a superconducting quantum circuits," *Nature*, vol. 454, pp. 310–314, July 2008.

[65] Y. Xiao, M. Klein, M. Hohensee, L. Jiang, D. F. Phillips, M. D. Lukin, and R. L. Walsworth, "Slow light beam splitter," *Phys. Rev. Lett.*, vol. 101, p. 043601, July 2008.

[66] B. R. Johnson, M. D. Reed, A. A. Houck, D. I. Schuster, L. S. Bishop, E. Ginossar, J. M. Gambetta, L. DiCarlo, L. Frunzio, S. M. Girvin, and R. J. Schoelkopf, "Quantum non-demolition detection of single microwave photons in a circuit," *Nat Phys*, vol. 6, pp. 663–667, Sept. 2010.

[67] G. Romero, J. J. Garca-Ripoll, and E. Solano, "Microwave photon detector in circuit QED," *Phys. Rev. Lett.*, vol. 102, p. 173602, Apr. 2009.

[68] Y. Yin, H. Wang, M. Mariantoni, R. C. Bialczak, R. Barends, Y. Chen, M. Lenander, E. Lucero, M. Neeley, A. D. O'Connell, D. Sank, M. Weides, J. Wenner, T. Yamamoto, J. Zhao, A. N. Cleland, and J. M. Martinis, "Dynamic quantum Kerr effect in circuit quantum electrodynamics," *Phys. Rev. A*, vol. 85, p. 023826, Feb 2012.

[69] A. A. Abdumalikov, O. Astafiev, Y. Nakamura, Y. A. Pashkin, and J. Tsai, "Vacuum rabi splitting due to strong coupling of a flux qubit and a coplanar-waveguide resonator," *Phys. Rev. B*, vol. 78, p. 180502, Nov. 2008.

[70] H. Paik, D. I. Schuster, L. S. Bishop, G. Kirchmair, G. Catelani, A. P. Sears, B. R. Johnson, M. J. Reagor, L. Frunzio, L. I. Glazman, S. M. Girvin, M. H. Devoret, and R. J. Schoelkopf, "Observation of high coherence in Josephson junction qubits measured in a three-dimensional circuit qed architecture," *Phys. Rev. Lett.*, vol. 107, p. 240501, Dec. 2011.

[71] K. Nemoto and W. J. Munro, "Nearly deterministic linear optical controlled-not gate," *Phys. Rev. Lett.*, vol. 93, p. 250502, Dec. 2004.

[72] I.-C. Hoi, A. F. Kockum, T. Palomaki, T. M. Stace, B. Fan, L. Tornberg, S. R. Sathyamoorthy, G. Johansson, P. Delsing, and C. M. Wilson, "Giant cross-Kerr effect for propagating microwaves induced by an artificial atoms," *Phys. Rev. Lett.*, vol. 111, p. 053601, Aug. 2013.

[73] S. Rebi, J. Twamley, and G. J. Milburn, "Giant Kerr nonlinearities in circuit quantum electrodynamics," *Phys. Rev. Lett.*, vol. 103, p. 150503, Oct. 2009.

[74] M. Fleischhauer, A. Imamoglu, and J. P. Marangos, "Electromagnetically induced transparency: Optics in coherent media," *Rev. Mod. Phys.*, vol. 77, pp. 633–673, July 2005.

[75] J. Clarke and B. A. I., *The Squid Handbook: Applications of Squids and Squid Systems*, vol. 2. Wiley-VCH, 2007.

[76] J. D. Teufel, D. Li, M. S. Allman, K. Cicak, A. J. Sirois, J. D. Whittaker, and R. W. Simmonds, "Circuit cavity electromechanics in the strong-coupling regime," *Nature*, vol. 471, pp. 204–208, Mar. 2011.

[77] K. Kakuyanagi, T. Meno, S. Saito, H. Nakano, K. Semba, H. Takayanagi, F. Deppe, and A. Shnirman, "Dephasing of a superconducting flux qubit," *Phys. Rev. Lett.*, vol. 98, p. 047004, Jan. 2007.

[78] S. M. Anton, C. Mller, J. S. Birenbaum, S. R. OKelley, A. D. Fefferman, D. S. Golubev, G. C. Hilton, H.-M. Cho, K. D. Irwin, F. C. Wellstood, G. Schn, A. Shnirman, and J. Clarke, "Pure dephasing in flux qubits due to flux noise with spectral density scaling as $1/f^{alpha}$.," *Phys. Rev. B*, vol. 85, p. 224505, June 2012.

[79] F. Wilczek, "Quantum mechanics of fractional-spin particles," *Phys. Rev. Lett.*, vol. 49, pp. 957–959, Oct. 1982.

[80] A. Kitaev, "Anyons in an exactly solved model and beyond," *Annals of Physics*, vol. 321, pp. 2–111, Jan. 2006.

[81] R. B. Laughlin, "Anomalous quantum Hall effect: An incompressible quantum fluid with fractionally charged excitations," *Phys. Rev. Lett.*, vol. 50, pp. 1395–1398, May 1983.

[82] G. Moore and N. Read, "Nonabelions in the fractional quantum Hall effects," *Nuclear Physics B*, vol. 360, pp. 362–396, Aug. 1991.

[83] M. H. Freedman, M. Larsen, and Z. Wang, "A modular functor which is universal for quantum computation," *Communications in Mathematical Physics*, vol. 227, no. 3, pp. 605–622, 2002.

[84] A. Kitaev, "Fault-tolerant quantum computation by anyons," *Annals of Physics*, vol. 303, pp. 2–30, Jan. 2003.

[85] M. Greiter, X.-G. Wen, and F. Wilczek, "Paired Hall state at half filling," *Phys. Rev. Lett.*, vol. 66, pp. 3205–3208, June 1991.

[86] A. S. S(ø)rensen, E. Demler, and M. D. Lukin, "Fractional quantum hall states of atoms in optical lattices," *Phys. Rev. Lett.*, vol. 94, p. 086803, Mar. 2005.

[87] Y.-F. Wang, Z.-C. Gu, C.-D. Gong, and D. N. Sheng, "Fractional quantum hall effect of hard-core bosons in topological flat bands," *Phys. Rev. Lett.*, vol. 107, p. 146803, Sept. 2011.

[88] T. Senthil and M. Levin, "Integer quantum hall effect for bosons," *Phys. Rev. Lett.*, vol. 110, p. 046801, Jan. 2013.

[89] I. Bloch, J. Dalibard, and W. Zwerger, "Many-body physics with ultracold gases," *Rev. Mod. Phys.*, vol. 80, pp. 885–964, July 2008.

[90] N. Cooper, "Rapidly rotating atomic gases," *Advances in Physics*, vol. 57, pp. 539–616, Nov. 2008.

[91] H. P. Buchler, A. Micheli, and P. Zoller, "Three-body interactions with cold polar molecules," *Nat Phys*, vol. 3, pp. 726–731, Oct. 2007.

[92] B. Paredes, T. Keilmann, and J. I. Cirac, "Pfaffian-like ground state for three-body hard-core bosons in one-dimensional lattices," *Phys. Rev. A*, vol. 75, p. 053611, May 2007.

[93] A. J. Daley, J. M. Taylor, S. Diehl, M. Baranov, and P. Zoller, "Atomic three-body loss as a dynamical three-body interaction," *Phys. Rev. Lett.*, vol. 102, p. 040402, Jan. 2009.

[94] L. Mazza, M. Rizzi, M. Lewenstein, and J. I. Cirac, "Emerging bosons with three-body interactions from spin-1 atoms in optical lattices," *Phys. Rev. A*, vol. 82, p. 043629, Oct. 2010.

[95] K. W. Mahmud and E. Tiesinga, "Dynamics of spin-1 bosons in an optical lattice: Spin mixing, quantum-phase-revival spectroscopy, and effective three-body interactions," *Phys. Rev. A*, vol. 88, p. 023602, Aug. 2013.

[96] S. P. Jordan and E. Farhi, "Perturbative gadgets at arbitrary orders," *Phys. Rev. A*, vol. 77, p. 062329, June 2008.

[97] D. R. Hofstadter, "Energy levels and wave functions of Bloch electrons in rational and irrational magnetic fields," *Phys. Rev. B*, vol. 14, pp. 2239–2249, Sept. 1976.

[98] M. Hafezi, A. S. S(ø)rensen, E. Demler, and M. D. Lukin, "Fractional quantum Hall effect in optical lattices," *Phys. Rev. A*, vol. 76, p. 023613, Aug. 2007.

[99] M. Hafezi, P. Adhikari, and J. M. Taylor, "Engineering three-body interaction and Pfaffian states in circuit QED systems," *Phys. Rev. B*, vol. 90, p. 060503, Aug. 2014.

[100] J. Koch, A. A. Houck, K. L. Hur, and S. M. Girvin, "Time-reversal-symmetry breaking in circuit-QED-based photon lattices," *Phys. Rev. A*, vol. 82, p. 043811, Oct 2010.

[101] E. Kapit, "Quantum simulation architecture for lattice bosons in arbitrary, tunable, external gauge fields," *Phys. Rev. A*, vol. 87, p. 062336, June 2013.

[102] M. Hafezi, E. A. Demler, M. D. Lukin, and J. M. Taylor, "Robust optical delay lines with topological protection," *Nat Phys*, vol. 7, pp. 907–912, Nov. 2011.

[103] R. O. Umucallar and I. Carusotto, "Artificial gauge field for photons in coupled cavity arrays," *Phys. Rev. A*, vol. 84, p. 043804, Oct. 2011.

[104] V. E. Manucharyan, J. Koch, L. I. Glazman, and M. H. Devoret, "Fluxonium: Single Cooper-pair circuit free of charge offsets," *Science*, vol. 326, no. 5949, pp. 113–116, 2009.

[105] D. Bozyigit, C. Lang, L. Steffen, J. M. Fink, C. Eichler, M. Baur, R. Bianchetti, P. J. Leek, S. Filipp, M. P. da Silva, A. Blais, and A. Wallraff, "Antibunching of microwave-frequency photons observed in correlation measurements using linear detectors," *Nat Phys*, vol. 7, pp. 154–158, Feb. 2011.

[106] J. M. Fink, M. Goppl, M. Baur, R. Bianchetti, P. J. Leek, A. Blais, and A. Wallraff, "Climbing the Jaynes-Cummings ladder and observing its nonlinearity in a cavity Qed systems," *Nature*, vol. 454, pp. 315–318, July 2008.

[107] K. Huang, *Statistical Mechanics*. New York: Wiley, 1987.

[108] P. Würfel, "The chemical potential of radiation," *Journal of Physics C: Solid State Physics*, vol. 15, no. 18, p. 3967, 1982.

[109] H. Ries and A. McEvoy, "Chemical potential and temperature of light," *Journal of Photochemistry and Photobiology A: Chemistry*, vol. 59, pp. 11–18, June 1991.

[110] F. Herrmann and P. Würfel, "Light with nonzero chemical potential," *American Journal of Physics*, vol. 73, pp. 717–721, 2005.

[111] G. Job and F. Herrmann, "Chemical potential–a quantity in search of recognition," *European Journal of Physics*, vol. 27, no. 2, p. 353, 2006.

[112] J. Klaers, J. Schmitt, F. Vewinger, and M. Weitz, "Bose-Einstein condensation of photons in an optical microcavity," *Nature*, vol. 468, pp. 545–548, Nov. 2010.

[113] J. Klaers, J. Schmitt, T. Damm, F. Vewinger, and M. Weitz, "Statistical physics of Bose-Einstein-condensed light in a dye microcavity," *Phys. Rev. Lett.*, vol. 108, p. 160403, Apr. 2012.

[114] C. Sun, S. Jia, C. Barsi, S. Rica, A. Picozzi, and J. W. Fleischer, "Observation of the kinetic condensation of classical waves," *Nat Phys*, vol. 8, pp. 470–474, June 2012.

[115] D. Snoke and S. Girvin, "Dynamics of phase coherence onset in Bose condensates of photons by incoherent phonon emission," *Journal of Low Temperature Physics*, vol. 171, no. 1-2, pp. 1–12, 2013.

[116] F. Dalfovo, S. Giorgini, L. P. Pitaevskii, and S. Stringari, "Theory of bose-einstein condensation in trapped gases," *Rev. Mod. Phys.*, vol. 71, pp. 463–512, Apr. 1999.

[117] P. Kirton and J. Keeling, "Nonequilibrium model of photon condensation," *Phys. Rev. Lett.*, vol. 111, p. 100404, Sept. 2013.

[118] A.-W. de Leeuw, H. T. C. Stoof, and R. A. Duine, "Schwinger-Keldysh theory for Bose-Einstein condensation of photons in a dye-filled optical microcavity," *Phys. Rev. A*, vol. 88, p. 033829, Sept. 2013.

[119] D. N. Sob'yanin, "Bose-Einstein condensation of light: General theory," *Phys. Rev. E*, vol. 88, p. 022132, Aug. 2013.

[120] Y. Subasi, C. H. Fleming, J. M. Taylor, and B. L. Hu, "Equilibrium states of open quantum systems in the strong coupling regime," *Phys. Rev. E*, vol. 86, p. 061132, Dec. 2012.

[121] N. Bergeal, R. Vijay, V. E. Manucharyan, I. Siddiqi, R. J. Schoelkopf, S. M. Girvin, and M. H. Devoret, "Analog information processing at the quantum limit with a Josephson ring modulator," *Nat Phys*, vol. 6, pp. 296–302, Apr. 2010.

[122] M. Aspelmeyer, T. J. Kippenberg, and F. Marquardt, "Cavity optomechanics," *arxiv:1303.0733*, 2013.

[123] M. D. Reed, L. DiCarlo, S. E. Nigg, L. Sun, L. Frunzio, S. M. Girvin, and R. J. Schoelkopf, "Realization of three-qubit quantum error correction with superconducting circuits," *Nature*, vol. 482, pp. 382–385, Feb. 2012.

[124] R. Blatt and D. Wineland, "Entangled states of trapped atomic ions," *Nature*, vol. 453, pp. 1008–1015, June 2008.

[125] T. Monz, K. Kim, W. Hnsel, M. Riebe, A. S. Villar, P. Schindler, M. Chwalla, M. Hennrich, and R. Blatt, "Realization of the quantum Toffoli gate with trapped ions," *Phys. Rev. Lett.*, vol. 102, p. 040501, Jan. 2009.

[126] D. C. Burnham and D. L. Weinberg, "Observation of simultaneity in parametric production of optical photon pairs," *Phys. Rev. Lett.*, vol. 25, pp. 84–87, July 1970.

[127] R. Vijay, M. Devoret, and S. I., "Invited review article: The Josephson bifurcation amplifiers," *Rev. Sci. Instrum.*, vol. 80, 2009.

[128] F. Beaudoin, M. P. da Silva, Z. Dutton, and A. Blais, "First-order sidebands in circuit QED using qubit frequency modulation," *Phys. Rev. A*, vol. 86, p. 022305, Aug. 2012.

[129] D. Kielpinski, D. Kafri, M. J. Woolley, G. J. Milburn, and J. M. Taylor, "Quantum interface between an electrical circuit and a single atom," *Phys. Rev. Lett.*, vol. 108, p. 130504, Mar. 2012.

[130] D. Leibfried, R. Blatt, C. Monroe, and D. Wineland, "Quantum dynamics of single trapped ions," *Rev. Mod. Phys.*, vol. 75, pp. 281–324, Mar. 2003.

[131] L. S. Brown, "Quantum motion in a Paul trap," *Phys. Rev. Lett.*, vol. 66, pp. 527–529, Feb. 1991.

[132] N. W. McLachlan, *Theory and Application of Mathieu Functions.* Oxford University Press, 1947.

[133] A. S. S(ø)rensen, C. H. van der Wal, L. I. Childress, and M. D. Lukin, "Capacitive coupling of atomic systems to mesoscopic conductors," *Phys. Rev. Lett.*, vol. 92, p. 063601, Feb. 2004.

[134] L. Tian, P. Rabl, R. Blatt, and P. Zoller, "Interfacing quantum-optical and solid-state qubits," *Phys. Rev. Lett.*, vol. 92, p. 247902, June 2004.

[135] P. Rabl, D. DeMille, J. M. Doyle, M. D. Lukin, R. J. Schoelkopf, and P. Zoller, "Hybrid quantum processors: Molecular ensembles as quantum memory for solid state circuits," *Phys. Rev. Lett.*, vol. 97, p. 033003, July 2006.

[136] D. Petrosyan, G. Bensky, G. Kurizki, I. Mazets, J. Majer, and J. Schmiedmayer, "Reversible state transfer between superconducting qubits and atomic ensembles," *Phys. Rev. A*, vol. 79, p. 040304, Apr. 2009.

[137] J. Preskill, "Quantum computing and the entanglement frontier," *Arxiv-1203-5813-v3*, 2012.

[138] C.-C. Tannoudji and J. Dupont-Roc, *Atom Photon Interactions: Basis Processes and Applications*. Wiley-VCH, 1992.